Modelling and Measuring 3D movements of a speed skater.

BSc. E. van der Kruk

Delft University of Technology
Section Biomechanical Engineering

September, 2013

Modelling and Measuring 3D movements of a speed skater

Author:
Eline van der Kruk

Thesis Committee:
Prof. dr. H.E.J. Veeger
Dr. ir. A.L. Schwab
Ir. O. den Braver

Extern:
Ir. J. Koopman

Preface

Conducting the research for this thesis was a challenge in many ways. Special thanks go out to Esther Brunner, Diederik Morsink and Bastiaan Petermeijer for their help and support during the field tests. Additionally I would like to thank Michiel Maeyaert (Nikon Metrology) for his participation in the project and his effort during the measurements. I also want to thank Aart van der Wulp(Innosportlab) and Thialf Heerenveen for the use of their facilities; the same holds for the companies ProMove and DVC machine vision. Of course I like to render special thanks to the participants in all tests. Last but not least I want to thank B.A.J. Lenseigne for his guidance concerning the image processing and Dr. Ir. A.L. Schwab, Ir. O. den Braver and Prof. Dr. H.E.J. Veeger for their guidance, advice and support during my master thesis trajectory.

Table of contents

Abstract

Ice-skating is a rather special form of locomotion. While in most types of human locomotion humans generate forces by pushing against the environment in the opposite direction of motion, in ice-skating the skater pushes sideward to propel himself forward; Insight in the details of this technique can help a speed skater improve his performance. Forward dynamic biomechanical models allow us to simulate motion, and thereby techniques, and generate the possibility to optimize motion. The aim of this thesis was to develop a reliable and valid three-dimensional biomechanical model that simulates the motion of a speed skater, to gain insight in the skating technique. In order to prove the reliability of the model, the model needs to be verified. Thus, the second goal of this thesis was to accurately measure the 3D kinematics of a speed skater, concerning the 2D positions of the skates and the 3D position of the upper body.

The speed skater was modelled by three point masses, an upper body and two feet, and skate constraints at the feet, based on prior studies. The input of the model were the changing distance between the mass modelled at the upper body and the mass modelled at the skate and the output were the global motion of the skater on the ice and the forces exerted. In order to verify the simple skater model, measured input and output data were needed. A comparative study was performed to find an accurate measurement system that could measure the positions of the upper body of the skater and the skates on the straight part of the ice rink and to find a measurement system that could measure the lean angle of the skates (roll motion).

The position measurement systems LPM (an electromagnetic based Local Position Measurement system, Xsens MTx (an inertial measurement unit), and iGPS (an optoelectronic based indoor GPS system) were tested in a comparative study. The iGPS system proved to be most accurate for the static and dynamic position measurements, with an accuracy of 6mm (maximum absolute error). The iGPS data suffered from data gaps, which resulted in coverage of about 67% in time. Therefore the goal of accurate position measurements was accomplished, but not satisfactory. Concerning lean angle measurements, ProMove and Xsens sensors were compared. The Xsens (MTx) measurement system showed to be most accurate, with an accuracy of 5^0 (mean error); however the required accuracy for verification (2.5^0) was not accomplished.

The results of the position measurements offered a new (quantitative) insight into the vertical upper body movement, which showed an amplitude of 7% of the average body height throughout a straight part. Additionally the results showed indication of a different take-off point of the skates compared to prior studies. The results of this study cannot be taken as evidence for a synchronisation or distortion error in the data used in prior research, however the findings do imply a likeability of such an error.

The goal of the development of a reliable and valid three-dimensional model was not satisfied in this study, since the verification of the model with accurate data could not be performed. No complete dataset for the verification of the three-dimensional model was obtained in this study, due to failing measurement systems. The constructed three-dimensional model was therefore studied using data from a prior study and a simulated vertical upper body movement. However exploratory, due to the inaccuracy of the used data, the three-dimensional skater model showed to do a good job of imitating forces and kinematics observed in actual speed skating for a skater throughout a whole straight part. Despite its preliminary character, the current study seems to indicate that it is possible to model the skater using only one mass at the upper body and two infinitesimal point-masses at the skates. The simulated upper body movements show that the power assimilated into the vertical direction is large compared to the total power output (23%). Therefore, the third dimension is a necessary addition to the prior developed two-dimensional skater model.

Table of contents

Contents

Nomenclature

Symbols	
g	gravitational acceleration
$J_{\min}$	net error between measured and simulated data
k_1	air friction coefficient
m	mass of the skater
u_{ls}, v_{ls}	generalized positions of the left skate
u_{rs}, v_{rs}	generalized positions of the right skate
x_b, y_b	x,y position of the mass at the upper body
x_{ls}, y_{ls}	x,y position of the left skate
x_{rs}, y_{rs}	x,y position of the right skate
α	mass distribution coefficient
μ	ice friction coefficient
θ_{rs}	clock wise angle of the right skate with respect to the length direction of the rink
θ_{ls}	counter clock wise angle of the left skate with respect to the length direction of the rink
θ_b	counter clock wise angle of the upper body with respect to the length direction of the rink

Abbreviations	
2D	Two- dimensional
3D	Three-dimensional
B	Modelled mass at the upper body
CoM	Center of Mass
FBD	Free Body Diagram
FBT	Fiducial Based Tracking
HS	High Speed (camera)
iGPS	Indoor GPS measurement system
LA	Lean Angle
LPM	Local Positioning Measurement system
LS	Modelled mass at the left skate
ProMove	The MEMS lean angle measurement system of the company ProMove
RS	Modelled mass at the right skate
TO	Take-off
ToF	Time of flight
Xsens	The MEMS lean angle measurement system of the company Xsens

“ The aim of this thesis is to develop a reliable and valid three-dimensional biomechanical model that simulates the motion of an speed skater, in order to gain insight in the skating technique. ”

Introduction

1.1 Ice skating

Ice-skating is a rather special form of locomotion. While in most types of human locomotion humans generate forces by pushing against the environment in the opposite direction of motion, in ice-skating the skater pushes sideward to propel himself forward; a curious but effective way to glide over the ice.

The ice skating movement can be divided into three phases: the glide phase, the push-off phase, and the repositioning phase (Figure 1). In the push-off phase the skate moves sideways with respect to the upper body (leg extension). In the glide phase, the skate moves forward with respect to the upper body. Double support (both skates are on the ice) exists in the first part of the glide phase of one leg and in the second part of the push-off phase of the other leg. This motion results in a sinus-wave like trajectory in the horizontal plane of the upper body over the ice.

Insight in the details of this technique can help a speed skater improve his performance.

The exact movement that results in optimal performance is unknown. Analysing the skating technique shows that the elite skaters have a variety of applied techniques. Insight might help skaters in selecting the best (individual) technique. It is therefore interesting for both science and sport to understand the dynamic principle of the ice skating motion.

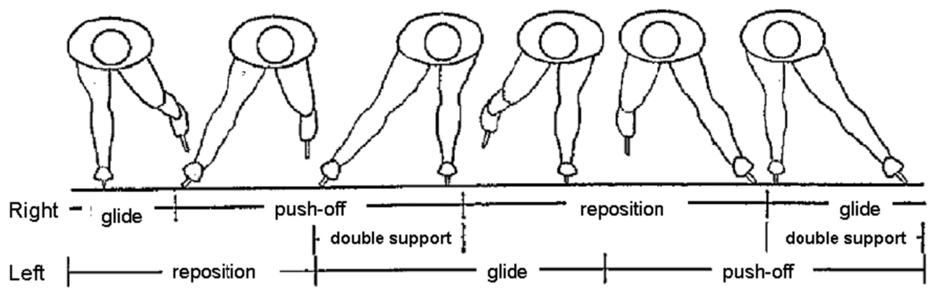

Figure 1 Ice skate phases

1.2 Research goal

The aim of this thesis is the development of a reliable and valid three-dimensional biomechanical model that simulates the motion of a speed skater, in order to gain insight in the skating technique. The reliability of the model needs to be proven by means of verification of the three-dimensional dynamic model. The second goal of this project is therefore to find a measurement system that can accurately measure 3D kinematic data of skaters on an ice rink.

1.3 Three-dimensional simple skater model

Forward dynamic biomechanical models allow us to simulate motion, and thereby techniques, and generate the possibility to optimize motion by comparing an athlete's present technique or form with that required for an ideal performance (Kurita 2011).
(Fintelman 2011) developed a two-dimensional biomechanical model of a speed skater, using only the leg extension as an input parameter. The model of Fintelman showed to simulate the skater motion rather well. The skater model of Fintelman is however a two-dimensional model, which entails that the implementation of the 2D model in the real world has shortcomings. In order to overcome this inadequacy, the model should be expanded into a three-dimensional model. In order to verify the three-dimensional model, accurate 3D kinematic measurements are required.

1.4 Three-dimensional measurements on an ice rink

Verification of a biomechanical model is done by comparing the modelled output with the measured parameters of the speed skater. Verification of the 3D skater model requires measured input and output data (5.5). The input of the model consists of position data (kinematic data), the output of the model includes position data and force data (kinetic data). In kinematics time-related movements are described without consideration of acting forces (Schwieger 2012); In kinetics also the acting forces are considered.

The acting forces can be measured using an instrumented skate (Appendix B). The kinematic data for the input and output of the model need a new measurement method. There are a couple of complicating aspects that render this measurement on an ice rink rather difficult. First the volume of the ice rink: measurements ideally cover both straight and curve, so the footprint of the rink covers up to almost 12000 m^2, while most kinematic measurement systems can acquire data only in a restricted volume. Typically the detection accuracy of a positioning system is inversely proportional to its coverage. Secondly, when measuring in an indoor ice rink the closed space(roof) is of high influence on the measurement systems used; however due to the available means in the Netherlands, indoor ice rinks are preferred for measuring speed skaters. Finally the characteristics of the environment, more specifically, a combination of high humidity, low temperature and high reflection are of influence on the measurement system performance. The search for an accurate kinematic measurement system in ice skating is part of this project.

1.5 Application of the model

The ultimate goal is to use the verified model to advise skaters on their technique; this is the validation of the model. In the long-run the model should give personal advice for individual speed skaters by inserting their variables, like mass and body length. However the application of the verified model (the validation) is left for prospective research (Figure 2). Short-term results can hand the coach and speed skater a tool by which variables can be easily changed, like friction or upper body position, and the performance can be simulated.

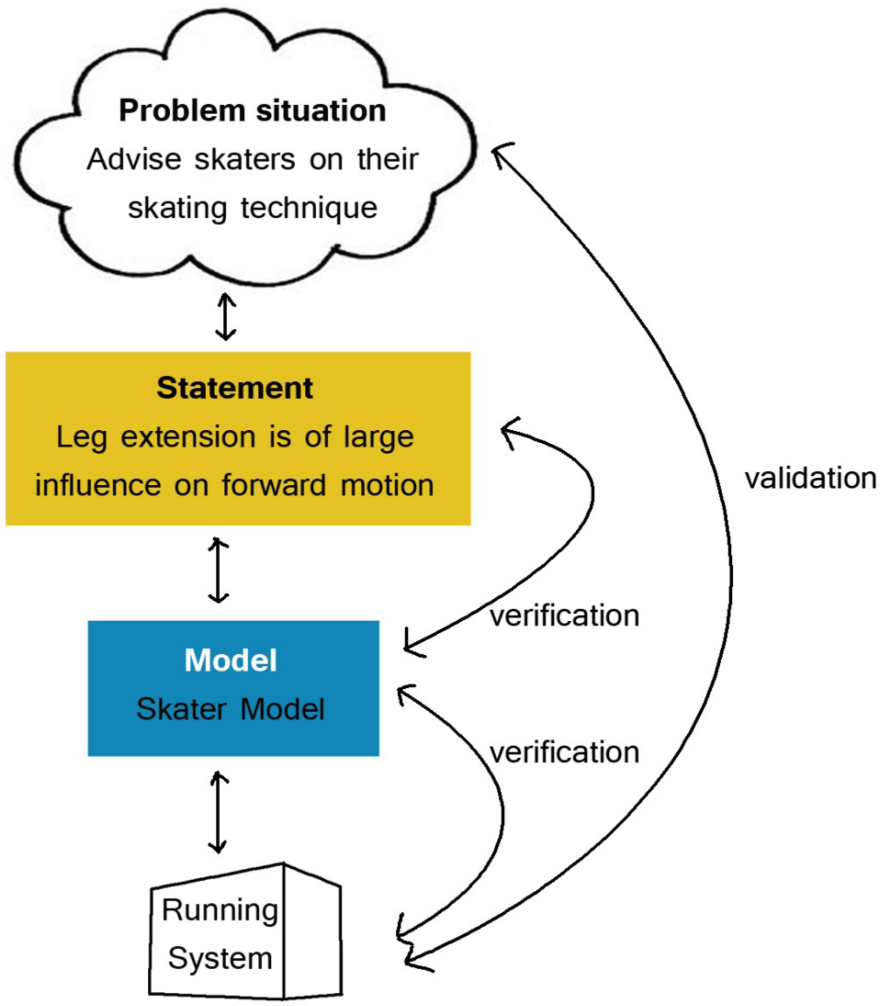

Figure 2 Overview of the steps made in this thesis. This thesis is mainly concerned with the verification of the skater model (blue square to white square). The validation of the verified model is left for prospective research.

1.6 Outline of the thesis

The outline of the thesis is sketched roughly in Figure 3. The report starts with the description and mathematics of the three-dimensional skater model. This reveals the necessary parameters to verify the skater model. Next the measurement systems are discussed and the research on finding the best kinematic measurement system is reported. The following part describes the data collection, followed by the final part of the thesis which holds the verification of the skater model.

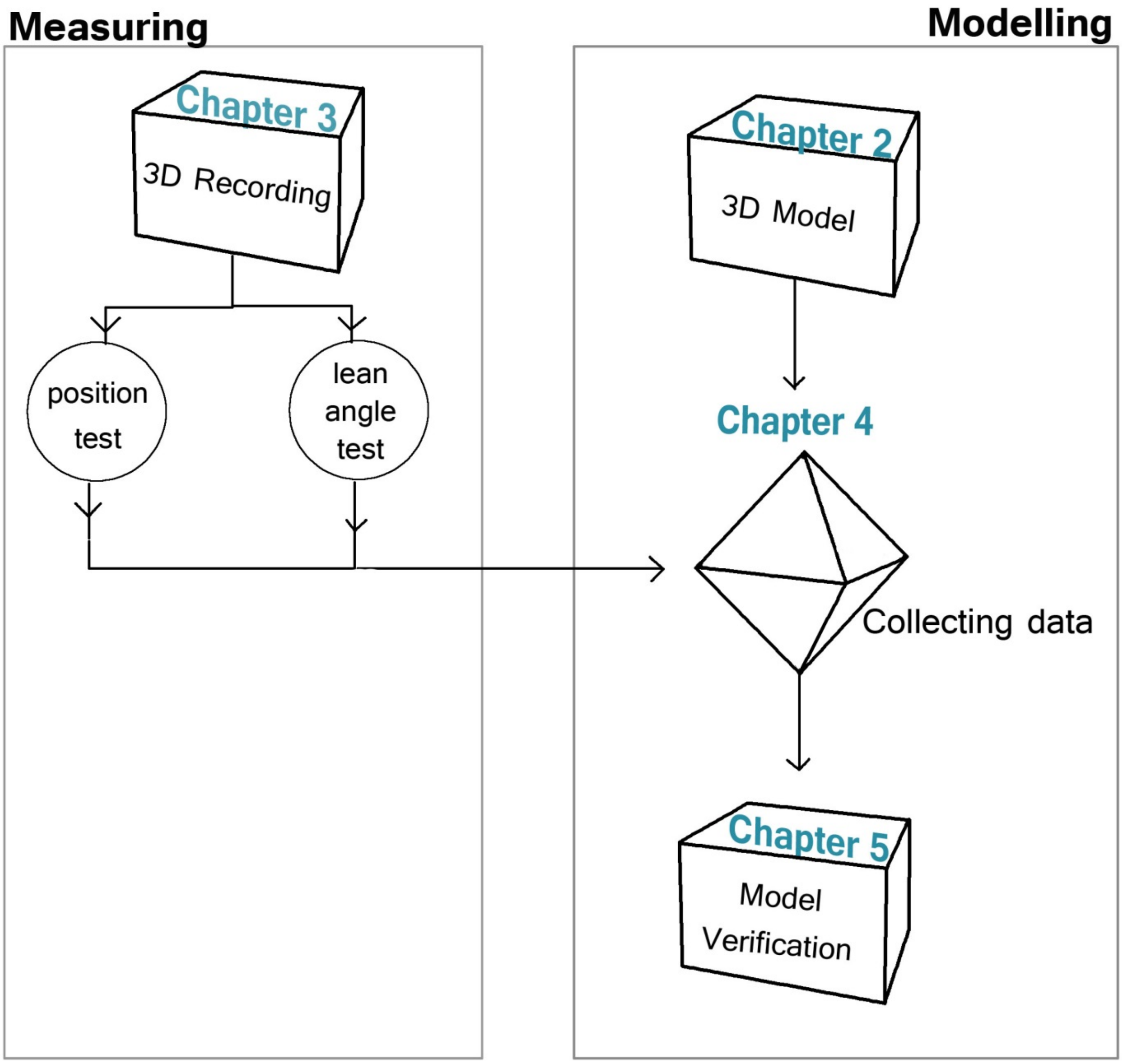

Figure 3 Outline of the report

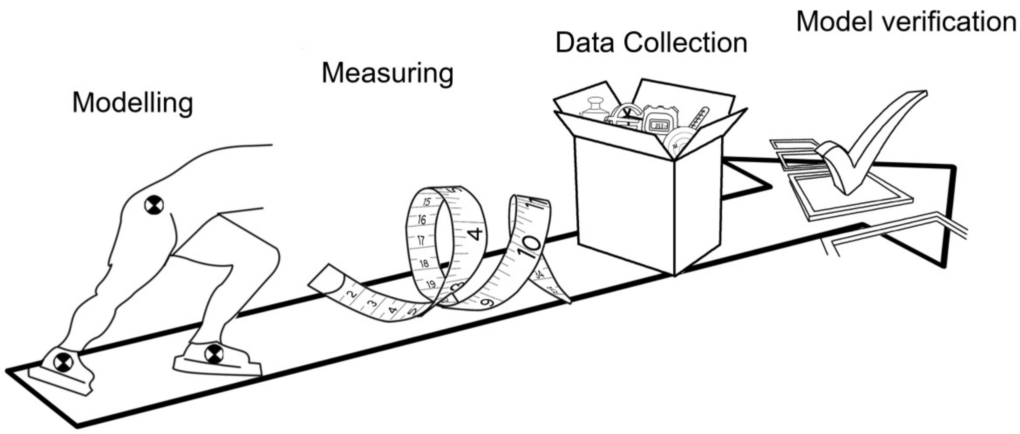
Modelling
Measuring
Data Collection
Model verification

“The speed skater is modelled by three point masses, an upper body and two feet, and skate constraints at the feet. The input of the model are the leg extensions and the output are the global motion of the skater on the ice and the forces exerted.”

3D Skater Model

2.1 Model generation

In this section a three-dimensional inverse dynamic model is derived. Literature on prior developed models can be found in (Fintelman 2010).

The model consists of three point masses: one at the upper body (B) and two on each skate (RS, LS) (Figure 4). The 3D model is driven by the changing distance between the mass B and the masses RS and LS, in line with the model of (Fintelman 2011). This distance will be called the leg extension in the remainder of this report. The output are the global motion of the skater on the ice and the forces exerted.

The model is developed in four stages; first the generalized coordinates and the Free Body Diagram (FBD) are determined. Secondly the equations of motion are derived. The third step is the formulation of the constraints of the model. Finally the equations are solved by numerical integration.

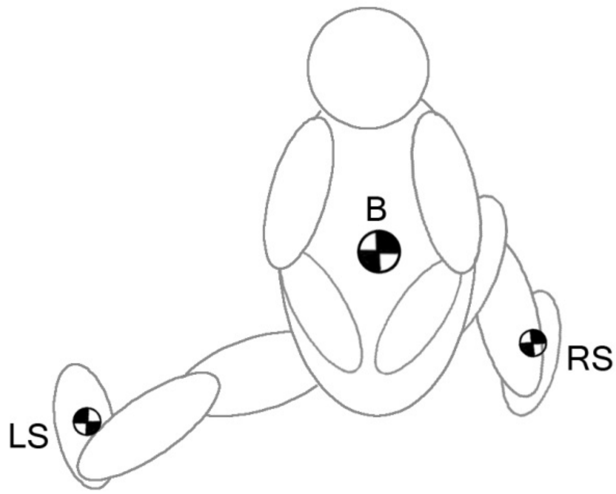

Figure 4 Masses of the 3D model. B = modelled mass at the upper body; LS = modelled mass at the left skate; RS = modelled mass at the right skate.

2.2 Creating the model

The purpose of the model is to express the coordination of the skater in terms of leg extension. The skater model consists of three masses, each with three coordinates (translations) and an angle (rotation), the heading, where we neglect all rolling and pitching motions of the rigid bodies. Additionally we neglect the double stance phase. This phase however proves to be very short (Fintelman 2011). The active skate is always on the ice. Furthermore the arm movements were neglected; The coordination of the skater is expressed in(1.2.1), see Figure 5 and Figure 6.

(1.2.1) $$x_i = \begin{bmatrix} x_b & y_b & z_b & \varphi_b & x_{ls} & y_{ls} & z_{ls} & \varphi_{ls} & x_{rs} & y_{rs} & z_{rs} & \varphi_{rs} \end{bmatrix}$$

(1.2.2) $$f_i = \begin{bmatrix} f_{xb} & f_{yb} & f_{zb} & M_b & f_{xls} & f_{yls} & f_{zls} & M_{ls} & f_{xrs} & f_{yrs} & f_{zrs} & M_{rs} \end{bmatrix}$$

In order to express the model in terms of leg extension, the generalized coordinates are used (Table 1), as given in (1.2.3).

Table 1 Clarification of the generalized coordinates.

q_i	Generalized coordinates
u_b	Absolute position of upper body mass in global x-direction
v_b	Absolute position of upper body mass in global y-direction
w_b	Absolute position of upper body mass in global z-direction
θ_b	Heading of the upper body mass (counterclockwise)
$u_{ls,rs}$	Distance between mass (LS,RS) and mass B in heading direction of the skate (global xy-plane)
$v_{ls,rs}$	Distance between mass (LS,RS) and mass B perpendicular to the heading direction of the skate (global xy-plane)
$w_{ls,rs}$	Vertical distance between mass (LS,RS) and mass B (global xz plane);
$\theta_{ls,rs}$	Heading of the (left, rigtht) skate (counterclockwise)

(1.2.3) $$q_i = \begin{bmatrix} u_b & v_b & w_b & \theta_b & u_{ls} & v_{ls} & w_{ls} & \theta_{ls} & u_{rs} & v_{rs} & w_{rs} & \theta_{rs} \end{bmatrix}$$

(1.2.4) $$F_i = \begin{bmatrix} Fu_b & Fv_b & Fw_b & M\theta_b & Fu_{ls} & Fv_{ls} & Fw_{ls} & M\theta_{ls} & Fu_{rs} & Fv_{rs} & Fw_{rs} & M\theta_{rs} \end{bmatrix}$$

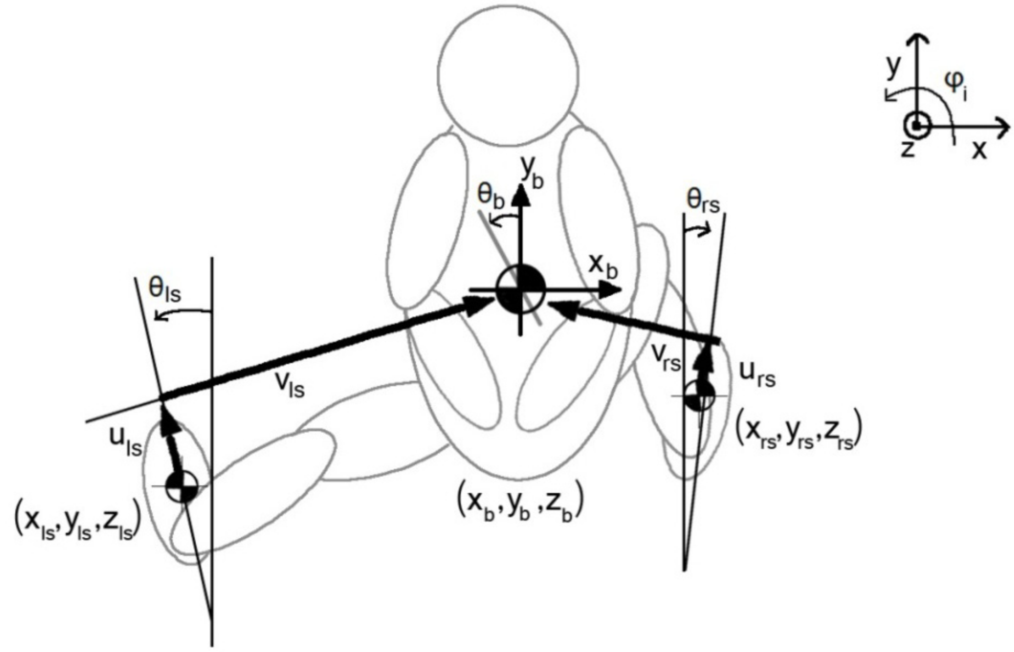

Figure 5 Top view of the 3D skater model. The coordinates of the three point masses are given (x_i,y_i,z_i,φ). The generalized coordinates are (u_i,v_i,w_i,θ)

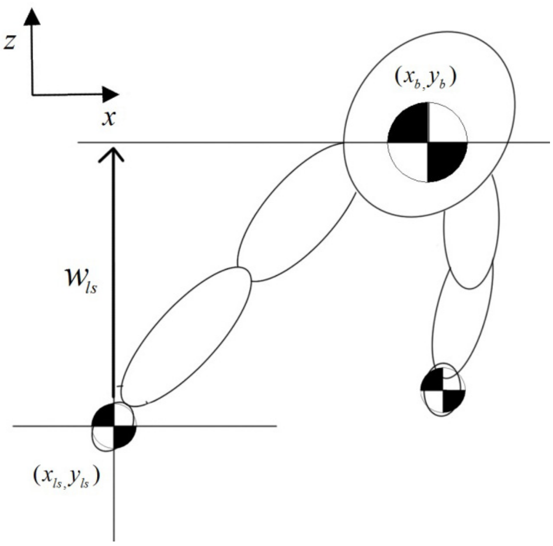

Figure 6 Rear view of the 3D skater model. Double stance phase is neglected, so there is only one active skate always on the ice.

2.3 Free body diagram

The free body diagram for the complete model is shown in Figure 7. In the vertical plane, it is assumed that only the gravitational forces act; the air friction on mass B in this direction is assumed to be insignificant. Figure 8 shows the free body diagram for both skates in the local coordinate system.

A)

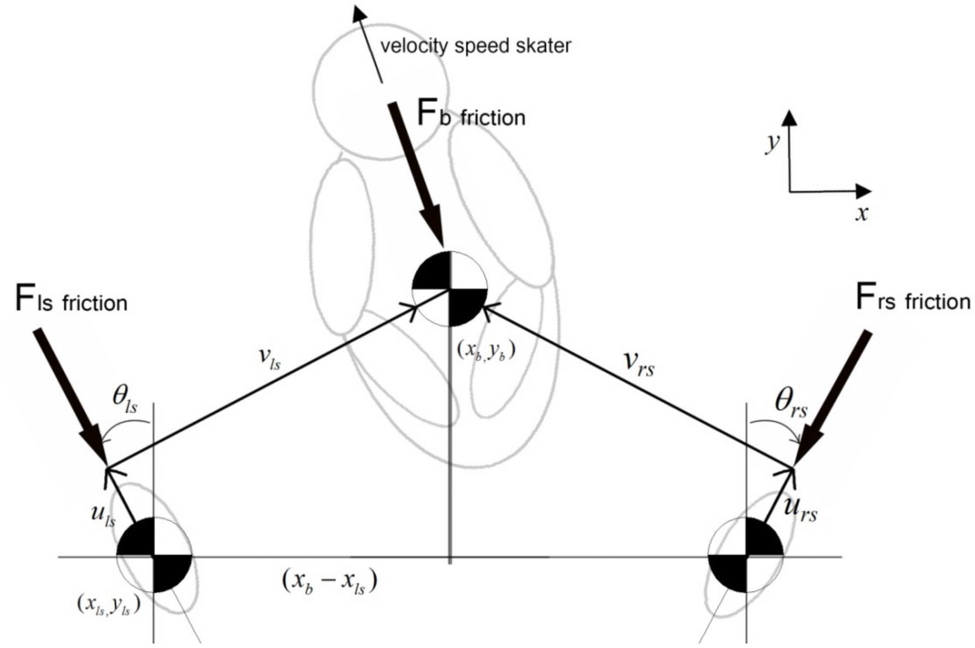

B)

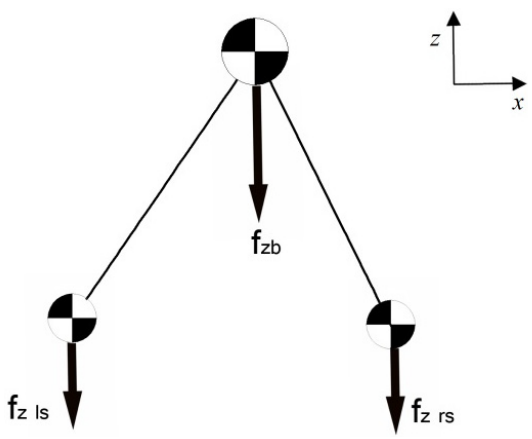

Figure 7 A) Top view of 2D Free body diagram of the skater. The skater consists of three masses, each withstand friction forces. The friction forces are due to air friction and ice friction. This will be further explained in section 2.6 B) Rear view of a skater and the vertical forces working on the bodies.

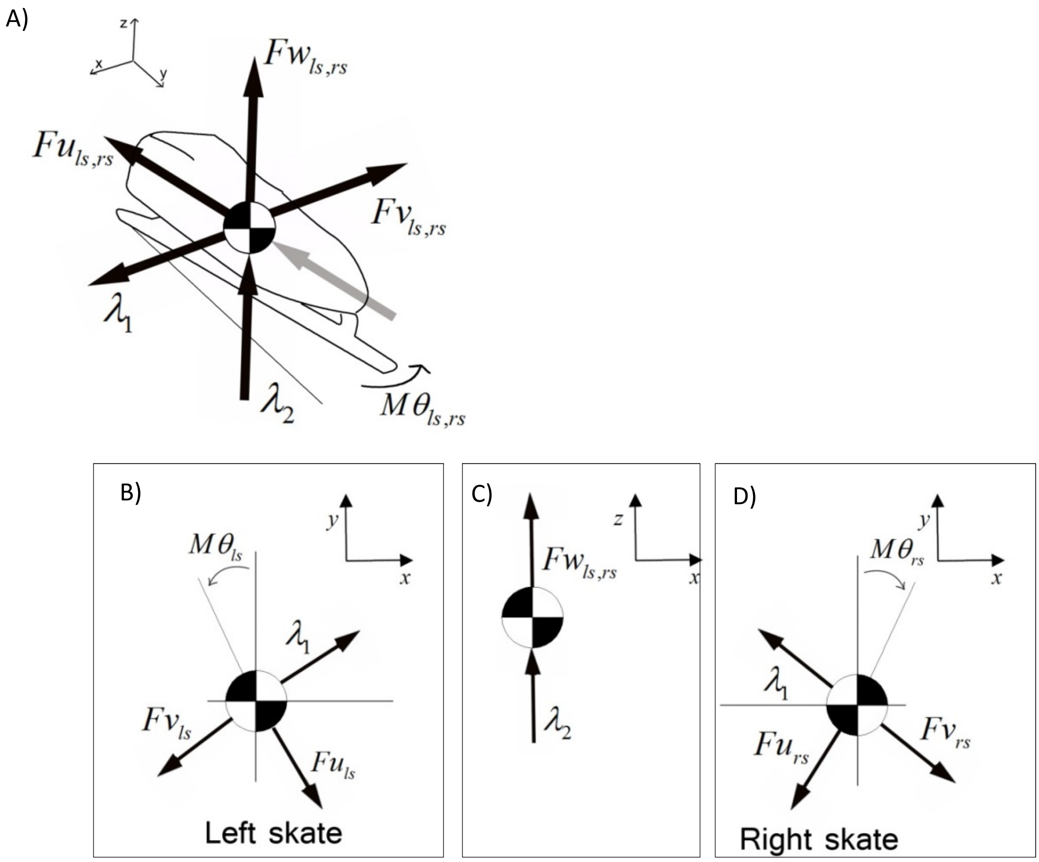

Figure 8 Free body diagram of the skates; A)three dimensional view of the FBD of the skate; B) Top view left skate; C) Rear view skate (RS and LS); D) Top view right skate; The constraint force λ_1 is due to the constraint of no lateral slip. The constraint force λ_2 is due to the constraint of the (active) skate being always on the ice. The constraints are explained in section 0.

2.4 Equations of Motion

Combining Newton's inertia law for all three bodies and leaving out all constraint forces results in:

(1.4.1) $$\sum f_i - M_{ij}\ddot{x}_j = 0$$

Where the mass matrix is given by (1.4.2).

(1.4.2) $$M_{ij} = diag\left(m_b,\; m_b,\; m_b,\; I_b,\; m_{ls},\; m_{ls},\; m_{ls},\; I_{ls},\; m_{rs},\; m_{rs},\; m_{rs},\; I_{rs}\right)$$

with the individual masses m_i and mass moments of inertia about the vertical axis I_i. Combined with the virtual velocities yields the virtual power equation

(1.4.3) $$\delta P = \delta\dot{x}_i\left\{\sum f_i - M_{ij}\ddot{x}_j\right\} = 0$$

Now we want to express all coordinates of the centre of mass of the bodies x_i in terms of generalized coordinates q_i (1.4.5).

(1.4.4) $$x_i = A_i(q_i)$$

$$\begin{bmatrix} x_b \\ y_b \\ z_b \\ \varphi_b \\ x_{ls} \\ y_{ls} \\ z_{ls} \\ \varphi_{ls} \\ x_{rs} \\ y_{rs} \\ z_{rs} \\ \varphi_{rs} \end{bmatrix} = \begin{bmatrix} u_b \\ v_b \\ w_b \\ \theta_b \\ u_b - v_{ls}\cos(\theta_{ls}) + u_{ls}\sin(\theta_{ls}) \\ v_b - v_{ls}\sin(\theta_{ls}) - u_{ls}\cos(\theta_{ls}) \\ w_b - w_{ls} \\ \theta_{ls} \\ u_b + v_{rs}\cos(\theta_{rs}) - u_{rs}\sin(\theta_{rs}) \\ v_b - v_{rs}\sin(\theta_{rs}) - u_{rs}\cos(\theta_{rs}) \\ w_b - w_{rs} \\ -\theta_{rs} \end{bmatrix} \tag{1.4.5}$$

The corresponding velocities are then

$$\dot{x}_i = \frac{\partial A_i}{\partial q_k} \cdot \dot{q}_k = A_{i,k} \cdot \dot{q}_k \tag{1.4.6}$$

$$T = jacobian(A(q_i), q_i) \tag{1.4.7}$$

And the virtual velocities are

$$\delta \dot{x}_i = T \cdot \partial \dot{q}_k \tag{1.4.8}$$

Substitution of these results in (1.4.3) yields

$$T \cdot \partial \dot{q}_k \left\{ \sum f_i - M_{ij} \ddot{x}_j \right\} = 0 \tag{1.4.9}$$

The virtual velocities of the generalized coordinates $\partial \dot{q}$, are independent, so every k equation must be zero as in

$$T \left\{ \sum f_i - M_{ij} \ddot{x}_j \right\} = 0 \tag{1.4.10}$$

The acceleration of the center of mass can be found by differentiating (1.4.6) twice, yielding

$$\ddot{x}_j = T \cdot \ddot{q}_l + T_{pq} \dot{q}_p \dot{q}_q \tag{1.4.11}$$

The second term will be addressed to as the convective acceleration term as in

$$g_j = T_{pq} \dot{q}_p \dot{q}_q \tag{1.4.12}$$

Substitution of (1.4.12) and (1.4.11) in (1.4.10) yields the equation of motion in terms of independent coordinates

$$T \left\{ \sum f_i - M_{ij} \left\{ T \cdot \ddot{q}_l + g_j \right\} \right\} + Q = 0 \tag{1.4.13}$$

$$\bar{M} \ddot{q} = \bar{F} \tag{1.4.14}$$

2.5 The constraints

We assume that the skate on the ice has no lateral slip. This slip will be modelled as a non-holonomic constraint, by constraining any lateral velocity. So In case of the left skate lateral slip is

(1.5.1) $$\mathrm{C}_{ls} = \sin(\theta_{ls}) \cdot \dot{y}_{ls} + \cos(\theta_{ls}) \cdot \dot{x}_{ls}$$

And the corresponding non-holonomic constraint is

(1.5.2) $$\mathrm{C}_{ls} = 0$$

In case of the right skate, the lateral slip and the corresponding non-holonomic constraint are

(1.5.3) $$C_{rs} = \sin(\theta_{rs}) \cdot \dot{y}_{rs} - \cos(\theta_{rs}) \cdot \dot{x}_{rs}$$

(1.5.4) $$C_{rs} = 0$$

Both these constraints can be expressed in generalized coordinates, using the equations of (1.5.5)

(1.5.5)
$$\begin{aligned}
\dot{x}_{ls} &= \dot{\mathrm{u}}_{\mathrm{b}} + \dot{\mathrm{u}}_{\mathrm{ls}} \cdot \sin(\theta_{\mathrm{ls}}) + \mathrm{u}_{\mathrm{ls}} \cdot \dot{\theta}_{\mathrm{ls}} \cdot \cos(\theta_{\mathrm{ls}}) - \dot{\mathrm{v}}_{\mathrm{ls}} \cdot \cos(\theta_{\mathrm{ls}}) + \dot{\theta}_{\mathrm{ls}} \cdot \mathrm{v}_{\mathrm{ls}} \cdot \sin(\theta_{\mathrm{ls}}) \\
\dot{y}_{ls} &= \dot{\mathrm{v}}_{\mathrm{b}} - \dot{\mathrm{u}}_{\mathrm{ls}} \cdot \cos(\theta_{\mathrm{ls}}) + \mathrm{u}_{\mathrm{ls}} \cdot \dot{\theta}_{\mathrm{ls}} \cdot \sin(\theta_{\mathrm{ls}}) - \dot{\mathrm{v}}_{\mathrm{ls}} \cdot \sin(\theta_{\mathrm{ls}}) - \dot{\theta}_{\mathrm{ls}} \cdot \mathrm{v}_{\mathrm{ls}} \cdot \cos(\theta_{\mathrm{ls}}) \\
\dot{x}_{rs} &= \dot{\mathrm{u}}_{\mathrm{b}} - \dot{\mathrm{u}}_{rs} \cdot \sin(\theta_{\mathrm{rs}}) - \mathrm{u}_{\mathrm{rs}} \cdot \dot{\theta}_{\mathrm{rs}} \cdot \cos(\theta_{\mathrm{rs}}) + \dot{\mathrm{v}}_{\mathrm{rs}} \cdot \cos(\theta_{\mathrm{rs}}) - \dot{\theta}_{\mathrm{rs}} \cdot \mathrm{v}_{\mathrm{rs}} \cdot \sin(\theta_{\mathrm{rs}}) \\
\dot{y}_{rs} &= \dot{\mathrm{v}}_{\mathrm{b}} - \dot{\mathrm{u}}_{rs} \cdot \cos(\theta_{\mathrm{rs}}) + \mathrm{u}_{\mathrm{rs}} \cdot \dot{\theta}_{\mathrm{rs}} \cdot \sin(\theta_{\mathrm{rs}}) - \dot{\mathrm{v}}_{\mathrm{rs}} \cdot \sin(\theta_{\mathrm{rs}}) - \dot{\theta}_{\mathrm{rs}} \cdot \mathrm{v}_{\mathrm{rs}} \cdot \cos(\theta_{\mathrm{rs}})
\end{aligned}$$

In order to use the constraints in our equations, the Jacobian of the constraints is used for the left side of the equation and the second derivative of the equations is used for the right side of the equation, see (1.5.6) and (1.5.7).

(1.5.6) $$C_k = jacobian(C, q_i)$$

(1.5.7) $$C_{k,lm} \dot{q}_l \dot{q}_m = jacobian(C_k \cdot \dot{q}_i, q_i) \cdot \dot{q}_i$$

Additionally the constraint of the skate being always on the ice is added, (1.5.8) and equation reference goes here(1.5.9).

(1.5.8) $$C_z = z_b - w_{ls}$$

(1.5.9) $$C_z = z_b - w_{rs}$$

Adding the constraints to the total equation(1.4.13), the total equation of motion is:

(1.5.10) $$\begin{bmatrix} \overline{M} & C_k{}^T \\ C_k & 0 \end{bmatrix} \begin{bmatrix} \ddot{q} \\ \lambda \end{bmatrix} = \begin{bmatrix} \overline{F} \\ -C_{k,lm} \dot{q}_l \dot{q}_m \end{bmatrix}$$

With the transformed mass matrix

(1.5.11) $$\overline{M} = T^T M_{ij} T$$

The forces working on the bodies are the forces acting on the global coordinates f_i, which are the friction forces and gravitational forces. The air friction working on the upper body in vertical direction is neglected, since this is assumed to be insignificant.

(1.5.12) $$f_i = \begin{bmatrix} f_{xb} & f_{yb} & f_{zb} & M_b & f_{xls} & f_{yls} & f_{zls} & M_{ls} & f_{xrs} & f_{yrs} & f_{zrs} & M_{rs} \end{bmatrix}$$

(1.5.13) $$f_i = \begin{bmatrix} \sin(\theta_b)\cdot F_{b-friction} \\ -\cos(\theta_b)\cdot F_{b-friction} \\ -m_b \cdot g \\ 0 \\ \sin(\theta_{ls})\cdot F_{ls-friction} \\ -\cos(\theta_{ls})\cdot F_{ls-friction} \\ -m_{ls} \cdot g \\ 0 \\ -\sin(\theta_{rs})\cdot F_{rs-friction} \\ -\cos(\theta_{rs})\cdot F_{rs-friction} \\ -m_{rs} \cdot g \\ 0 \end{bmatrix}$$

(1.5.14) $$gcon = jacobian(T\cdot\dot{q}_i, q_i)\cdot\dot{q}_i$$

The forces f_i have to be converted into the local coordinate system (generalized coordinates), using the transformation matrix T. Additionally the forces exerted in de local frame (forces exerted by the skater) are added Q.

(1.5.15) $$\overline{F} = T^T(f_i - M\cdot gcon) + Q$$

2.6 Friction forces

The friction forces can be divided into air friction and ice friction. The ice friction force however only works on the skates. The formula for the air friction found in (de Koning, de Groot et al. 1992) is:

(1.5.16) $$F_{air} = \frac{1}{2}\cdot A\cdot C_d\cdot\rho\cdot\left|v_{xyz}\right|^2 = k_1\cdot\left|v_{xyz}\right|^2$$

Where C_d represents the drag coefficient, A the frontal projected area of the skater, ρ the air density, $\left|v_{xyz}\right|$ the velocity of the air with respect to the skater and k_1 represents the total air friction coefficient (Ingen Schenau 1982) . Ice friction arises when the skates are in contact with the ice. Ice friction force can be found by Coulomb's law

(1.5.17) $$F_{ice} = \mu F_n = \mu mg$$

In which μ is the ice friction coefficient, m is the mass of the skater and g is the gravitational acceleration. This equation only holds if we assume that the normal force (λ_2)is equal to the mass times gravitational acceleration, which is not exactly the case in the three-dimensional skater model, however this assumption can be made, since the approach is close to correct and leaves us with a problem that can be solved.

The air friction is a function of the projected frontal area, and therefore indirectly a function of the mass. The friction forces can therefore be found by the formulas

(1.5.18) $$\begin{aligned} F_{b,friction} &= (1-\alpha)k_1(rvel_b)^2 \\ F_{ls,rs,friction} &= \left(\frac{\alpha}{2}\right)k_1(rvel_{ls,rs})^2 + \mu\cdot m\cdot g \end{aligned}$$

With α the mass distribution coefficient, $m = m_b + m_{ls} + m_{rs}$ and $rvel_i$ the relative velocities of the air with respect to the speed skater.

2.7 Finding the solution

The input for the skater model are the leg extensions. These leg extensions are the generalized, known, coordinates q^o. Furthermore we have the unknown coordinates, which are the generalized coordinates of the upper body mass B, q^d. Further elaboration on obtaining these data is given in section 5.2.

(1.6.1) $$q^d = \begin{bmatrix} x_b & y_b & z_b & \theta_b \end{bmatrix}$$

(1.6.2) $$q^o = \begin{bmatrix} u_{ls} & v_{ls} & w_{ls} & \theta_{ls} & u_{rs} & v_{rs} & w_{rs} & \theta_{rs} \end{bmatrix}$$

When we apply this division onto(1.5.10), we obtain the matrix

(1.6.3) $$\begin{bmatrix} M^{dd} & M^{do} & {C_k}^d \\ M^{od} & M^{oo} & {C_k}^o \\ {C_k}^d & {C_k}^o & 0 \end{bmatrix} \begin{bmatrix} \ddot{q}^d \\ \ddot{q}^o \\ \lambda \end{bmatrix} = \begin{bmatrix} \overline{F}^d \\ \overline{F}^o \\ -C_{k,lm}\dot{q}_l\dot{q}_m \end{bmatrix}$$

Furthermore we assume that either the left skate, or the right skate is on the ice and eliminate thereby the double stance phase. Therefore if the left skate is on the ice, only $q^o(1:4)$ is used in the equations of motion. When the right skate is on the ice, only $q^o(5:8)$ is applied in the equations of motion.

In addition to the unknown q^d , the vectors λ and $\overline{F}^o$ (the forces working on the mass at the skates) are also unknown variables. The equation first can be solved for $\ddot{q}^d$ and λ using (1.6.4). Secondly the system can be solved for $\overline{F}^o$ using (1.6.5).

(1.6.4) $$\begin{bmatrix} \ddot{q}^d \\ \lambda \end{bmatrix} = \begin{bmatrix} M^{dd} & {C_k}^d \\ {C_k}^d & 0 \end{bmatrix}^{-1} \cdot \begin{bmatrix} \overline{F}^d - M^{do} \cdot \ddot{q}^o \\ -C_{k,lm}\dot{q}_l\dot{q}_m - {C_k}^o \cdot \ddot{q}^o \end{bmatrix}$$

(1.6.5) $$\overline{F}^o = [M^{od} \quad M^{oo} \quad {C_k}^o] \cdot \begin{bmatrix} \ddot{q}^d \\ \ddot{q}^o \\ \lambda \end{bmatrix}$$

Summarizing we insert the known coordinates q^0, which we define as the leg extension, from this we obtain the unknown coordinates q^d which is the motion of the upper body; this motion strategy is then used to find the vector of forces applied.

2.8 ODE solver and Coordinate Projection method

In order to solve the equations of motion to obtain the 3D position of the upper body in relation to the leg extension, an ODE solver is applied for integration of the differential equations. An ODE solver can only handle differential equations of first order, therefore we need to rewrite the equations of motion as a first order differential equation, wherefore y will be introduced.

(1.7.1) $$y = \begin{bmatrix} q^d \\ \dot{q}^d \end{bmatrix},\ \dot{y} = \begin{bmatrix} \dot{q}^d \\ \ddot{q}^d \end{bmatrix}$$

Based on the report of (Fintelman 2011), the method of Runge Kutta was chosen as integration method (Press, Flannery et al. 1992). The stepsize h is held constant during simulation. The integration time t_n is chosen the sample time of the measurements ($T_s = 0.01$) and the step size is chosen to be one.

After numerical integration of the equations of motion for one time increment, the state variables in general do not fulfil the constraints. This is solved by applying a 'coordinate projection method'. This method pictures the constraints as a sort of surface in a higher dimensional space, where a state q is represented by points in that space. Using this surface we can formulate a minimization problem such that the distance from the predicted solution $\tilde{q}_{n+1}$ to the solution which is on the constraints surface is minimal:

(1.7.2) $$\left\| \tilde{q}_{n+1} - q_{n+1} \right\|$$

Where all q_{n+1} have to fulfil the constraints

(1.7.3) $$D(q_{n+1}) = 0$$

The non-linear constraints least-square problem can be solved using a Gauss-Newton Method. The explanation of this complete method can be found in (Field; 2005). The process of the ODE solver and the Coordinate Projection method is summarized in Appendix C.

2.9 Preliminary conclusion

2.9.1. Skater model

The skater is modelled as three point masses, each with three translations and one rotation, the heading, where we neglect all rolling and pitching motions of the rigid bodies. Movements of the mass B in both the horizontal plane and the vertical plane are considered. It is assumed that the active skate is always on the ice, there is no double stance phase. Air friction and ice friction are included in the model. The arm movements are neglected. The ideal contact of the skate on the ice is modelled by a holonomic constraint in the vertical direction and a non-holonomic constraint in the lateral direction. The model is driven by the changing distance between the mass B and the masses RS and LS (leg extension). The outcomes of interest of the model are the translations and heading of mass B (upper body) and the forces acting on mass RS and LS (skates) (Figure 9 and Appendix A).

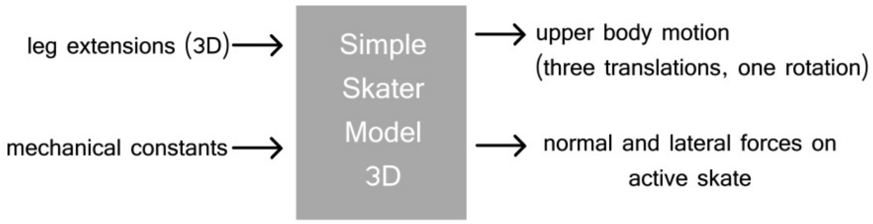

Figure 9 Input and output of interest of the skater model; Input is the leg extension (changing distance between the mass B and the masses RS and LS) and the mechanical constants (mass, mass distribution, air and ice friction coefficient); Output of interest are the upper body motion (x,y,z-direction and the steer angle) and the lateral and normal forces working on the 'active' skate (skate that is on the ice).

2.9.2. Verification of the skater model

In order to verify the model, we need to compare the model outcome with the true outcome. Therefore 3D measurements are necessary in order to obtain kinematic input and kinetic output. Additionally the lean angle of the skate is needed to convert the measured forces to the coordinate system of the model (Figure 10). The leg extension will be measured by the distance between a sensor at the upper body and a sensor at the skate. The measured variables needed in order to verify the model are given in Table 2. Further elaboration on these variables is given in section 3.2 and 5.5.

Table 2 Measured variables needed to verify the inverse dynamic skater model

Measured for input		Measured for output	
Changing distance between the 2D positions of a sensor at each skate (RS and LS) and the 3D positions of sensor at the upper body (B)	[m]	3D positions of sensor at the upper body (B)	[m]
		Normal and lateral forces acting on the skates	[N]
		Lean angle of both skates	[^{0}]

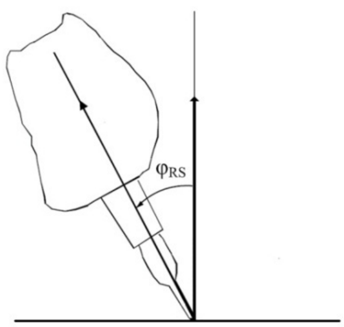

Figure 10 Lean angle of the skater.

“The outcome of the comparative study shows that the iGPS system is most accurate (6mm maximum absolute error) in dynamic position measurements. Attention has to be drawn to the necessary line of sight. Xsens proves to be accurate up to 5^0 (mean) error in the lean angle measurements for ice skating.”

3D Recording

3.1 Introduction

As mentioned in section 2.9.2, kinetic data is needed to verify the biomechanical model. The forces exerted by the skater are measured with an instrumented skate (Appendix B). This part of the report is therefore only concerned with finding the best measurement system for measuring kinematic data to verify the biomechanical model of a speed skater. First the requirements are given, followed by the outcome of the literature review. Next the position accuracy test is described, followed by the choice for a lean angle measurement system (Figure 11).

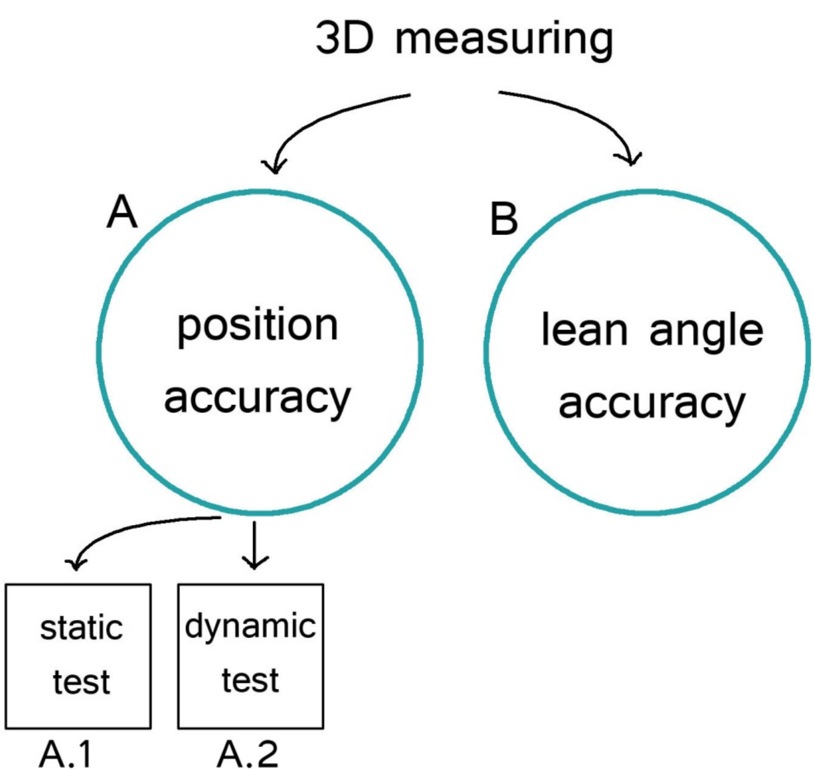

Figure 11 Overview of the research section.

3.2 Requirements

Preferably we would like to collect real-time accurate kinematic data of the positions of both skates, the lean angle of the skates and the three-dimensional position of the upper body, in order to gain insight in the performance of the speed skater. The required accuracy for position, based on a 5% error, is set to 50 mm in all three directions, whereas the required accuracy on the lean angle of the skate is assumed to be 2.5^0. The required temporal accuracy of the system is 0.05 seconds, for more details see (Kruk 2013). The skater model demands for separate ice-skating strokes as an input in order to eliminate the double stance phase. The difficulties of measuring on an ice rink, as mentioned in the introduction, have to do with the size of the rink (cover up to almost 12.000 m^2), the closed space of the stadium and the environmental conditions, including the high humidity, low temperature and high reflection of the ice.

3.3 Literature review

In a literature review four leading systems that might meet the requirements as stand-alone system or in combination were selected, based on their characteristics and results (Appendix D):

- the Fiducial based image processing tracking system (FBT)
- the electromagnetic based Local Position Measurement system (LPM, Inmotio),
- an inertial measurement unit (Xsens or combined in a MVN suit),
- an optoelectronic based indoor GPS system (iGPS, Nikon) (Appendix E).

The benefits and drawbacks of these systems are given in Table 3. For further details on the specifications and application the author refers to (Kruk 2013).

Table 3 Drawbacks and benefits of the measurement systems. For further details about the accuracy and the application see (Kruk 2013).

	Metric	Benefit	Drawback
FBT	3D	Non-invasive	New application
LPM	2D	Already applied in ice skating	Low found accuracies in prior tests (>130mm error) (Fintelman 2011)
Xsens	3D	Already applied in sports	Drift
iGPS	3D	Very accurate (<0.2mm) (Nikon 2013)	Unknown with dynamic applications
MVN suit	3D	Already applied in ice skating	Not available for this research + unknown accuracy

The accuracy of a system is highly dependent on the measurement volume; in general an increasing volume decreases the accuracy. The exact correlation of this relation is however unknown, therefore an independent test with all systems in the same situation and environment is needed in order to establish the true position accuracy of a system.

3.4 Research

The research part on 3D recording on an ice rink is separated into two parts; first the position measurement system will be established; the research performed to determine the accuracy of the position measurement system is described in that part. Second the selection of the right lean angle measurement system is described.

A. Position accuracy research

The kinematic position measurement systems are appointed an expected accuracy based on the literature found (Table 4).

The position accuracy measurements are divided into static measurements and dynamic measurements. All measurements were performed in the ice rink stadium of Thialf without ice on the rink. This thesis describes the results for the iGPS, LPM and Xsens measurements on the straight part of the rink (measurement data of the curve are available in the digital appendix for future use). The FBT measurement system was incorporated into this research, however it did not show results as expected; more on the FBT system can be found in Appendix G.

Table 4 Accuracy of the measurement systems found in literature

Measurement System	Accuracy position [mm]	Coverage
Indoor GPS (Nikon 2013)	0.2	$100m^2$ to $1600\ m^2$
LPM (Inmotio)	50	$5000\ m^2$
Fiducial based tracking (FBT) (Klous, Muller et al. 2010)	9-13	$525\ m^2$
Xsens (Xsens 2013)	2 [^{0}]	-

A.1 Static measurements

A.1.1 Method

In the static test the sensors of the measurement systems (two Nikon iGPS single detectors (30Hz), two LPM transponders (100 Hz)), were positioned on a frame (measurement cube, 320x320x320mm), thereby maintaining a constant relative position. The global position of the cube was changed, into nine different positions in the xy-plane at two different height positions (A=0.5m and B=0.9m) (Figure 12, Appendix H). This test was repeated twice.

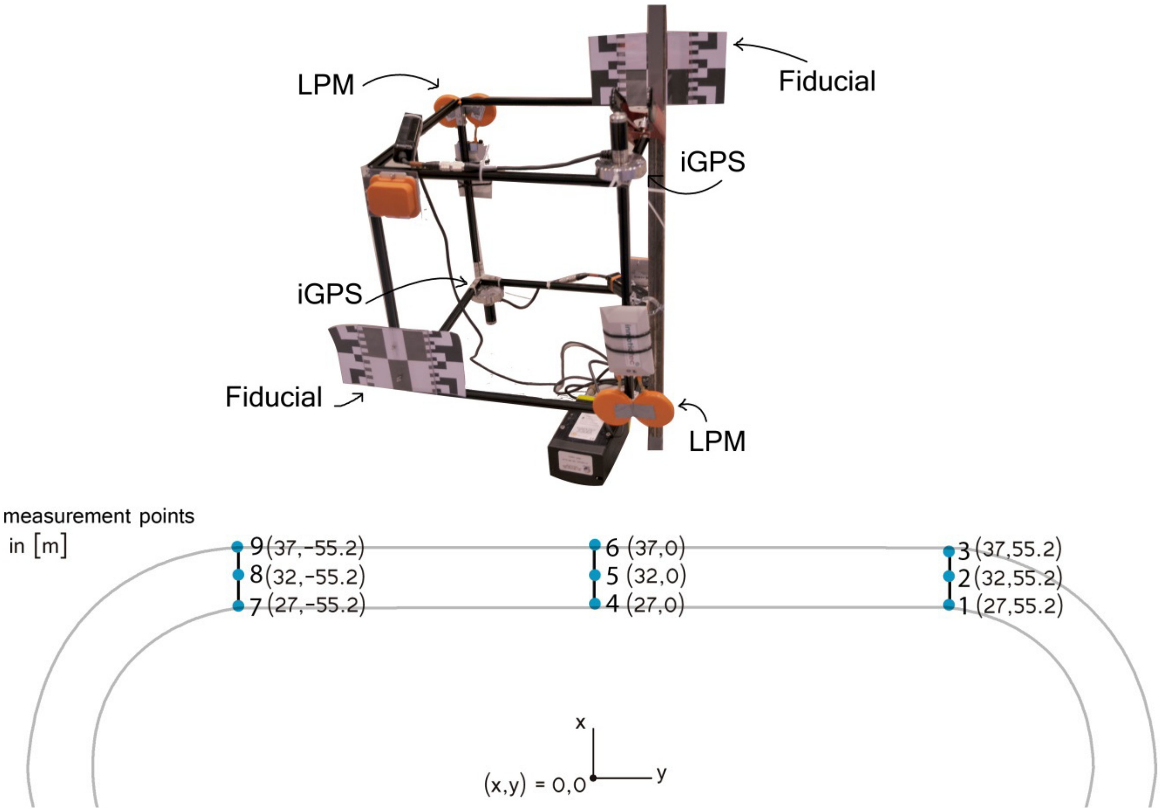

Figure 12 Measurement Cube (320mmx320mmx320mm) and the measurement positions.

The output variables of this test are the relative position error and the correlation between the relative error and the global position. The LPM data were filtered using a Kalman filter which is integrated in the LPM hardware and by using a linear filter of the LPM Software. The iGPS data were unfiltered. The set value of the relative positions of the sensors is given in Table 5.
The accuracy of a system is low when the results show a large variation in distance between the two sensors or a large deviation compared to the set value.

Table 5 Set value of the relative positions of the sensor. Accuracy is within ±10 mm.

Set value	LPM [mm]	iGPS [mm]
X	320	260
Y	300	300
Z	-	400

A.1.2 Results

A.1.2.1 LPM

Relative position error

The results show a very large deviation, ranging up to almost 790 mm difference in Δx-position (Table 6). The maximum error and standard deviation indicate that the variation in longitudinal direction (in line with the straight) (y) is lower than the perpendicular measurements (x). The measurements in x direction have however a smaller deviation from the set value.

Global versus relative position error

In Figure 13 the relative position error versus the global position on the ice rink is given. One outlier was removed (position 4A). Overall the lower position (A) performs worse than the upper height position (B).

Table 6 Results from the static measurements performed with a LPM system. The numbers indicate the distance difference between two sensors in either x or y direction. Mean is the average value of the distances found; STD is the standard deviation of the distances found; Min is the minimum distance found; Max is the maximum distance found Max error is the maximum difference between the mean and the extremes;

	Set-value	Mean [mm]	STD [mm]	Min [mm]	Max [mm]	Max error [mm]
Test 1						
Δx-position	320 mm	505	228	48.9	1052	547
Δy-position	300 mm	73	90	-205	165	278
Test 2						
Δx-position	320 mm	494	348	-0.64	1284	790
Δy-position	300 mm	56.5	299	-704	533	761

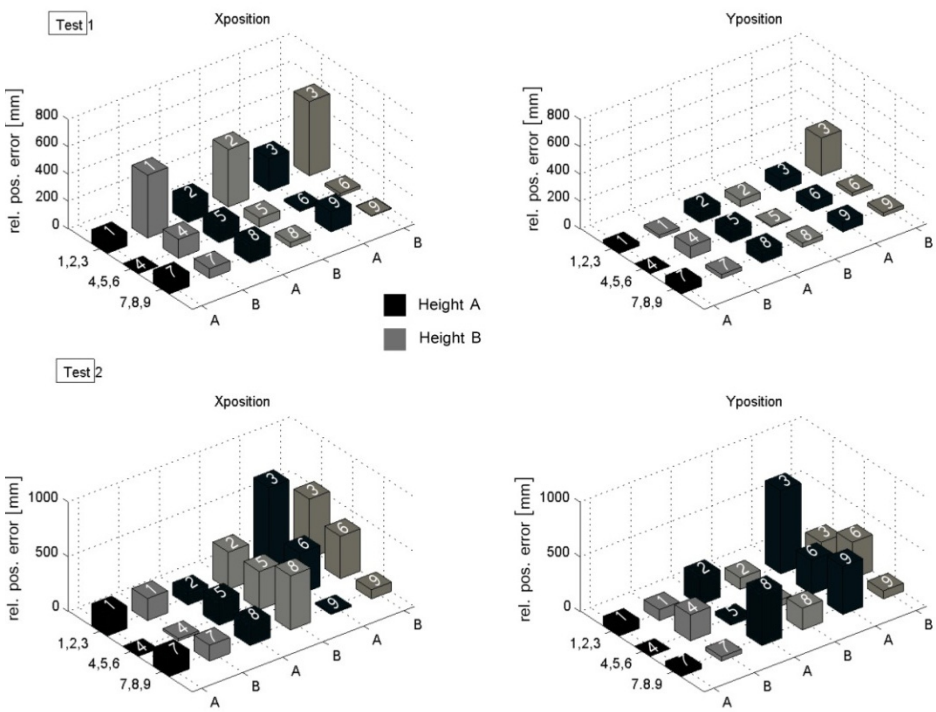

Figure 13 Relative position error versus the global position of the sensors. A and B indicate the different height positions.

A.1.2.2 iGPS

Relative position error

The variation in iGPS is much smaller compared to LPM (Table 7). The maximum deviation for the iGPS system is about 20 mm (in y direction). There is no significant difference in performance for the three separate directions.

Relative versus global position error

The data of the iGPS relative position is shown for each global position in Figure 14. There was a structural problem at the positions 3A and 3B, probably due to a bad line of sight. These points are considered outliers and were removed from the data.

Table 7 Results from the static measurements performed with an iGPS system. The numbers indicate the distance difference between two sensors in either x, y or z direction. One outlier was removed; Mean is the average value of the distances found; STD is the standard deviation of the distances found; Min is the minimum distance found; Max is the maximum distance found; Max error is the maximum difference between the mean and the extremes;

	Set value [mm]	Mean [mm]	STD [mm]	Min [mm]	Max [mm]	Max Error [mm]
Test 1						
Δx-position	260	249	7.4	245	274	18.4
Δy-position	300	308	9.2	294	326	19.6
Δz-position	400	400	4.0	390	405	10.9
Test 2						
Δx-position	260	265.6	7.7	247	276	18.7
Δy-position	300	305.6	7.5	293	319	12.9
Δz-position	400	401.3	3.9	394	409	7.9

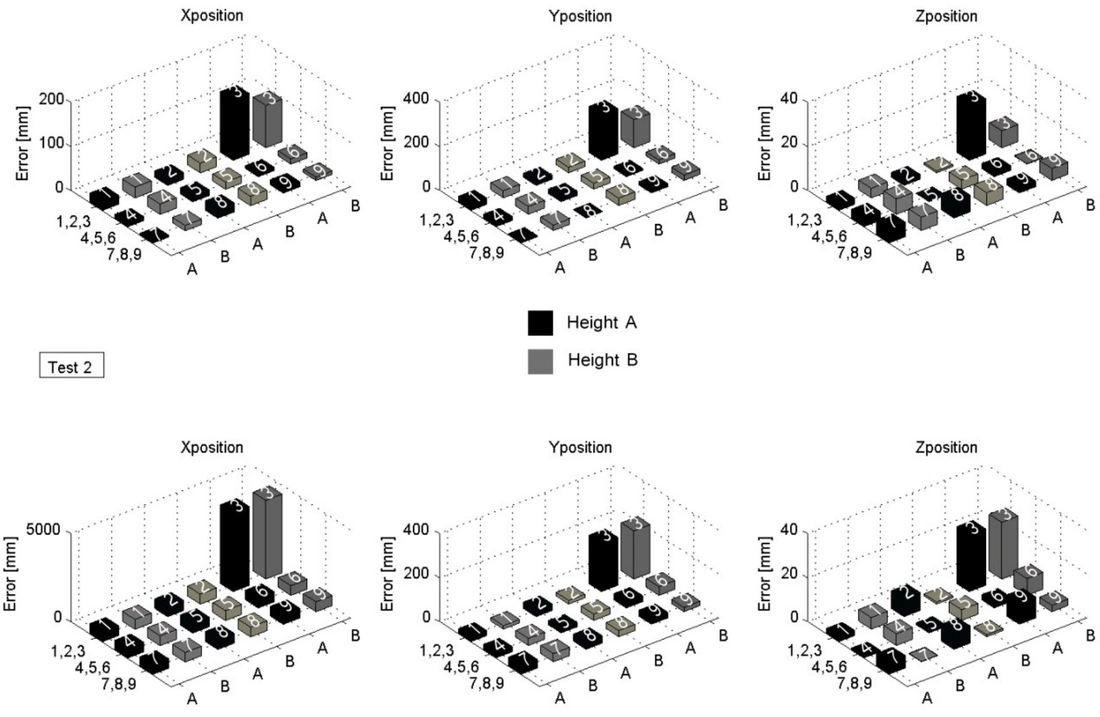

Figure 14 Relative error versus the global positioning of the iGPS data

A.1.3 Discussion on static measurements

The static LPM results are in line with the results found in (Fintelman 2011), where the static error ranged up to 730mm with an average standard deviation of 240mm; the current research shows a range up to 790 mm with an average standard deviation of 241 mm. The sensors perform better at a height 0.9m compared to 0.5m, which is in line with the fact that manufacturer (Inmotio 2013) recommends to wear the sensors at the shoulders (shoulder height is around 1000mm for ice skating).

The LPM system in principle was not designed to perform static measurements, this has contributed to the poor performance of the LPM system in this static test. The internal (dynamic) Kalman filter was probably the major cause. The company Inmotio accounted an additional reason for the deviations due to the use of steel in the frame of the measurement cube. To the best knowledge of the author however, steel has two possible consequences on electromagnetic waves (the working principle of LPM), namely an increasing amplitude and reflection. This first consequence will not affect the working principle of the LPM system, since it is based on Time of Flight (ToF). Reflection could influence the ToF of the system and is therefore an important fact. However in order to interfere with the system, there need to be large reflections (caused by for instance reinforced concrete) and the author doubts if the 10mm ribs of the steel frame can have such an interference.

The iGPS system performed worse than expected. The system was expected an accuracy of 0.2 mm, while the outcome of the research showed an outcome of almost 20 mm error. This however still is in the accuracy range needed to perform the kinematic measurements. The use of old sensors (Appendix E) and the large measurement volume probably caused this decrease in accuracy.

A.2 Dynamic measurements

A.2.1Method

The purpose of the dynamic measurement is to find the accuracy of the systems with regard to position and velocity in a dynamic situation. A measurement cube (320x320x320mm) with the sensors attached to it (two Nikon iGPS single detectors (30 Hz), two LPM transponders (Inmotio) (100 Hz), Xsens MTx (100 Hz), Xsens MTi-G (100 Hz)) was placed on the rear of a bike (Figure 12, Figure 15), thereby changing the global position dynamically while maintaining the relative positions of the sensors. The Xsens sensors were attached to a mini laptop, which was also placed on the back of the bike (Appendix I).

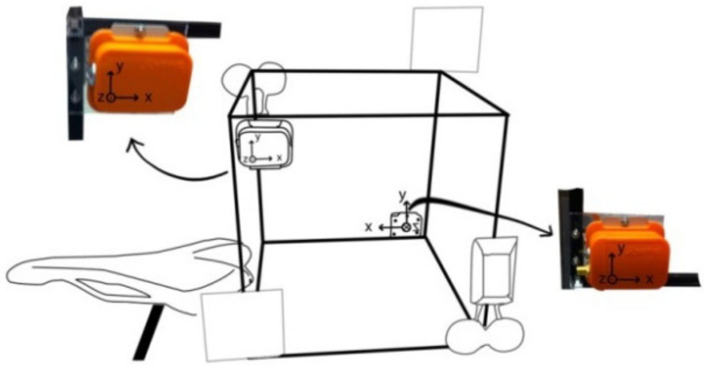

Figure 15 measurement set-up

The bike with cube was cycled along the rink at three different speeds (15 km/h, 20km/h and 25km/h), each test was performed three times, each ending with a coasting exercise (the cyclist stops pedalling). The velocity of the bicycle was kept constant by the cyclist with the aid of a laser trainer and the indication of the cycling computer. Additionally a data logger was used (Arduino) to examine afterwards if the average velocity was as intended. Only the straight parts were measured.

The relative position accuracy was established by the sensor positions on the measurement cube. Since the measurement cube was not always aligned with the rink, the diagonal was used (2D for LPM and 3D for iGPS) for the relative position measurement (Figure 16). The actual distance of this 2D diagonal is 439(±17) mm. The distance of the 3D diagonal is 564(±17) mm. In case of the Xsens the relative acceleration error was used in longitudinal direction; this relative acceleration should be zero.

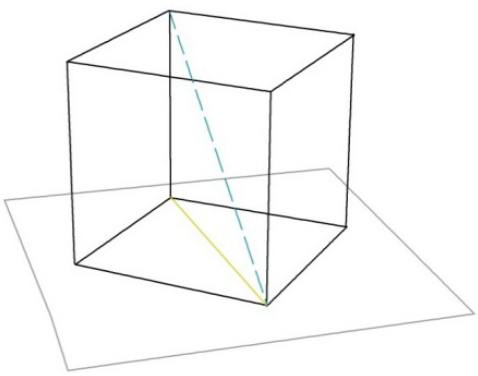

Figure 16 Figure indicating the 2D diagonal (yellow line, 453 mm) and the 3D diagonal (blue dotted line 564 mm)

The LPM data was filtered with a Kalman filter in the hardware. In the software the outliers were removed and the data is filtered with a linear or a Gaussian filter. The analysis of the iGPS data was done using the raw data. The raw data showed outliers which were removed (Appendix J). In the Xsens data the outliers were removed and the data were filtered using a low-pass Butterworth filter, with a normalized cut-off frequency of 0.8/100 Hz.

A.2.2 Results

A.2.2.1 LPM

Relative position accuracy

In Figure 17 the results are shown for the first test performed by LPM at a speed of 15 km/h. More results can be found in Appendix J. The mean, standard deviation and maximum absolute error of the tests at 15 km/h averaged over nine straight parts are given in Table 8. The results show that the standard deviation of the error is around 130 mm for all measured speeds. The results also indicate a large deviation from the set value (>180mm).

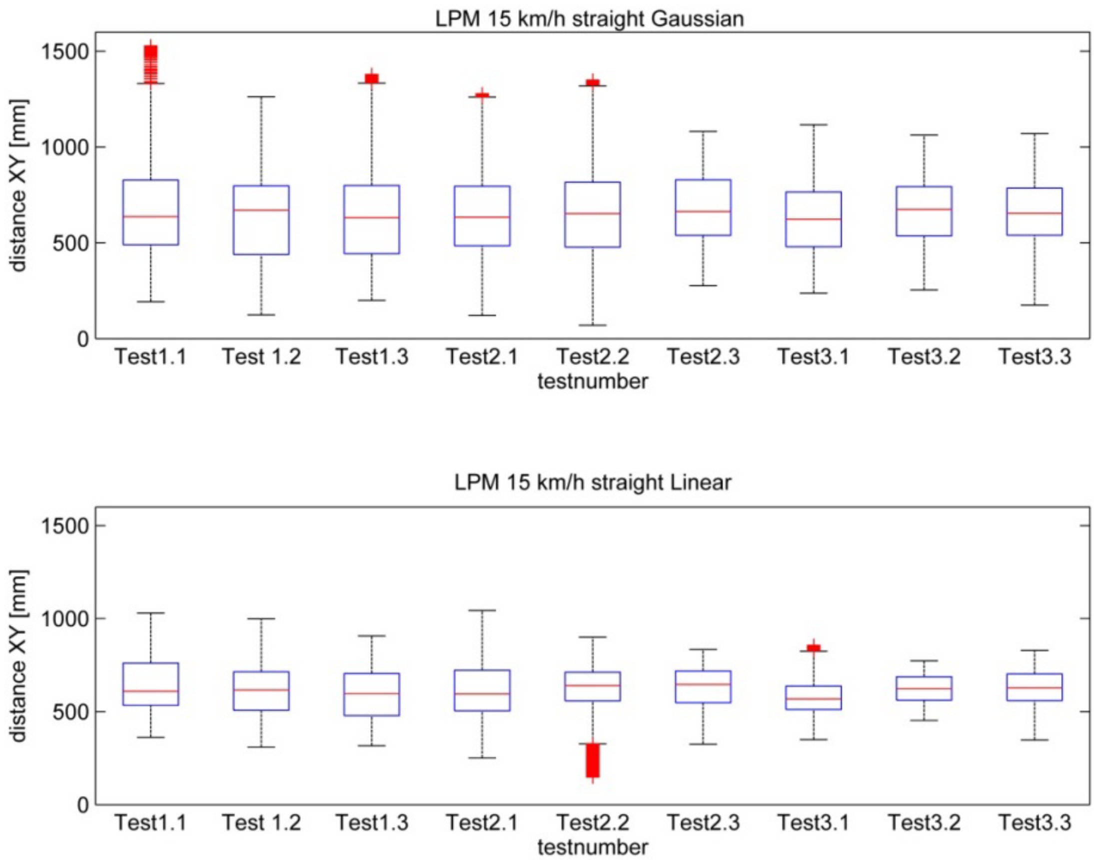

Figure 17 Boxplot indicating the relative distance between sensor 1 and sensor 2 (2D diagonal). This test was performed at the straight part of the rink with a speed of 15 km/h. The upper graph shows the data that is filtered with a Gaussian filter, the lower graph shows the results of the data filtered with a Linear filter.

Table 8 The mean STD and maximum absolute error of the dynamic LPM tests. The numbers are averaged over nine straight parts.

Relative position	Set value [mm]	Mean [mm]	STD [mm]	Max abs error [mm]
15km/h linear	439(±17)	616.7	128.7	329.7
25 km/h linear	439(±17)	614.6	131.9	312.1

A.2.2.2 iGPS

Relative Position Accuracy

The results show that the iGPS data were very accurate and had almost no variation in the data (Figure 18). The standard deviation of the error ranges between 1.2 mm and 1.7 mm for the increasing speeds (Table 9.). The largest deviation from the set value found was at 20 km/h with a difference of about 40 mm from the found mean value. (test 2, Appendix J).

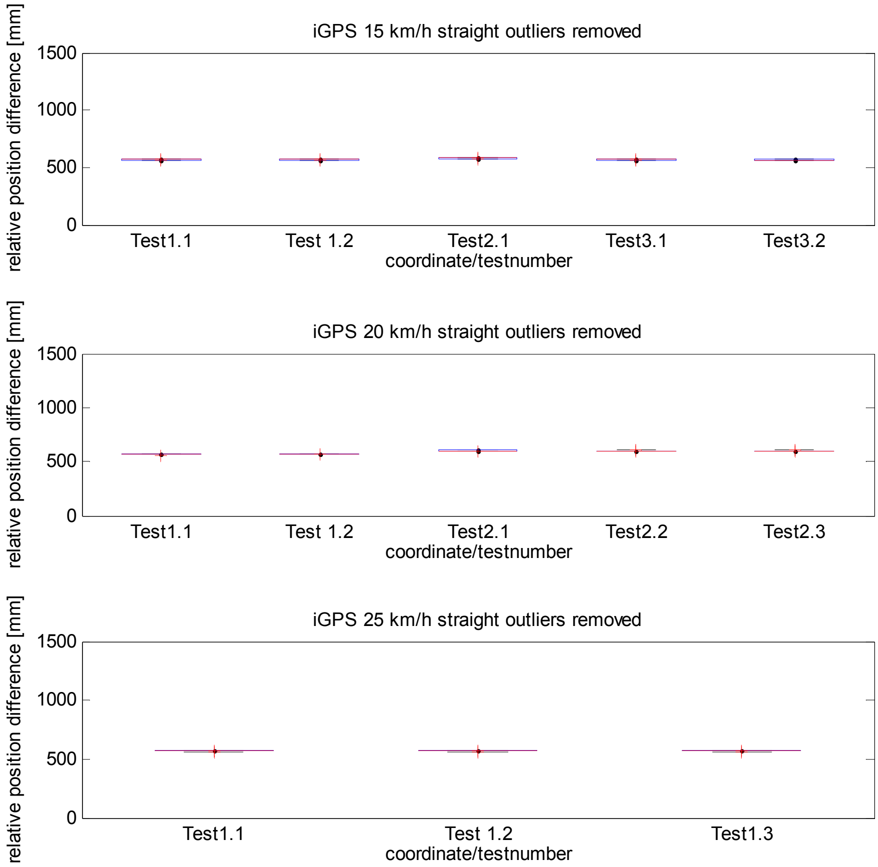

Figure 18 Boxplot indicating the relative position between sensor 1 and sensor 2. This test was performed at the straight part of the rink with a speed of 15 km/h, 20 km/h and 25 km/h. The outliers are removed from this data.

Table 9 mean, standard deviation and maximum error for the iGPS position measurements, averaged over 5 trials for the velocities of 15km//h and 20km/h and averaged over 3 trials for the velocity of 25 km/h

Relative Position	Set value [mm]	Mean	STD	Max error (abs)
15 km/h	564(±17)	569.8	1.2	4.3
20 km/h	564(±17)	587.8	1.5	4.7
25 km/h	564(±17)	567.0	1.7	5.9

Number of samples

The number of samples in time of the iGPS system fluctuates due to the loss of signal during the measurements. Table 10 shows the average number of samples found on each straight and the duration of this measurement (Appendix J). The number of samples per time is negatively related to the velocity.

Table 10 N = number of samples (outliers removed), OR = number of outliers that are removed, Time, Distance measured and the Time divided by the number of samples averaged over the trials Appendix J.

iGPS	N	OR	Time [s]	Distance	Time/N
15 km/h	511.8	21	17.99	75.56	28.16
20 km/h	425.8	14.2	14.72	79.52	28.82
25 km/h	287.4	11.7	11.4	71.2	24.4

A.2.2.3 Xsens

The results for the relative acceleration in direction of the cycling movement are given in Table 11. The data show more variations and errors when the speed is increased.

Table 11 Relative acceleration averaged over 3 trials for the velocities of 15km/h, 20km/h and 25 km/h.

Relative Acceleration	Set value	Mean [m/s^2]	STD [m/s^2]	Max error [m/s^2]
15 km/h	0 m/s^2	0.03	0.05	0.16
20 km/h	0 m/s^2	0.05	0.07	0.22
25 km/h	0 m/s^2	0.10	0.17	0.44

A.2.2.4 Global velocity error

The performance of the systems in terms of velocity can be easily scrutinized with the analysis of the coasting exercise (Figure 19). The speed can only decrease since the cyclist stops cycling. The LPM results show accelerations in the data; iGPS only shows decelerations. The data obtained at the straight part with a constant velocity show a correct global average velocity (4.2 m/s), however the LPM system shows far more fluctuations than the iGPS system.

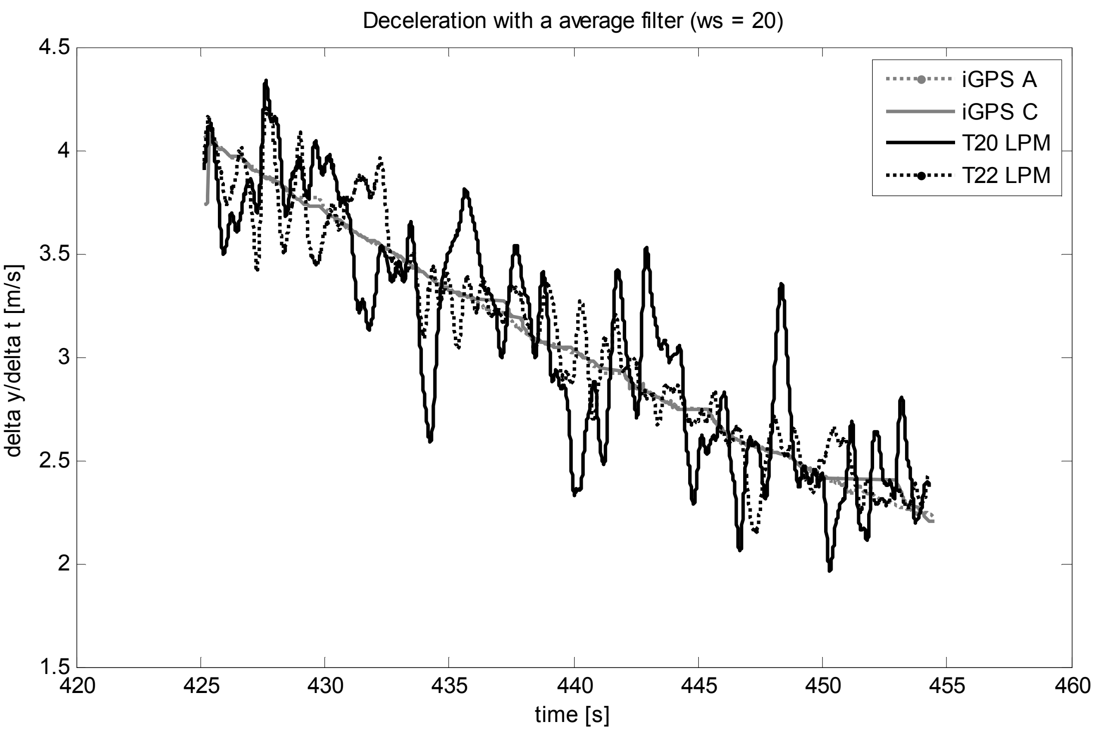

Figure 19 Figure indicates the difference in y position over time. The figure should give a smooth deceleration. The LPM data is filtered with a linear filter and sampled at 100 Hz. The data from the iGPS system was sampled at 30 Hz and filtered using an averaging filter with a windowsize of 20.

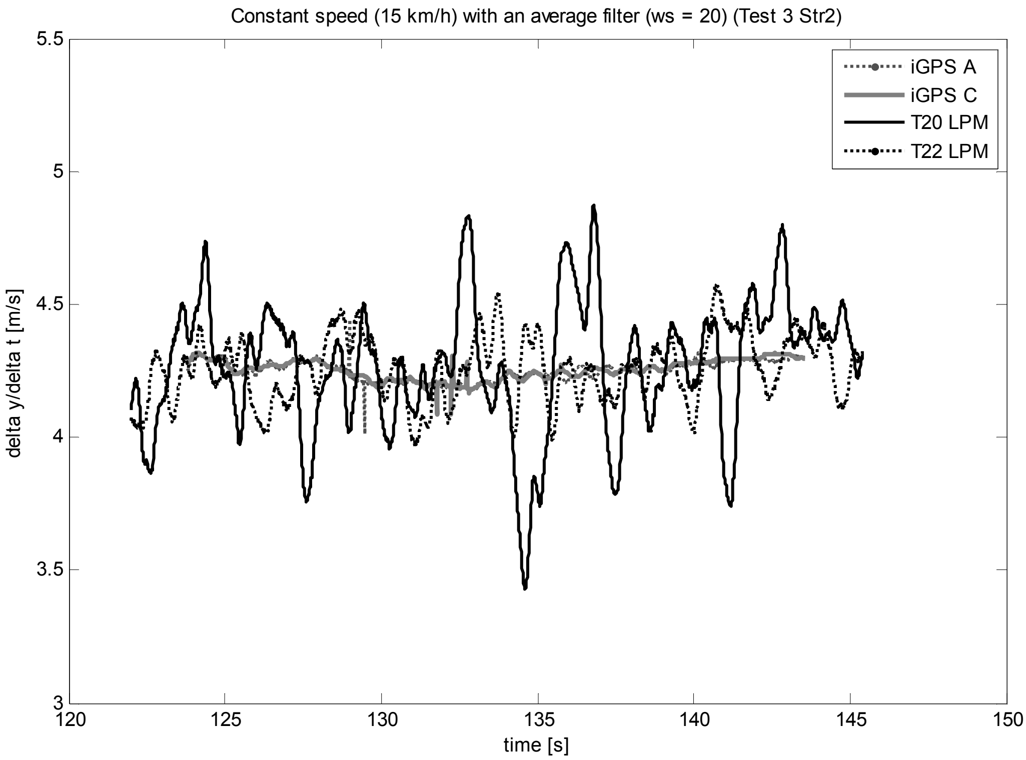

Figure 20 This plot indicates the difference in y position over time. The data should show an average speed of 15 km/h. The LPM data is filtered with a linear filter and sampled at 100 Hz. The data from the iGPS system was sampled at 30 Hz and filtered using a averaging filter with a windowsize of 20.

A.2.3 Discussion on the dynamic measurements

The results for the LPM system show a maximum error comparable to the maximum error found in the static measurements. The found constant error of the LPM system (180 mm) and the standard deviation of the error (130 mm) are in line with the values found in prior research, where an constant error of 160 mm and standard deviation of 130mm were established (Fintelman 2011). The LPM results do not indicate a dependency on velocity.

The iGPS system has maximum errors of 6 mm which are lower than the errors found in the static test (20 mm), possible cause was the different transmitter placement. Increased speed leads to lower position accuracy and a decreased number of samples. The average number of samples at 25 km/h (24.4 samples per second), lead to a time accuracy of 0.04 s, which is within the requirement for the model verification (0.05s). Care has to be taken, since the gaps are clustered and therefore at some points in time the data have larger time gaps. Solution would be interpolation of the data or selection of data parts.

The velocity measurement of both LPM and iGPS on average indicate a right estimation; the velocity over time in the LPM data however suffers from incorrect fluctuations. Again the Kalman filter might have been an influencing factor in these fluctuations.

The variance of the Xsens relative acceleration data goes from 0.03 m/s^2 for the trials at 15 km/h up to 0.1 m/s^2 for 25 km/h. The results show that there is a positive relation between the velocity and variance. This variance restricts integration to obtain position data, due to the time iterative related error. The findings suggest that the Xsens is no option for stand-alone position measurements. Combined, in sensor fusion, the acceleration data could be functional for very short periods of time. Sensor fusion between Xsens and iGPS can combine the sampling rate of the Xsens system with the accuracy of the iGPS system.

A.3 Preliminary conclusion

A.3.1 Position accuracy research outcome

The position accuracy of four measurement systems was tested in this research. The FBT system unfortunately showed to be too undeveloped to use the data in the comparison. The results show that the iGPS system has the best static accuracy (with a maximum error of 19.6 mm to the maximum error of LPM of 447.9 mm) and the best dynamic position accuracy (with a mean maximum error of 5.9 mm at 25 km/h to a mean maximum error of 312.1 mm of LPM at the same speed). The iGPS system reaches the required position accuracy of 50 mm for the ice skating data collection. The time accuracy of 0.05s can be reached with the iGPS system, however the data contain large time gaps.

A.3.2 iGPS optimizations

The iGPS system shows to be very dependent on the line of sight and on the transmitter placement. Both influence the number of sampled data points (and therefore the time accuracy). Two additional tests were performed in order to establish the optimization points of the iGPS system. These measurements are described in Appendix K and Appendix M. In order to improve the iGPS system for use in the ice skating data collection, based on the tests the following optimizations were taken into account:

1. Positioning and fixation of the sensors;
   In order to have a clear line of sight, the sensors at the skate are best placed at the tip of the blade (Figure 21). In order to have a clear line of sight of the sensor at the upper body, the battery is best placed at the bottom of the back, so the battery is never in line of sight of the sensor.

2. Positioning of the transmitters
   The data of a speed skater is only collected at the necessary part of the ice rink, the straight, due to a limited number of transmitters available. The iGPS system has trouble resuming the measurement when the sensor has been out of the measurement area for a while. It is therefore beneficial to place transmitters in front of the necessary measurement area (the area of interest), that can localize the sensor before it enters the straight part.
   Concerning the height of the transmitters, it proves to be most beneficial to use an alternating height positioning: some transmitters directly on the ice and some at tripods (±1.2 m)(Figure 21).

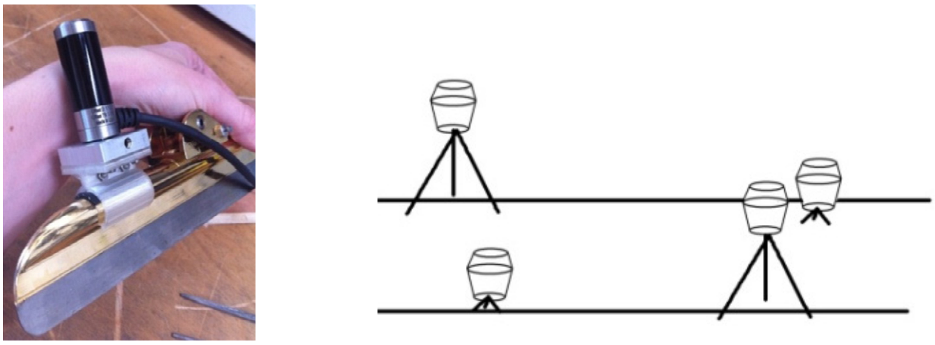

Figure 21 Left: sensor placement at the tip of the blade of the skate; Right: transmitter placement.

A.3.3 Further recommendations for the data collection.

Main issues with the iGPS measurement system are the data gaps and the (therefore) low time accuracy. The iGPS system can be improved by combining the measurements from the iGPS system with data obtained from accelerometers at the skates. Sensor fusion can combine the accurate position data from the iGPS system with the high sampling rate from an accelerometer. The accelerometer used in the data collection (section 4.2) is the one of Xsens.

Although it was established that the LPM system is not accurate enough to measure the skate movements, it is still interesting to measure the position of the upper body and the skates with both LPM and iGPS. This could establish if the shape of the curves shown by LPM is realistic and gives opportunity to link the new insights to prior research.

B. Lean Angle research

The lean angle measurement system used to verify the three-dimensional skater model requires an accuracy of 2.5^0. Two measurement systems, a wired Xsens sensor and a wireless ProMove sensor, were tested on their accuracy using a video analysis tool to quantify the lean angle. The tests are described in Appendix N, this section holds the results.

B.1 Results

The results show that the Xsens measurement system has a higher accuracy compared to the ProMove measurement system (Table 12). The Xsens measurements are closest to the angles found by the video analysis with a mean difference of 4.9^0. These data are based on few selected points in time in both trials, but the result is in accordance to (Fintelman 2011).

Table 12 Differences between the lean angle measured by the MEMS systems and the video analysis GIMP tool

	Trial	ProMove [^{0}]	Xsens [^{0}]
Average difference	**1**	**12.7**	**4.9**
Maximal difference	1	17.9	5.1
Minimal difference	1	-6.7	-4.6
Average difference	**4**	**9.7**	**4.4**
Maximal difference	4	15.3	7.5
Minimal difference	4	-14	-12.4

B.2 Discussion

The lean angle is used in the verification of the skater model to convert the forces measured by the measurement skate into a global coordinate system, determined by the model. An inaccurate lean angle measurement introduces errors in these converted forces. Notwithstanding its limitations, the lean angle measurement study suggests that the required accuracy of 2.5^0 (3.2) will not be reached with the wired Xsens system used. This implies an error in the converted forces of 9% for an angle inaccuracy of 5^0 and 23% for the maximum angle inaccuracy found of 12.4^0 (Table 13).

Table 13 Influence of the inaccuracy of the lean angle measurements on the converted forces.

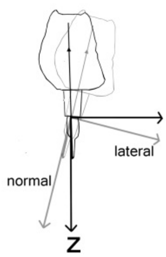

Angle inaccuracy [^{0}]	Fx error [%]	Fz error [%]
2.5	4	4
5	9	8
12.4	24	20

Recalibration moments at motionless (in terms of lean angle) periods, could improve the measurement performance. This method is often applied in walking or running. Due to developing time, this is left for future purposes.

Data collection of the model verification was performed using the Xsens sensors, due to available means; in attempt to improve the lean angle accuracy, the measurements were monitored with the use of a camera. Additionally, the inaccuracy of the Xsens system is taken into account in the analysis.

“No complete dataset was obtained for the verification of the three-dimensional skater model. The three-dimensional position data do however show an upper body movement with an amplitude of 7% of the average upper body position (1.1m). Additionally new insight was gained concerning the data of prior research and based on the experience of the current study, a synchronisation or distortion problem in Fintelman’s data cannot be ruled out.”

Data Collection

4.1. Introduction

The input for the skater model is the leg extension (position change of the modelled masses at the skates relative to the modelled mass at the upper body) and the mechanical constants; the outputs of interest of the skater model are the position of the modelled mass at the upper body (B) and the forces acting on the modelled masses at the skates (RS,LS). The variables that need to be measured to obtain this input and output data are given in Table 14. The necessary accuracy is given in Table 15. Section 3 established that the iGPS measurement system was best used for the dynamic position measurements (6mm maximum error) and the Xsens sensors for the lean angle measurements (accuracy of 5^0 (mean error)).

Due to problems with the measurement equipment, no complete data set was obtained in this data collection. The data described in this section were therefore eventually not used for the verification of the model. This section does hold the results for the 3D position measurements performed with the iGPS system.

Table 14 Variables needed to verify the inverse dynamic skater model

Measured for input		Measured for output	
Changing distance between the 2D positions of a sensor at each skate (RS and LS) and the 3D positions of	[m]	3D positions of sensor at the upper body (B)	[m]
		Normal and lateral forces acting on the skates	[N]
		Lean angle of both skates	[^{0}]

Table 15 Necessary accuracy for the verification of the skater model

Measurement systems	accuracy	unit	System
2D positions of both skates	50	[mm]	Indoor GPS (Nikon)
3D positions of CoM	50	[mm]	Indoor GPS (Nikon)
Forces exerted on the skate	60	[N]	Instrumented skate
Lean angle of both skates	2.5	[^{0}]	Xsens sensor

4.2. Method and set-up

Each participant (skater) was equipped with two iGPS single detectors (I4is) at the skates (30 Hz) (Figure 22). At the upper body the skater is equipped with an iGPS double detector (I4is) (30 Hz). The benefit of the double detector is an increased accuracy and robustness. All iGPS sensors were connected to an amplifier and to the battery on the back of the skater. The iGPS sensors measured the position coordinates of the skates and the upper body. Additionally two LPM sensors (100 Hz) were attached to both skates. These offer extra position measurements. The lean angle of both skates was measured using two Xsens sensors (MTx and MTi-G) (100 Hz). The Xsens sensors were mounted on the skates and connected through a USB cable with a mini laptop at the back of the skater. MATLAB(R2012a) was used to record the Xsens data. The normal forces exerted on the skates were measured using instrumented skates (100 Hz) (Appendix B).

Additionally a Casio Exilim high speed camera was used to capture motion of the speed skaters in high speed (300 fps) (Figure 23). A video camera was used to record the lean angle of the skater (30 fps). Four AutoDome 800 serie HD PTZ cameras were used to capture the whole research (25fps). These cameras were linked to the LPM system, so their panning movement was initiated by the movement of the LPM sensors. The skater therefore carried a LPM sensor at the upper body.

The synchronization procedure was based on the internal clock of the High Speed camera. The complete synchronisation procedure is described in Appendix Q.

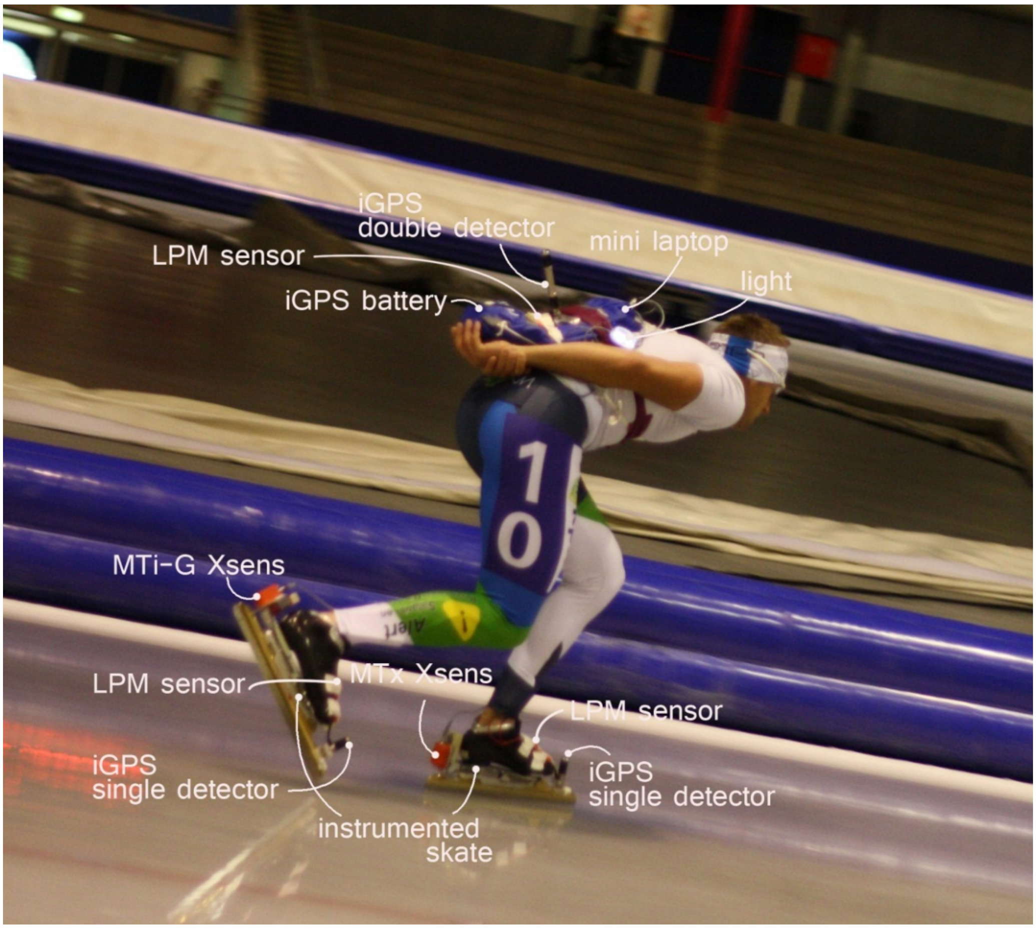

Figure 22 Equipped skater

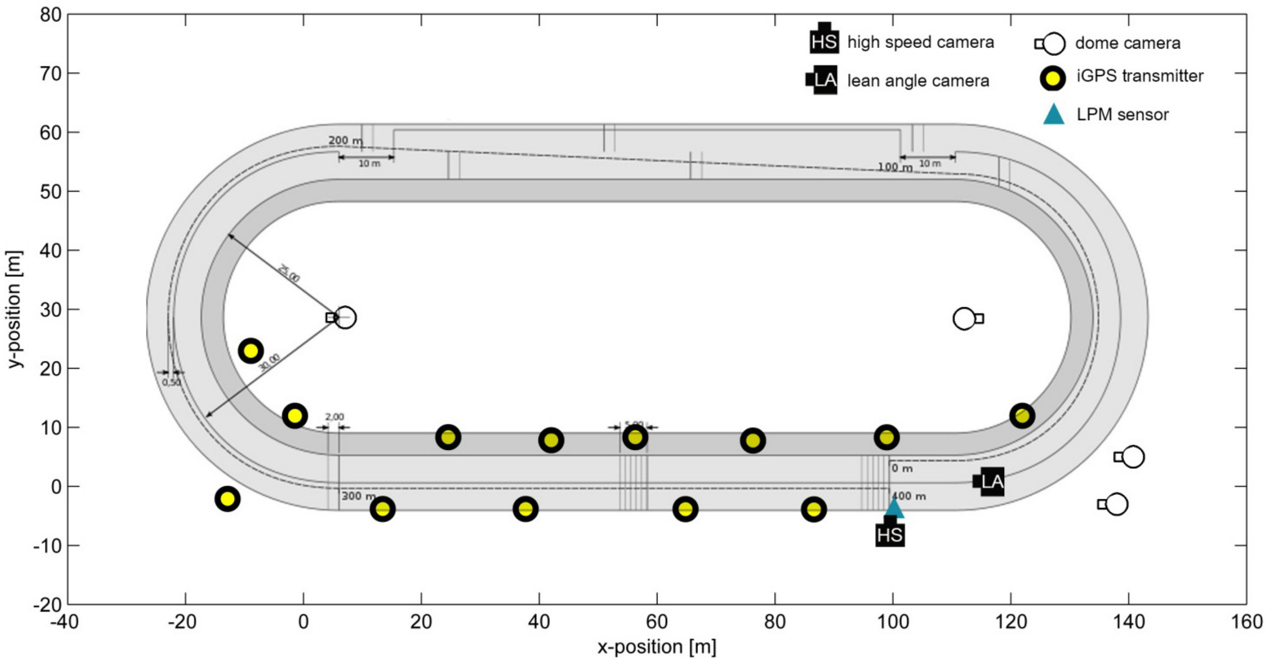

Figure 23 Research set-up for the data collection at the ice rink of Thialf.

4.3. Subjects

The data collection was performed with four subjects, who differed in skate level, but who were all highly-skilled skaters. The subjects are listed in Table 16 .

Table 16 Subjects used in this research. Elite = top athlete; Competitive = competitive athlete; Ex-competitive = ex competitive athlete;

Subject	Gender	Skating level	Weight [kg]
Participant 1	Male	Competitive	84
Participant 2	Male	Ex-competitive	76
Participant 3	Female	Competitive	-
Participant 4	Male	Competitive	80

4.4. Results

The data collection involved position measurements, lean angle measurements and force measurements. In Appendix P the collected data for each trial are shown. This overview shows that the first trial of participant 1 is most complete.

4.5.1 Force measurements

The force measurements suffered from time gaps in the data. The left and right skate were not automatically synchronized; therefore the time gaps (which occurred independent of the other skate) resulted in shifts between the right and left force data. Also the synchronisation in the analysis with other measurement systems was impossible due to the measurement deficiencies. As a consequence no reliable force data time series could be constructed and force data could therefore not be used for the verification of the skater model (Appendix R).

4.5.2 Lean angle measurements

The lean angle measurement system (Xsens) also suffered from data gaps in the measurement data (Appendix R). The data did sample at a frequency of 100 Hz, however the mini laptop used to collect the data was not capable of buffering the data in time. This resulted in irregular data gaps. Therefore the collected data cannot be used for the verification of the skater model.

4.5.3 Position measurements

Upper body sensor

The results of the iGPS sensor on the upper body show that the upper body of the participants is moving up and down throughout the skate movement. Figure 24 shows the upper body movement in the 3D environment. The upper body shows a sinusoidal movement in both xy-plane and xz-plane. In the xy-plane this pattern is caused by the change of feet during a stroke: this changes the direction of movement of the skater. This indicates that the skater not only propels itself forward, but also initiates a sideward movement by pushing against the environment. This figure shows that the upper body position in z-direction is lowest just after the points of inflection of the upper body in xy-plane, which is probably the point of take-off of the skates (just before the skates steer back, see Appendix S); The results seem to indicate that the skaters move their body up and back down again within a stroke (Figure 25), although the exact ending of the stroke is unknown. The amplitude of the upper body movement is about 7% of their average upper body height (Table 17).

A)

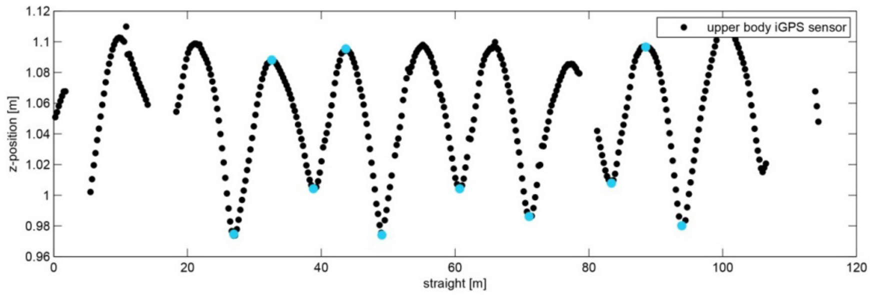

B)

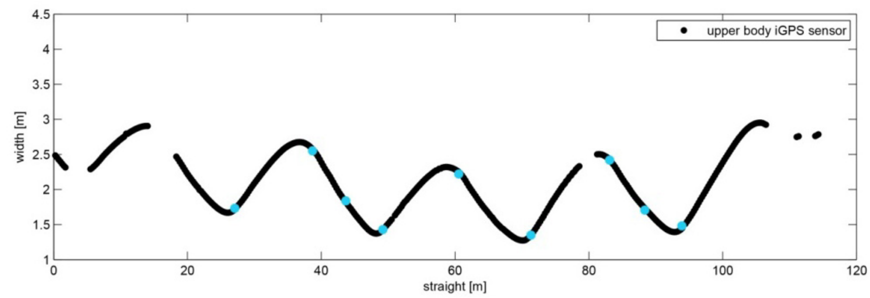

Figure 24 This figure illustrates the upper body movement of the speed skater. A) vertical position of the sensor at the upper body. B) The sensor at the upper body in horizontal plane. The lowest point is reached just after point of inflection of the upper body. The vertical movement shows an asymmetry between the left and right strokes of participant (3). The gaps in the data are due to a line of sight problem.

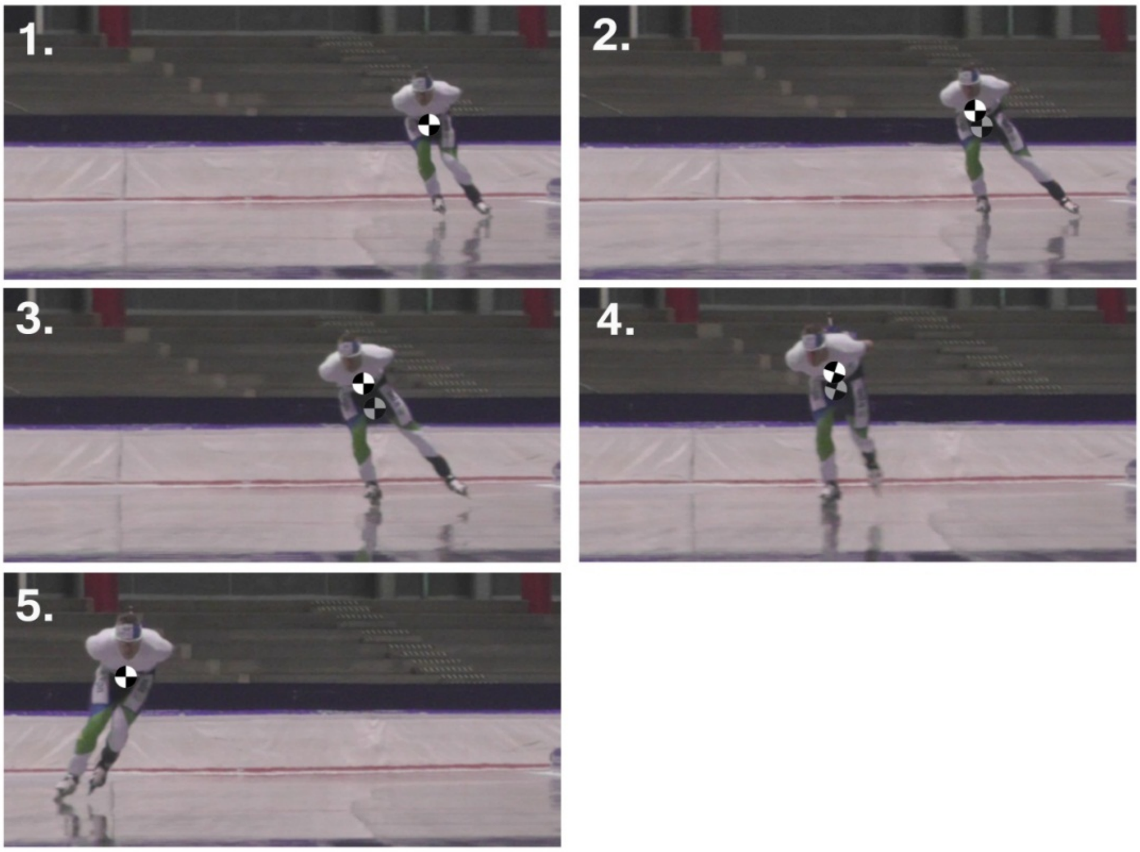

Figure 25 This figure illustrates the upper body movements from one inflection point to the other. Picture 1 illustrates the double support of both skates; the left skate is in push-off and the right skate is in the glide phase. The skater is at the lowest point in this case. The skater then moves his upper body upwards, which is shown in picture 3 and 4 during the glide phase of the right skate. Towards the end of the reposition phase of the left skate and the start of the push-off phase of the right skate, the upper body is lowered again.

*Table 17 #S is the number of straight parts analysed in this trial; Mean is the average body height of the skater during the trial at the straight parts; STD is the standard deviation of the body height of the skater; The amplitude of the vertical upper body position is defined as (2*STD/mean)*100%*

	Participant 1			Participant 2		Participant 3	Participant 4
	Trial 1	Trial 2	Trial 3	Trial 1	Trial 2	Trial 1	Trial 1
#S	4	4	4	2	2	2	1
Mean	1.11 [m]	1.10 [m]	1.08 [m]	1.18 [m]	1.15 [m]	1.05 [m]	1.11 [m]
STD	0.04 [m]	0.04 [m]	0.05 [m]	0.03 [m]	0.03 [m]	0.03 [m]	0.04 [m]
A	7 [%]	8 [%]	9 [%]	5 [%]	6 [%]	7 [%]	7 [%]

Sensors at the skate

The iGPS system measured the position of the skates in 3D. Therefore the point of take-off can be established with only the position data, eliminating any possible synchronizing error. The data from the sensors at the skates however contain a lot of noise and data gaps due to reflection of the ice (which is increased after each ice resurface). Therefore separate trials were used to find the point of take-off. Before the take-off, the iGPS sensor moves down, due to the lean angle, after which it is lifted. An example is given in *Figure 26*.

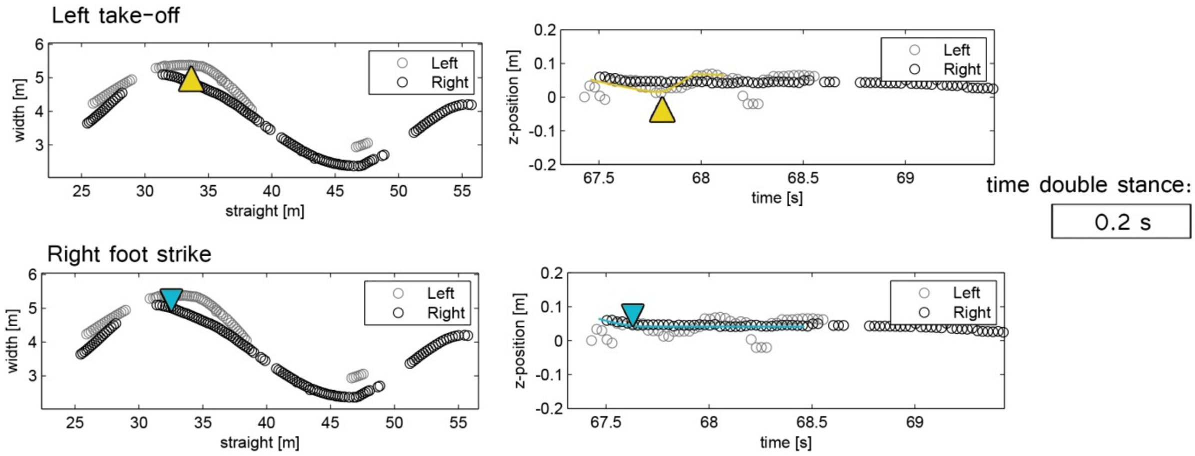

Figure 26 iGPS data of the skates. Left the position in xy-plane, right the position in z-direction. The green triangle indicates a foot strike; the yellow triangle indicates a take-off. The double stance phase time is the time between the foot strike of one skate and the take-off of the next. The sensor is positioned at the tip of the skate. (Figure 22 Equipped skater).

4.5. Discussion

4.5.1 Measurement systems

Verification of the skater model demands a complete set of data, including position data, lean angle data and force data. The faulty data from both the lean angle measurements and the force measurements rendered the collected data unfit for verification of the three-dimensional skater model. Recommendation would be to run all the different measurement systems on one global time stamp, a unified synchronisation time. This would solve both problems of synchronisation (which is very time consuming) and data gaps, since the data gaps can then be quantified.

4.5.2 Collected data

Upper body position

In speed skating the skating position is seen as an important factor of the performance (van Ingen Schenau, de Groot et al. 1985). The trunk position is of influence on both the aerodynamics of the skater, and therefore the air friction, and the skating technique in terms of push-off. (Boer and Nilsen 1989) reported a more or less constant vertical position of the upper body during the entire stroke; (Fintelman 2011) already found, using an accelerometer, that there is an upwards movement of the upper body during speed skating, but could not quantify it.
The current study shows a periodic movement. The study of Boer was performed with male and female athletes who participated in the 1500 and 5000 m races during the Winter Olympic games in Calgary 1988, which entails higher skilled participants compared to the current study. Other difference was the technique of the skaters; the current study was performed on clap skates. Both causes could have contributed to the difference in outcome.
Unfortunately we are unable to determine from these data what and if there is a relation between the average upper body position and the amplitude during the skating movement. Assumed is for now that the amplitude is linearly related to the average body height, however the amplitude (7% of the average upper body position) might also be independent from the average body height or related differently.

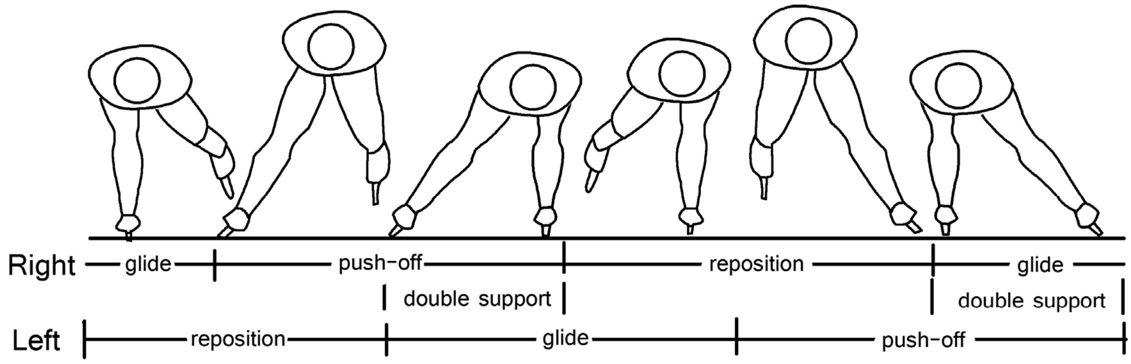

Figure 27 Adjusted schematic drawing of the phased of a stroke, based on Allinger(Allinger and Bogert 1997)

Skate position

The results from (Fintelman 2011), based on the force data synchronised with the LPM data, showed that the skate steers back towards the upper body before leaving the ice (Figure 28).
However exploratory, the current study indicates that the first ice contact (foot strike) and the take-off of the skate were timed differently; in the current study the skate took off before actually steering back. The difference between Fintelman's data and the results from this study might be caused by two different factors:
First the difference in skill-level of the speed skaters or the velocity of the skaters might have been a possible cause. The velocity of the skaters used in the current study was lower (respectively 7.4 m/s versus 9.4 m/s). Although steering back the skate is probably inefficient in terms of performance (the direction of push off is then partly opposite of the skating direction), the speed might be the reason for the delay in take-off of the skate.

Second, Fintelman's research used force data and LPM data and based on the experience of the current study, a synchronisation or distortion problem in Fintelman's data cannot be ruled out. Comparing the data measured with LPM and iGPS, the LPM has a more smooth pattern, consisting of only symmetric curves (Figure 29); this pattern is probably initiated due to the use of a (sinusoidal function in the) Kalman filter in the LPM software. This might deform the data of LPM, whereby the point of take-off differs in the data.

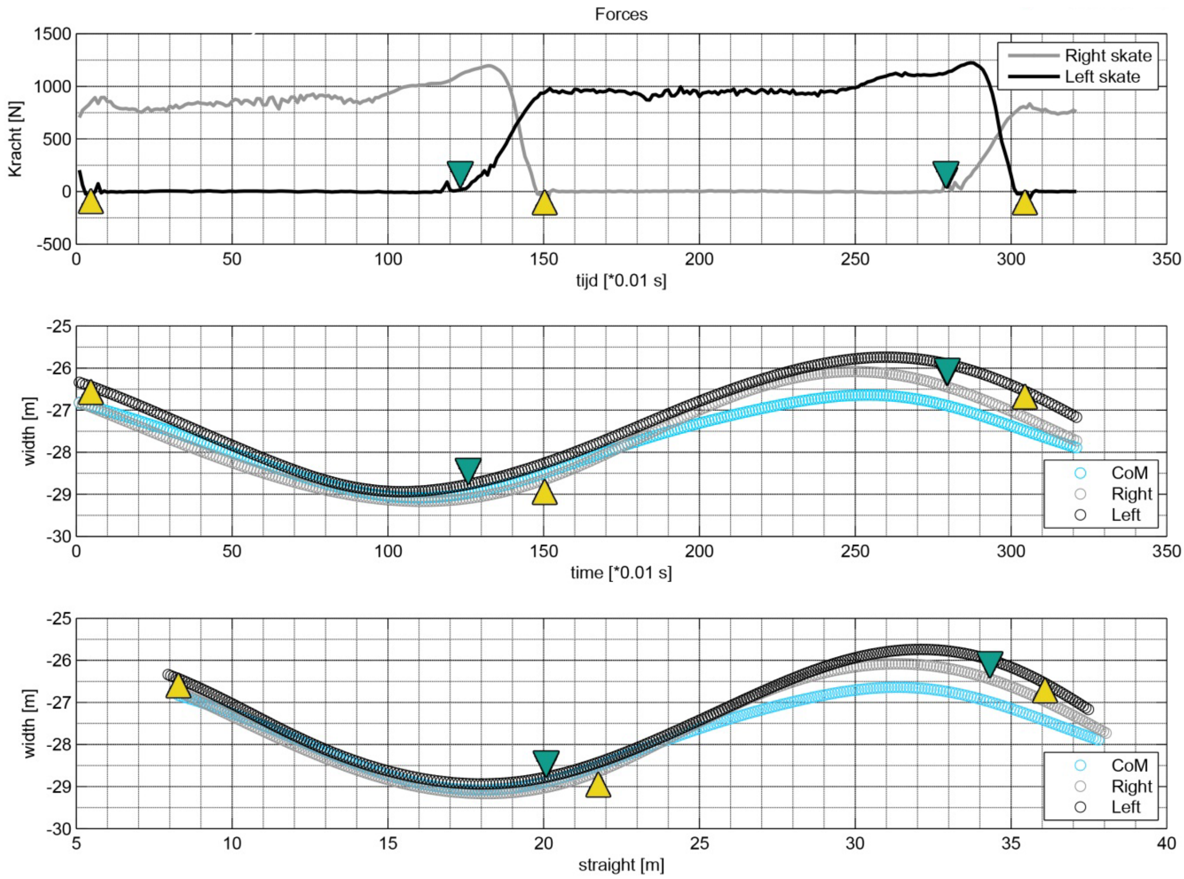

Figure 28 The synchronised position and force data of Fintelman with the points of take-off(yellow triangle) and foot strike(green triangle) indicated by the triangles.

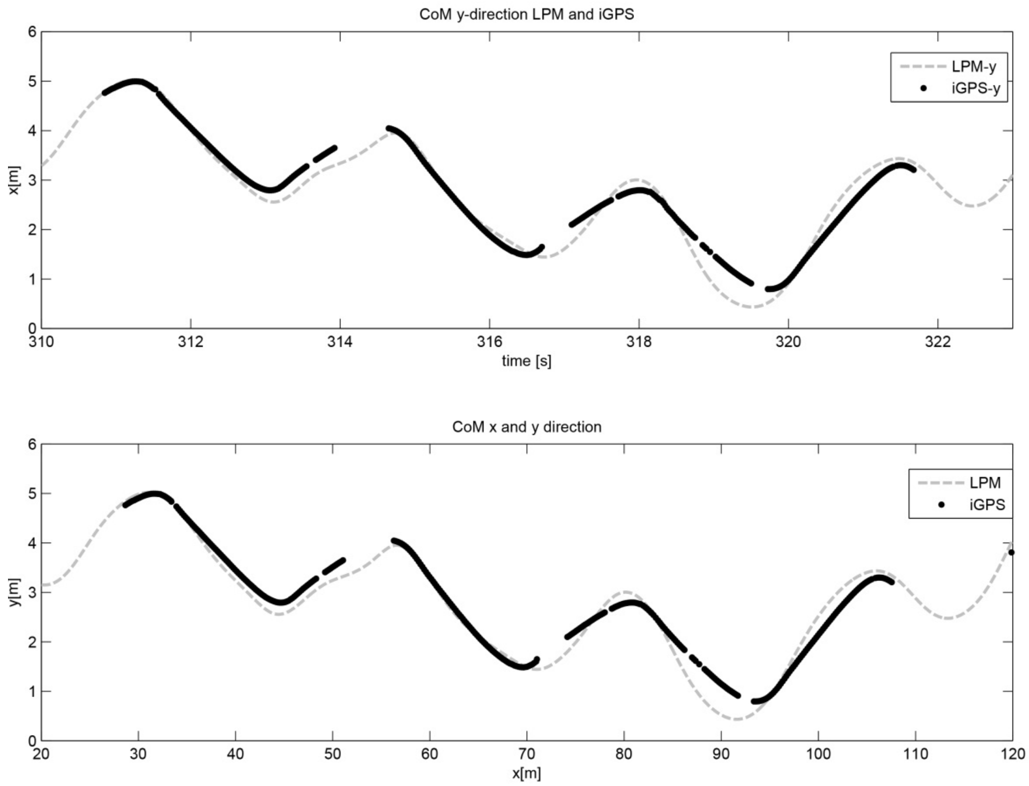

Figure 29 Position of the LPM and iGPS sensor at the upper body. The LPM data show more symmetric curves, while the iGPS data show asymmetry.

“The constructed simple three-dimensional skater model does a good job of imitating forces and kinematics observed in actual speed skating for a skater during a whole straight part. The vertical upper body movement shows to be of high influence on the total power output of the model (8%).”

Model Verification

5.1 Introduction

Model verification is done by feeding the model with an input (leg extension) and comparing the output of the model, which the global motion of the skater on the ice and the forces exerted, to the true outcome measured at the ice rink section (5.5). Unfortunately the data collection did not meet the expectations in terms of the accuracy and comprehensiveness and therefore these three-dimensional data cannot be used to verify the 3D dynamic model.

The 2D data from prior research (Fintelman 2011) is however still available, although (as found through the current research) limited in accuracy. Complementary the current data collection offered new insights into the upper body movements of a speed skater and moment (position) of take-off of the skates.

This section of the report will first establish if the developed three-dimensional model generates the expected outcome, based on the 2D data collected in (Fintelman 2011), keeping the upper body levelled.

Additionally an upper body movement will be simulated to complement the 2D position data. Using these data as an input for the model can indicate what the influence of the upper body movements is on the forces obtained by the model.

Finally the model verification and development will be discussed in terms of necessity and recommendations.

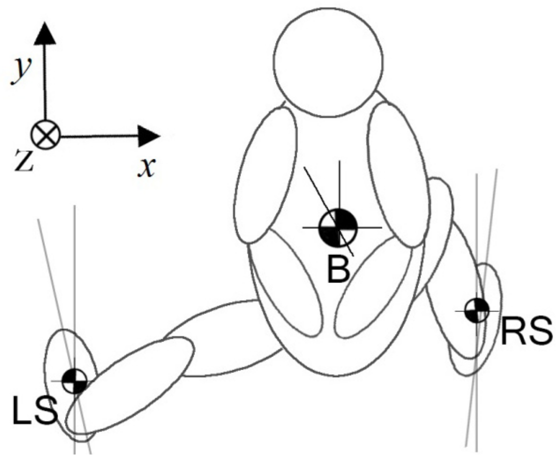

Figure 30 Top view of the skater model with the masses and the coordinate system. B = modelled mass at the upper body; LS = modelled mass at the left skate; RS = modelled mass at the right skate.

5.2 Data

5.2.1 Measured data

The data used in this section are measured data from (Fintelman 2011) (Figure 31). The data were collected at the ice rink of Thialf, Heerenveen in 2010. The position data were collected by means of LPM sensors at the skates and a double LPM sensor at the upper body of the skater. The accuracy of this system is 330 mm (maximum absolute error). The LPM position data are parameterized, since numerical differentiation of the position data is necessary. The parameterization functions are combinations of linear and geometrical functions and can be found in (Fintelman 2011). The parameterization did not alter the accuracy significantly(Fintelman 2011), but does eliminate the (LPM) fluctuations in the velocity data. The conversion of these data into the leg extension and heading (obtained by the velocity in x and y direction) can be found in Appendix T.

The forces were measured with the instrumented skate (before the installation of the wireless component)(Appendix B). The accuracy of this system is 4.3N in normal direction and 2.4N in lateral direction. The forces were converted into the global coordinate system using lean angle measurements obtained by Xsens. These introduce an additional inaccuracy of 9% of the found force.

The mass of the skater and equipment was 77 kg; based on (Ackland, Blanksby et al. 2013) the mass moment of inertia of the upper body is set to 1.26 [kgm^2]. The skater was a highly skilled skater (competitive level).

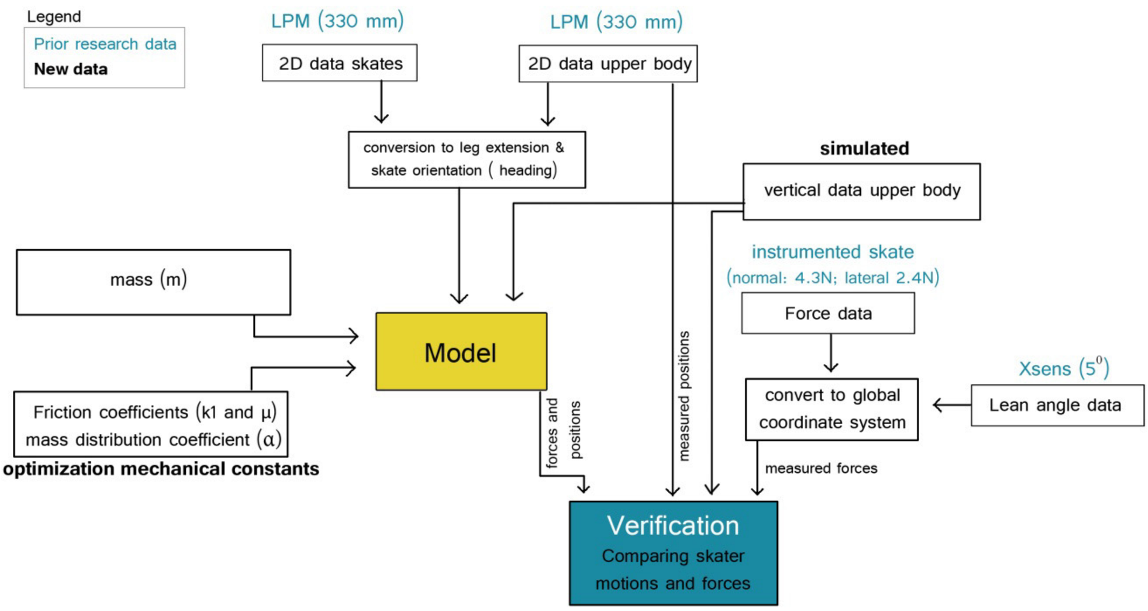

Figure 31 Input and output data used to verify the 3D skater model. The method used to collect the data is mentioned in blue words for the data obtained from Fintelman; the black bold methods indicate data from the current research.

5.2.2 Mechanical constants

There are three mechanical constants that were estimated, since measuring these variables is too elaborate. These three variables are the friction coefficient for both the ice(μ) and the air(k_1) and the mass distribution coefficient(α). This was done by use of the net error between the model and the measurements. The net error is defined as in equation(5.2.1).

(5.2.1) $$E = \frac{1}{N}\sum_{j=1}^{N}(\tilde{y}_{ij} - y_{ij})^2$$

Where N is the number of collected data points, $\tilde{y}_{ij}$ the simulated value from the model and y_{ij} the measured value. The total net error was calculated including the position in x and y direction and including the local normal force (5.2.2). This minimization problem was solved using the optimization function of MATLAB *fmincon*.

(5.2.2) $$J_{\min} = \frac{\sum_{j=1}^{M} w_j \left(\frac{1}{N} \sum_{i=1}^{N} \frac{(\tilde{y}_{ij} - y_{ij})^2}{\bar{y}_{ij}^{\ 2}} \right)}{\sum_{j=1}^{M} w_j \bar{y}_{ij}^{\ 2}}$$

5.2.3 Simulated data

Since the LPM data only concerned 2D data, where needed, a simplified vertical upper body movement was simulated, based on the knowledge found in the data collection research (section 4.5.2), equation(5.2.3).

(5.2.3) $$z_{sim} = z_{ave} + A \cdot \sin\left(\frac{t}{T} + t_d \right)$$

(5.2.4) $$A = a \cdot z_{ave}$$

With an average body height (z_{ave}) of 1.2 m (Fintelman 2011), an amplitude (A) of 7% of the average body height and a constant period (T) of 1400 ms (average of the stroke duration during the run). A minimization function was applied (minimizing(5.2.2)) in order to find the optimal initial time shift (t_d) for the simulated upper body motion. The time shift obtained by the minimization function creates an upper body movement as expected from the research in section 4.5.2: the z-position of the upper body is lowest just after point of inflection in the xy-plane (Figure 32.).
Since the upper body movement was simulated with a constant time period, while the skate strokes all have different periods, the simulated upper body movement is restricted in accuracy.

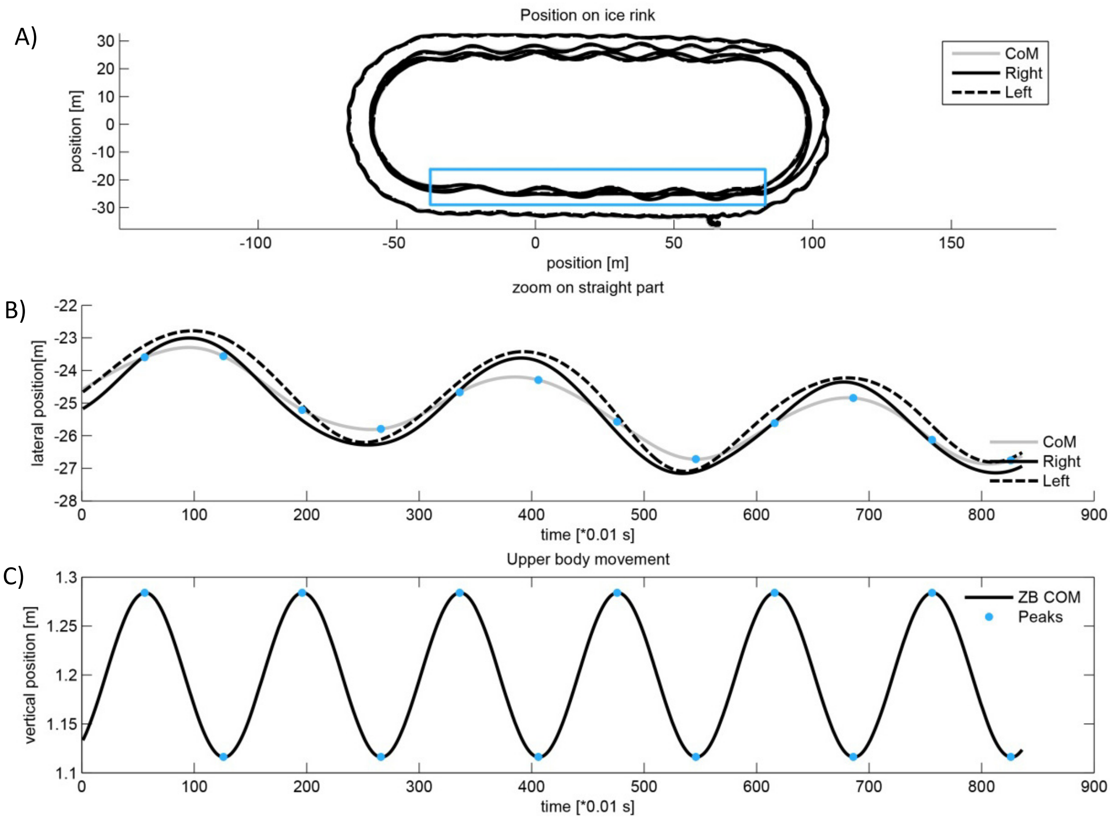

Figure 32 A) position of the sensors at the upper boy and skates over time, the blue rectangular indicates the area that is shown in graph B; B) Selected straight part of A; C) the simulated upper body movement (run26, straight 1). The

simulated data were shifted using a minimization function. The obtained motion agrees with the found upper body motion in the prior research section: the lowest point of the upper body is at the point of inflection in the xy-plane.

5.3 Method

5.3.1 Residuals

The total net error from (5.2.2) was used to compare the 3D model to the 2D model, in order to have an indication of the feasibility of the model. The total net error was thereby divided by the number of optimization parameters. Additionally the residuals were calculated similar to (Allinger and Bogert 1997) (5.2.5), which gives an indication of the error of the model for different variables.

(5.2.5) $$R_j = \sum_{i=1}^{N} \frac{\left|\tilde{y}_{ij} - y_{ij}\right|}{N}$$

5.3.2 Tests

In order to establish the feasibility of the three-dimensional model, three tests were performed.

5.3.2.1. Constant upper body position

The three dimensional model was fed with 2D data from the prior research. The upper body was kept levelled at 1.2 m.

5.3.2.2. Shifting the data

In section 4.5.2 the iGPS data implicated a different take-off of the skate compared to what was established in prior research. The stroke separation is based on the synchronisation between the force data and position data (Figure 33). In case of a synchronisation or distortion error between the force data and the position data, a distorted stroke separation would occur. When this is the case, the performance of the model outcome would improve when the position data is shifted relatively to the force data. Therefore a minimization problem was formulated, based on(5.2.2), adding the optimization parameter of a time shift between the force and position data.

The upper body was kept levelled at 1.2m for this test.

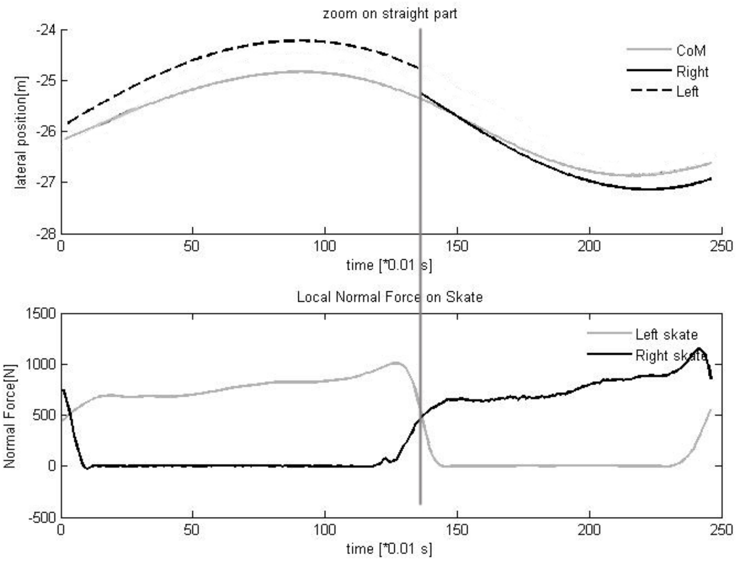

Figure 33 Stroke separation based on the force data. The stroke is cut at the intersection point between the normal forces measured in the skates.

5.3.2.3. Simulated upper body position

The three-dimensional model was fed with the 2D data from the prior research, supplemented with the simulated vertical upper body movement.

5.4 Results

5.4.1 Constant upper body position

The mechanical constants found through optimization are given in Table 18. The results of two straight parts (each 6 strokes) are shown in Table 19. The modelled and measured force and position data are shown in Figure 34. Figure 35 shows the movement of the skater over the straight part in the horizontal plane (equal axes), the lower graphs give an indication of estimated velocity over the length of the straight. Based on the residuals of Table 19 and the graphs, the 3D model estimation gives accurate results for the position and force estimation; however the force data seem to lack the force peak at the end of the stroke.

Table 18 Values of parameters in the simulations; S1 = straight 1; S2 = straight 2; α = mass distribution, k1 = air friction coefficient; μ = ice friction; m = mass skater; g = gravitational acceleration.

Variable	Value		Description
	Straight 1	Straight 2	
α	0 [-]	0.1478 [-]	Mass distribution
k1	0.2816 [N/(m/s)]	0.3133 [N/(m/s)]	Drag coefficient (air)
μ	0.001 [N/(m/s)]	0.001 [N/(m/s)]	Ice friction
m	77 [kg]	77 [kg]	Mass skater
g	9.81 [m/s^2]	9.81 [m/s^2]	Gravitational acceleration

Table 19 Table of residuals between the measured and simulated values of the variables (averaged over six strokes for the values of the 2D model). x_b = upper body position in x-direction(perpendicular to straight) [m], y_b = upper body position in y-direction (in line with the straight) [m], $\dot{x}_b$ = upper body velocity in x direction [m/s], $\dot{y}_b$ = upper body velocity in y-direction [m/s], F_n = the local normal force on the skates [N].

Residuals	2D model		3D model	
	Straight 1 [m]	Straight 2 [m]	Straight 1 [m]	Straight 2 [m]
x_b	0.0217	0.0411	0.1672	0.1429
y_b	0.0732	0.1364	0.2651	0.3002
$\dot{x}_b$	0.0519	0.0733	0.0712	0.0581
$\dot{y}_b$	0.1772	0.2370	0.2219	0.1691
F_n	67 [N]	41 [N]	86 [N]	74 [N]

Table 20 Net error Jmin of the subject for both the 2D and 3D model. The number is divided by the number of optimization parameters.

Total net	2D model		3D model	
	Straight 1	Straight 2	Straight 1	Straight 2
Jmin	0.0115	0.0101	0.0131	0.0145

A)

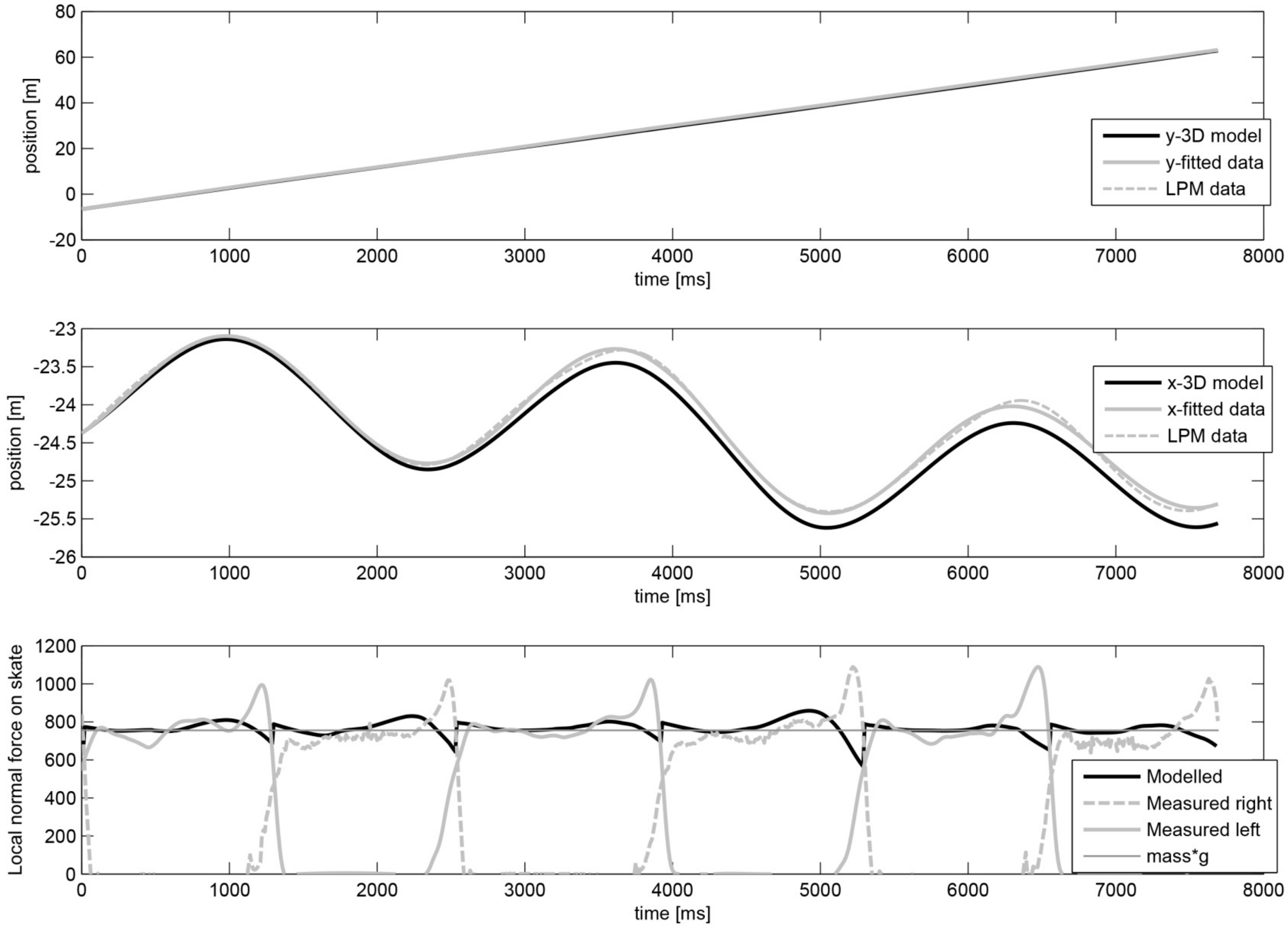

B)

C)

Figure 34 Modelled data versus measured data of the mass (B) of run 26 straight 2. A) The y-position data of mass (B) over time (in line with the straight part); B) The x-position data of mass (B) over time (perpendicular to the straight); C) The local normal force exerted on the active masses at the skate (alternately RS and LS) and measured with the instrumented skates (in plane with the skate blade).

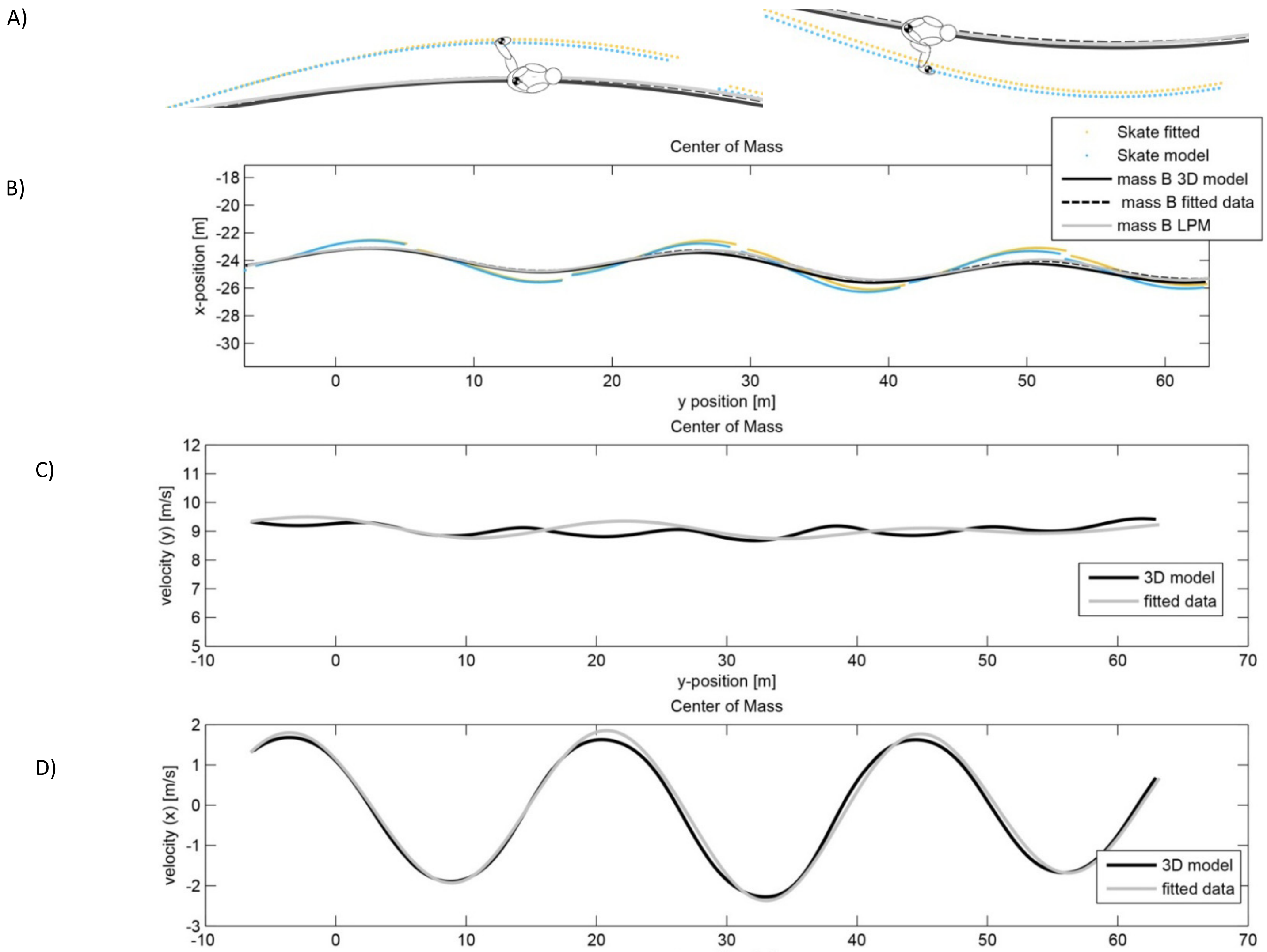

Figure 35 Modelled data versus measured data of run 26 straight 2. A) A graphical explanation of how to interpret the results. B) Position of the upper body and skates on the straight part; C) Velocity of the modelled mass B and the fitted data of the upper body in line with the straight (y-direction). The fitted data was chosen, due to the fluctuations in the LPM data. D) Velocity of the modelled mass B and the fitted data of the upper body perpendicular to the stroke (x-direction).

5.4.2 *Shifting the data*

The result of the test whereby the position and force data are shifted relatively to each other is shown in Table 21 and visualized in Figure 36. The time shift indicated in the table refers to a sooner take-off (Figure 37). The results show that the shift has a positive effect on the modelled movement (Jmin is decreased), mainly the force estimation is improved (Figure 38), although the force peak at the end of the stroke is still lacking.

Table 21 Table of residuals between the measured and simulated values of the variables. x_b is the upper body position in x-direction(perpendicular to straight) [m], y_b is the upper body position in y-direction (in line with the straight) [m], $\dot{x}_b$ is the upper body velocity in x direction [m/s], $\dot{y}_b$ is the upper body velocity in y-direction [m/s], F_n are the local normal forces on the skates [N].The time shift indicates a shift between the LPM (position) data and the measured force data.

Residuals	3D model		3D model shifted input data	
	S1 [m]	S2 [m]	S1	S2
Time shift	0	0	-0.188 [s]	-0.120 [s]
x_b	0.1672	0.1429	0.1431 [m]	0.1427 [m]
y_b	0.2651	0.3002	0.9281 [m]	0.4679 [m]
$\dot{x}_b$	0.0712	0.0581	0.0723 [m]	0.06 [m]
$\dot{y}_b$	0.2219	0.1691	0.2315 [m]	0.1785 [m]
F_n	86 [N]	74 [N]	75 [N]	72 [N]
Jmin	0.0131	0.0145	0.0106	0.0134

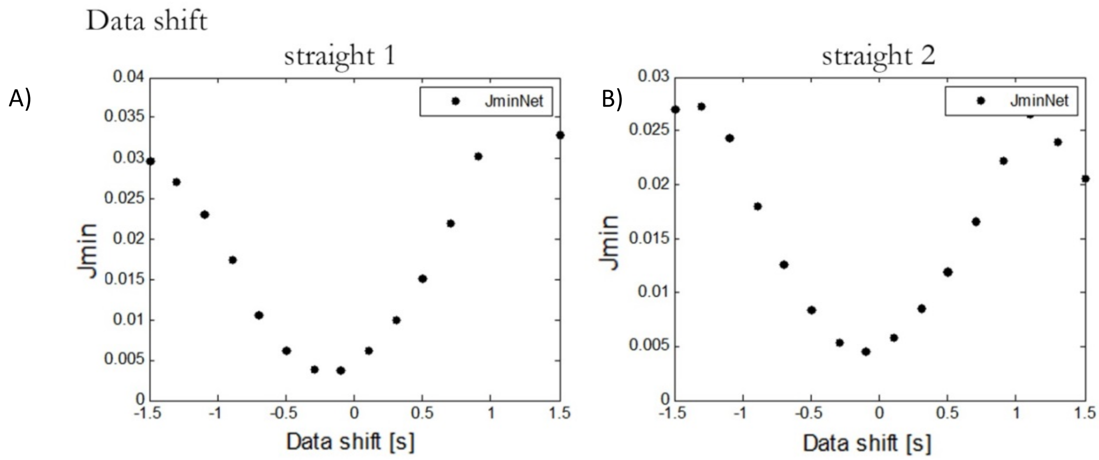

Figure 36 Jmin versus the time shift. The minimal Jmin is at a timeshift smaller than zero.

A)

B)

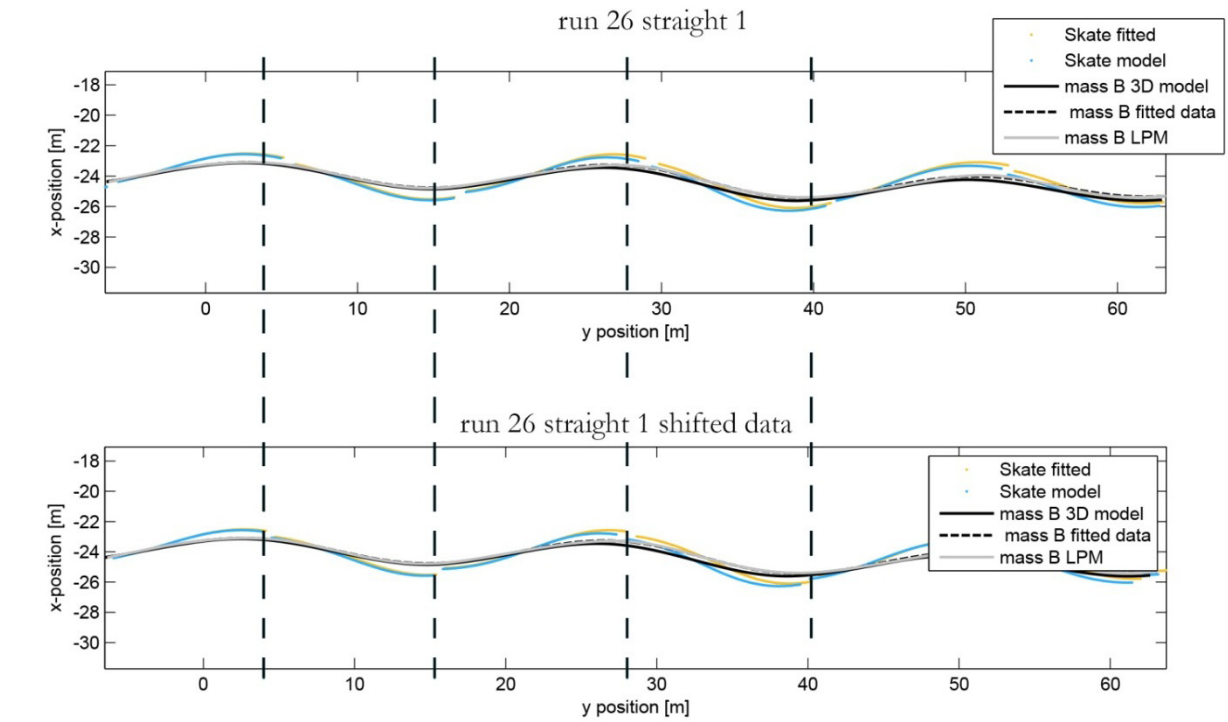

Figure 37 A) non-shifted data used as input for the 3D model; B) shifted data obtained by optimization

A)

B)

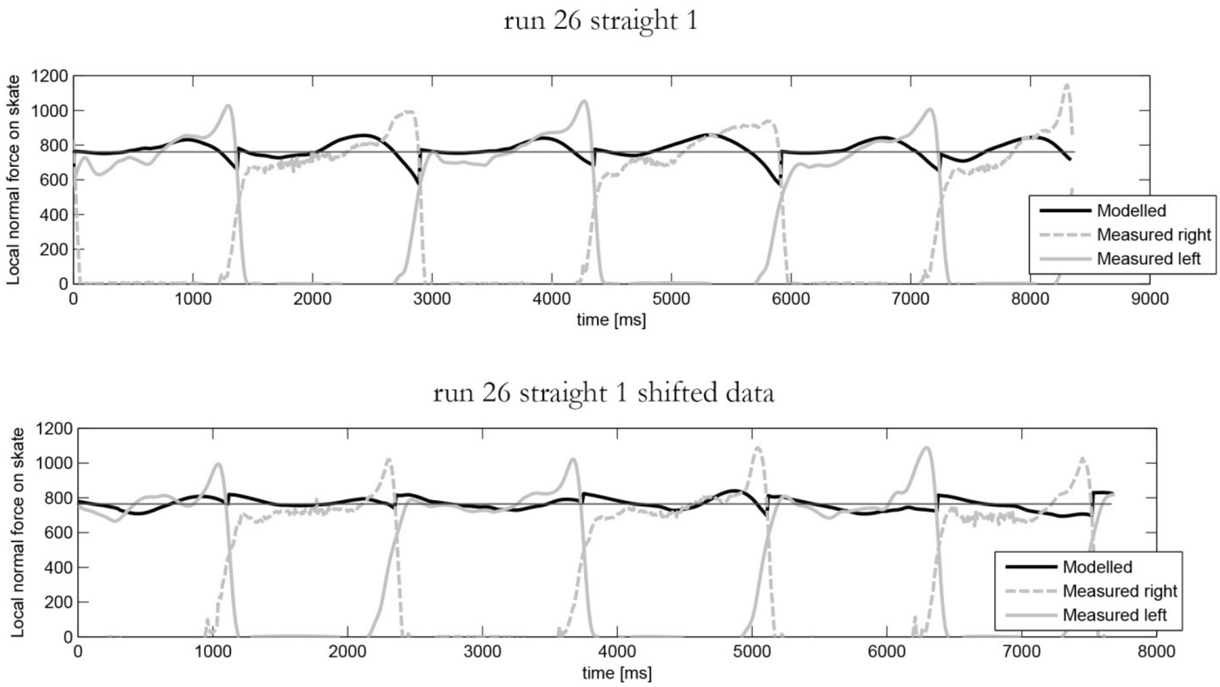

Figure 38 A) Non-shifted data outcomes for the force data; B) shifted data outcomes for the force data

5.4.3 Simulated upper body movement

In this test the data time shift is zero and the vertical upper body movement is simulated. The residuals for this test are given in Table 22 . The force and position outcome is given in Figure 39. On the whole the results show a reduced net error. For the first straight this improvement is introduced due to the better force estimation; the second straight part has a reduced force estimation, but an improved position estimate. Taking into account the estimated mechanical constants, straight 1 shows a more realistic result concerning the air friction coefficient. Although simplified, due to the very simple simulated upper body movement, a force peak is introduced in the force data.

Table 22 The residuals of the 3D model with and without a simulated upper body motion. The mass distribution coefficient, the air friction and the ice friction are respectively 0.0774, 0.3596, 0.001 for straight1 and 0.3923, 0.5265, 0.001 for straight2.

Residuals	3D model constant upper body		3D model upper body motion	
	Straight 1	Straight 2	Straight 1	Straight 2
α	0	0.1478	0.0908	0.3904
k1	0.2816	0.3133	0.3697	0.5199
μ	0.001	0.001	0.001	0.001
x_b	0.1672[m]	0.1429[m]	0.1535 [m]	0.1198 [m]
y_b	0.2651[m]	0.3002[m]	0.4151 [m]	0.1519 [m]
$\dot{x}_b$	0.0712[m]	0.0581[m]	0.0751 [m]	0.0577 [m]
$\dot{y}_b$	0.2219[m]	0.1691[m]	0.2429 [m]	0.1646 [m]
F_n	86 [N]	74 [N]	77 [N]	79 [N]
Jmin	0.0131	0.0145	0.0108	0.0141

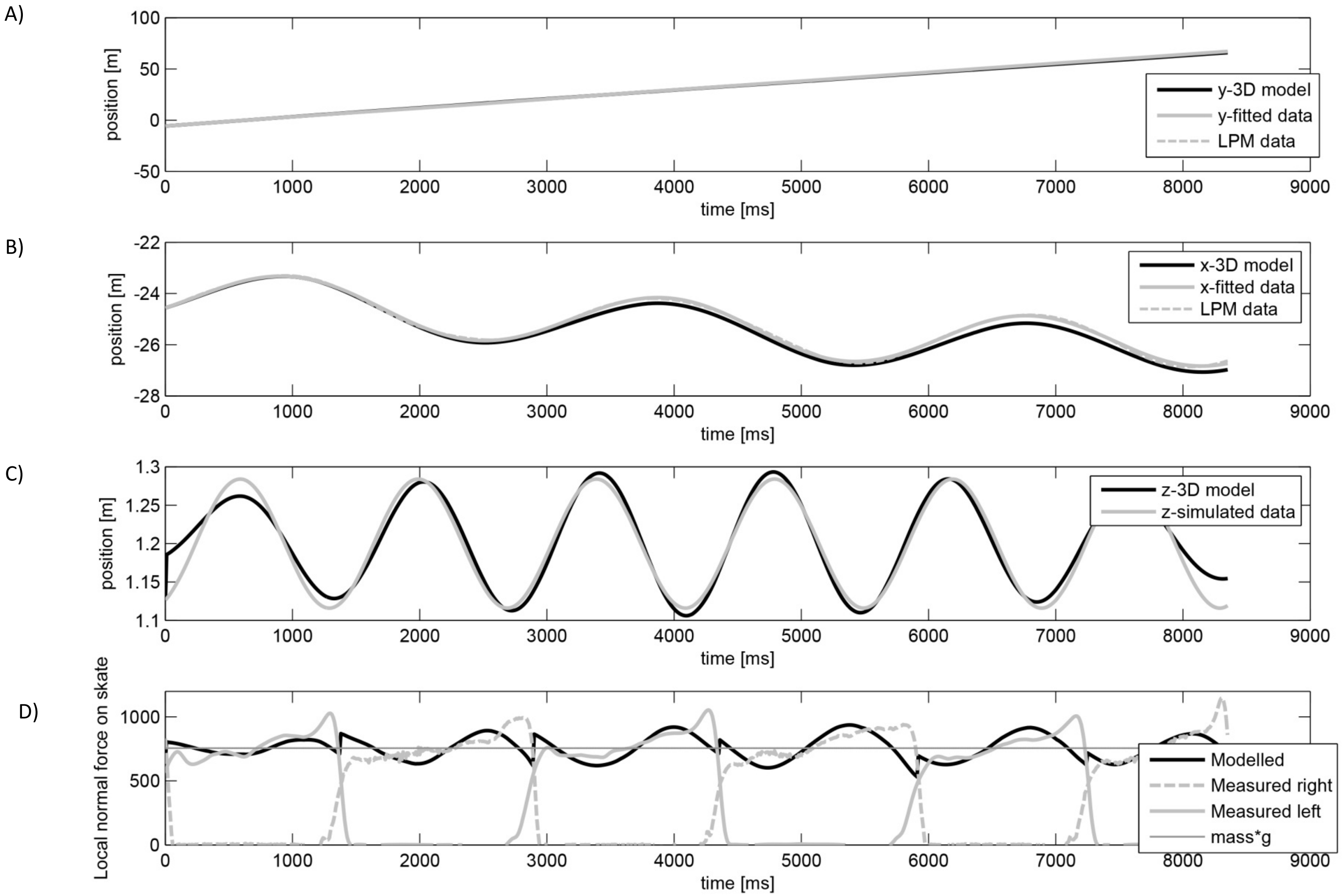

Figure 39 Modelled data versus measured data of run 26 straight 1. A) measured and modelled y-position of the upper body over time B) measured and modelled x-position of the upper body over time C) Modelled and simulated z-position data of the upper body over time.; D) The local normal force exerted on the skates (in plane with the skate blade).

5.5 Discussion

5.5.1 Constant upper body position

5.5.1.1 Model error

Considering the residuals of the 2D model, the 3D model results indicate higher errors. This result has two causes; first the 3D model differs from the 2D model in terms of stroke input; the 2D skater model is applicable for single strokes, while the 3D model is modelled to insert sequential strokes. The second difference occurs in terms of mechanical constants. In the 2D model these were optimized for each single stroke, while the 3D model uses constant mechanical constants for the whole modelled straight part (consisting of six strokes). Both these differences explain the lower position accuracy for the 3D model, while more realistic. The velocity accuracy is independent of time and shows that the 3D model is similar to the 2D model outcome concerning the model error.

The maximum position error outcome of the 3D model (300mm) is within the maximum error found for the LPM system (330 mm). Taking into account a 9% distortion error on the maximum measured force, due to the lean angle measurement system, the measured force accuracy for straight 1 and 2 is 103 N and 98 N respectively. The modelled outcome of the 3D model fulfils this accuracy.

At the start of the thesis, a 5% accuracy was requested from all measurement systems. This is only useful if the model can fulfil this same accuracy. Therefore the residuals of the 3D model for the positions and forces are divided by the average values of these variables on both straights (Table 23) to test if this accuracy can be reached. Although the measured positions are inaccurate, the model estimation fits the data rather well; not unexpected, since these (inaccurate) data are used for both input and output. Advantageous is that the accuracy in line with the straight (y) is most accurate, since the displacement in that direction is most important in terms of performance of the skater. The consequence of the inaccuracy of the measurement system was expected in the force estimation, which indeed is confirmed by the results. These force estimations are expected to improve with more accurate position data.

Notwithstanding its limitations due to inaccuracy of the data, looking at the position estimations, the 5% accuracy is expected to be reached by the model when accurate kinematic data is available.

Table 23 In column 2 and 4 the area of the position data is indicated (length of the straight part and width of the strokes) and the average velocity and local normal force. The error is the ratio between the residuals and values given in the prior mentioned columns.

Variable	Straight 1: measured average or distance	Error [%]	Straight 2: measured average or distance	Error [%]
x_b	3.5 [m]	4.8	2.3 [m]	6.2
y_b	72.9 [m]	0.36	69.7 [m]	0.43
$\dot{x}_b$	1.4 [m/s]	5	1.2 [m/s]	4.8
$\dot{y}_b$	8.7 [m/s]	2.5	9.1 [m/s]	1.9
F_n	772 [N]	11.1	762 [N]	9.7

5.5.1.2 Mechanical constants

The sensitivity of the mechanical constants can be found by fixing all parameters except one. In Figure 40 the net error is plotted as function of the mechanical constants. The results prove a sensitivity of the model to all mechanical constants, which endorses the credibility of the model.

The optimization of the mechanical constants results in a low mass distribution coefficient, which leads to small to no mass at the skates. Notwithstanding its limitations due to inaccurate and few data, this study suggests that the skater could be modelled using only one mass at the upper body and two infinitesimal point-masses at the skates, comparable to the simplest walking model (Garcia, Chatterjee et al. 1998), which has two rigid massless legs hinged at the hip, a point-mass at the hip, and infinitesimal point-masses at the feet. The mechanical constants obtained for the ice friction are in the order of magnitude of the ice friction found in (Koning, Groot et al. 1992) (0.0046[N/(m/s)]). Notable is the plausible correlation between the mass distribution and the ice friction: an increased mass distribution (more mass at the skates) leads to a higher ice friction coefficient (Appendix U). The air friction coefficient is within realistic values.

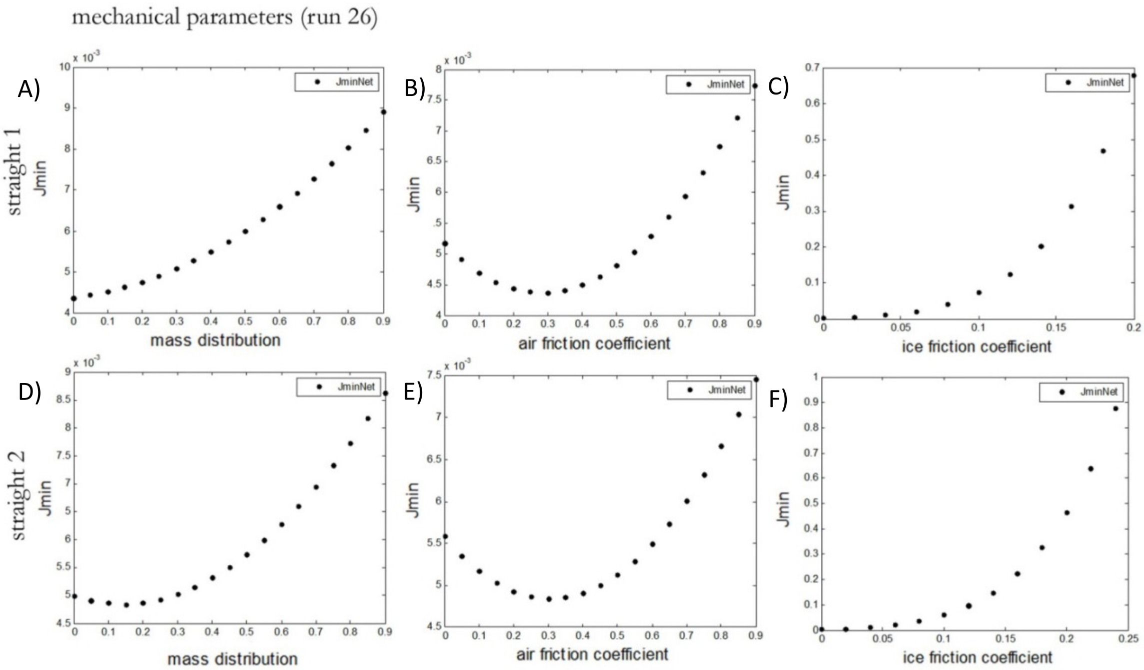

Figure 40 Sensitivity analysis of the parameters. The net error between the measurements and the model versus the minimization parameters: A,D) mass distribution; B,E) air friction coefficient; C,F) ice friction coefficient.

5.5.1.3 Fitting false data

The mechanical constants are optimized in order to obtain the right values. The risk exists that the results obtained are therefore a consequence of good curve fitting. Therefore false data is implemented into the model, adding a sinusoidal function to the velocity input of the model in x and y direction:

(5.5.1) $$A \cdot \cos\left(\frac{2\pi}{T} \cdot t\right)$$

Were A is the amplitude of the sine wave and the period T is set at 140 ms. The result is shown in Figure 41. These results suggest that it is unlikely that the fits are a result of curve fitting; this endorses the reliability of the model.

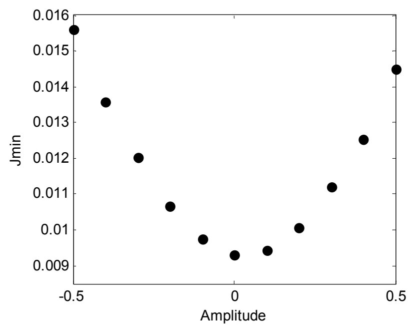

Figure 41 Jmin versus the amplitude of the sine wave corrupting the input velocity data.

5.5.2 Data shift

The main result for the data shift is the improvement of the force estimation. Without the shift of data, the force estimated by the model shows a decrease at the end of the stroke; this dip is eliminated after the data shift. The results of this study cannot be taken as evidence for a synchronisation error in the data used in prior research, however the findings do imply a likeability of such a synchronisation or distortion error, since the measurements for the straight parts each show a comparable optimal time shift, in accordance to the results found by iGPS.

5.5.3 Simulated upper body position

The simulated upper data positions show a positive influence on the estimated force data and position data, although the vertical upper body movement might have been too easily simulated, which could lead to inexact timing of the vertical upper body movement.

5.5.3.1 Power output

Power is the amount of energy consumed per unit time. In case of a speed skater it indicates the energy needed from the athlete to complete the exercise of skating. There exist a number of power models in literature, based on the power output of the skater (Koning, Foster et al. 2005). Power gives a good indication of the performance of the skater and therefore the influence of the power used to move the upper body up and down will be of influence on the total performance. The exact upper body movement is unknown, however the amplitude obtained in the data collection, gives an indication and with that the ratio of power in all three directions can be established. According to (Koning, Foster et al. 2005) the rate of change of the kinetic energy of the skater can be expressed as (5.5.2).

(5.5.2)
$$\begin{aligned} m\ddot{x} &= F_h - F_w \\ (m\ddot{x})\,\dot{x} &= (F_h - F_w)\,\dot{x} \\ \frac{d\left(\frac{1}{2}mv^2\right)}{dt} &= P_h - P_w \end{aligned}$$

With F_h the forces exerted by the human, F_w the friction forces, P_h the power generated by the human and P_w the power generated by friction. The power can be expressed as (5.5.3). For the human power output, also the absolute power P_{h_abs} is given, since negative power also needs to be generated by the human.

(5.5.3)
$$\begin{aligned} P_h &= F_{u,i}\cdot\dot{u}_i + F_{v,i}\cdot\dot{v}_i + M_i\cdot\dot{\theta}_i + \lambda_2\cdot\dot{z}_b \\ P_{h\_abs} &= \left|F_{u,i}\cdot\dot{u}_i\right| + \left|F_{v,i}\cdot\dot{v}_i\right| + \left|M_i\cdot\dot{\theta}_i\right| + \left|\lambda_2\cdot\dot{z}_b\right| \\ P_w &= F_{i,friction}\cdot\dot{u}_i + F_{b,friction}\cos(\theta_b)\cdot\dot{y}_b + F_{b,friction}\sin(\theta_b)\cdot\dot{x}_b \\ i &= [rs, ls] \end{aligned}$$

5.5.3.2 Human power output

Applying these formulas to the runs with the simulated upper body positions (Table 24) shows an absolute average power output of 350W on a straight part. These results are comparable to the results found in (Koning, Foster et al. 2005), who found an average power output of 370W for speed skaters on longer distances, determined experimentally, based on aerobic and anaerobic energy output.

Table 24 mean power output obtained for run 26 with a simulated upper body motion.

Power Output	Straight 1	Straight 2
P_{h_abs}	348 [W]	352 [W]
P_w	251 [W]	226 [W]

In Figure 42 the power output is drawn. The absolute power generated by the human indicates at which parts the skater has a higher power output compared to the friction output, so at which part the skater is accelerating. The grey areas indicate these positions. The skater has a higher power output at the middle of the stroke when the upper body is moving down.

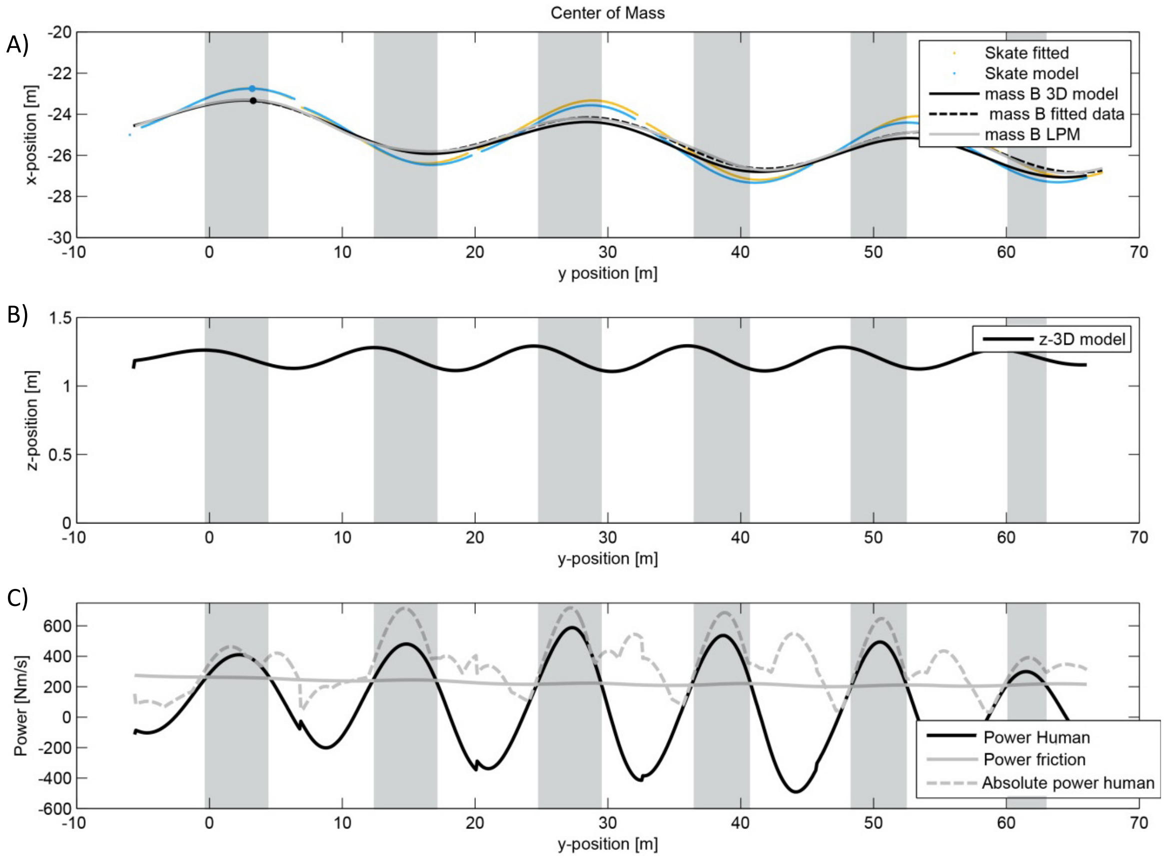

Figure 42 A) Modelled position of the upper body and skates; B) Modelled height position of mass B;C) Power output of the three dimensional model with a simulated upper body position; the grey areas indicate the parts of the straight where the power output is higher than the friction output.

5.5.3.3 Power direction

For the division of power in all three directions, the whole skater is assumed a single rigid body, with only the constraint forces working on the speed skater and the velocity of the total skater in x,y and z direction (5.5.4). The results show that most power is generated in y-direction, along the straight part of the rink. In vertical direction the power is 23% of the total assimilated power. This indicates that the addition of a third dimension to the simplest skater model is very useful and necessary in order to provide the skaters with constructive feedback in the future.

(5.5.4)
$$P_{xy} = \lambda_{1,xy} \cdot v_{b,xy}$$
$$P_z = \lambda_2 \cdot \dot{z}_b$$
$$i = [rs, ls]$$

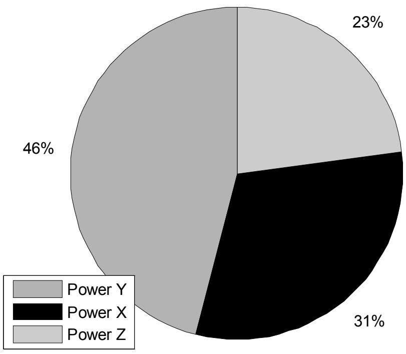

Figure 43 Pie chart of the power output division in all three directions for straight 1 with a simulated upper body movement. The results for straight two are similar (24%, 47% and 29% for the x,y,z-direction respectively).

5.5.4 Limitations of the model

5.5.4.1 Leg extension

In section 2.1 the leg extension was defined as the difference in position between the modelled upper body mass (B) and the modelled skate masses (RS and LS). Two issues have to be considered with this assumption. First this parameter is not the true leg extension, since it is not just the leg that is included in this expression (part of the upper body is included); additionally the leg is piston-like modelled, while the true leg extensions is affected by the knee and ankle angles. Secondly the sensors used to measure the positions are placed at the back of the skater and at the skates. These positions were assumed to be the CoM of these bodies, however the exact positions of the CoM is unknown (and may shift). This probably causes small errors between the modelled and measured data.

5.5.4.2 Kinematic assumptions

The model is a simplified representation of the skate movement. The double stance phase was therefore not included in the model. This phase however proves to be very short (Fintelman 2011). Furthermore the arm movements were neglected; however the model only simulates the straight part at steady speed, where the arms are mainly placed on the back of the skater. Finally the opening of the clap skate is not included in the model, but (Houdijk, Bobbert et al. 2003) found that this only occurs at the last 50ms of the stroke, and will therefore be of reduced influence on the skating dynamics. Additionally the rolling and pitching motions of the upper body were neglected; these were assumed to be small, but quantitative data on this variable is to this date unavailable.

5.5.4.3 Physiological limitations

The inverse dynamic model is built without any consideration of muscles, rigid bodies or physiological characteristics of the speed skater. The model is therefore not suitable for the investigations of long term effects, due to for instance fatigue or rotations of separate body parts. These characteristics were irrelevant from a mechanical point of view, but will be important for future application of the model.

5.5.4.4 Measurements

The kinetic data used in this thesis is limited in terms of accuracy. This holds for both the position and force measurements and for the simulated vertical upper body motion. This may have led to errors between the modelled and measured data, mainly in the force estimate.

5.5.5 Practical use of the model

The ultimate goal of the dynamic skater model is to provide skaters with feedback on their skating technique in order to improve their performance. The model as such is not sufficient to provide this feedback. At this point, the model can provide insight in the influence of several variables on the skating technique; for instance the influence of the ice and air friction or mass of the skater in relation to the leg extension (according to the definition used in this report) or the influence of the upper body movement on the performance of the speed skater. Additionally, the forces and moments at the skates can be analysed and the power assimilated in different directions can be estimated.

5.6 Preliminary conclusion

However exploratory, the constructed simple three-dimensional skater model seems to do a good job of imitating forces and kinematics observed in actual speed skating for a skater during a whole straight part, using the changing distance between a mass modelled at the upper body and a mass modelled at the skate (leg extension) as an input. Despite its preliminary character, the reported research seems to indicate that that the skater could be modelled using only one mass at the upper body and two infinitesimal point-masses at the skates. These results are however based on the two-dimensional data available with limited accuracy and the simulated vertical upper body position. The results prove that the added third dimension is of large influence on the total power output of the model.

The results of this study cannot be taken as evidence for a synchronisation or distortion error in the data used in prior research, however the findings do imply a likeability of such an error.

Conclusion

The aim of this thesis was to develop a reliable and valid three-dimensional biomechanical model that simulates the motion of a speed skater, to gain insight in the skating technique. In order to prove the reliability of the model, the model needs to be verified. Thus, the second goal of this thesis was to accurately measure the 3D kinematics of a speed skater, concerning the 2D positions of the skates and the 3D position of the upper body.

In the comparative study performed (LPM, iGPS and Xsens), iGPS proved to be most accurate (6mm maximum error) for dynamically measuring the 3D positions. The accuracy of the system proved to be within the requirement for verification of the model (<50mm error). The iGPS data suffered from data gaps, which resulted in coverage of about 67% in time. Therefore the goal of accurate position measurements was accomplished, but not satisfactory. Concerning lean angle measurements, the Xsens (MTx) measurement system showed an accuracy of 5^0 (mean error) ; the required accuracy for verification (2.5^0) was not accomplished.

The results of the iGPS measurements showed a sinusoidal movement of the upper body in vertical direction with an amplitude of approximately 7% of the average body height throughout a straight part. Additionally the results showed indication of a different take-off point of the skates compared to prior studies. The results of this study cannot be taken as evidence for a synchronisation or distortion error in the data used in prior research, however the findings do imply a likeability of such an error.

The goal of the development of a reliable and valid three-dimensional model was not satisfied in this study, since the verification of the model with accurate data could not be performed. No complete dataset for the verification of the three-dimensional model was obtained in this study. The constructed three-dimensional model was therefore studied using 2D position data from the LPM system, forces measured with the instrumented skate, and a simulated vertical upper body movement. However exploratory, due to the inaccuracy of the used data, the three-dimensional skater model showed to do a good job of imitating forces and kinematics observed in actual speed skating for a skater throughout a whole straight part. Despite its preliminary character, the current study seems to indicate that it is possible to model the skater using only one mass at the upper body and two infinitesimal point-masses at the skates. The simulated upper body movements show that the power assimilated into the vertical direction is large compared to the total power output (23%). Therefore, the third dimension is a necessary addition to the two-dimensional skater model.

Recommendations

Considering future work in the field of research on speed skaters, this section holds some recommendations, based on the study performed. The recommendation section is divided into a practical part describing possible improvements on recording speed skaters. Additionally some recommendations for prospective research possibilities are employed.

7.1 Recording of speed skaters.

7.1.1. Position measurements

The current study shows that the position measurements performed with an iGPS measurement system are accurate, but not satisfying, due to the coverage of the system; the data contain many data gaps. Possible solution to this problem would be sensor fusion of the iGPS data with data obtained from for instance an inertial sensor. This was not accomplished in the current study due to the lack of Xsens data. Additionally the sensors at the skates suffered badly from ice reflections; these influences might be reduced in the new release of the iGPS hardware and software (Nikon 2013), which are more robust.
The fiducial based tracking measurement system still is a promising system for the position measurements in sports. The recommendation is to further develop this system in order to test its accuracy in speed skating.
Recommendation for the local position measurement system, which is currently installed at the ice rink, would be to adjust the applied Kalman filter in the hardware, since the current study implies a possible position distortion or synchronisation error potentially introduced by this filter.

7.1.2. Lean angle measurements

None of the tested lean angle measurement systems reached the accuracy necessary for verification of the skater model. The current measurement system applied (Xsens) could be improved by introducing a recalibration moment. Prior knowledge is necessary to find a moment where recalibration is possible. Additionally in the future a wireless system would be a requirement.

7.1.3. Synchronisation

The main issue of recording speed skaters in this study occurred in the synchronization of the (different) measurement systems. It would therefore be beneficial if all measurement systems could run on the same timestamp or have a global synchronization point. Additionally it is recommended when working with several measurement systems to design software (GUI) in order to instantly check all data at the field.

7.2 Prospective research

7.2.1. Upper body movements

The current study shows an upper body movement with an amplitude of 7% of the average height of the upper body during ice skating. Hereby is assumed that there is a linear relation between the average upper body height and the amplitude; however more data is necessary to confirm this assumption. The new insight into the movement of the upper body and possibility to quantitatively measure it, leads to several new research questions. The correlation between the amplitude of de vertical upper body movements and the performance of the skater could be useful in terms of performance improvement. Additionally factors as fatigue and skill-level of the speed skater could be analysed in terms of causality. Currently the pitching and rolling motion of the upper body were neglected, since these were assumed to be small. However there is no quantitative data on these rotations. Research on these rotations should establish if these rotations should be implemented in the three-dimensional model.

7.2.2. Take-off of the skate

The take-off of the skates found by iGPS measurements in the current study, show that the skate is hardly steering back before take-off. Accurate measurements on the exact heading of the skate during take-off will give important feedback to the skater; In case of a heading towards the upper body, the force applied might oppose the forward propulsion. In this case, knowledge on the point of take-off could provide the skater with a good handle to improve his performance.

7.2.3. Skater model

Although the three-dimensional skater model shows promising results, the model still needs to be verified with accurate three-dimensional kinetic data. When the model is verified, it is advised to add a graphical interface to the model. The skater can be supplied with feedback on his power output and kinetics. Additionally small adjustments can be made to the measured input to simulate what the influence is on the skating motion. Interesting point for the skate-equipment would be to see where the point of action of the force introducing the moment on the skate is located.

Further research should rebuild the model into an optimization model with constraints on physiological parameters (maximum power output and leg extension). This optimization should provide a comprehensive feedback that can be used by coaches and speed skaters, so validation of the model is possible in the future.

Appendix A Overview input and output

This appendix shows the necessary steps and variables in order to verify the biomechanical 3D model.

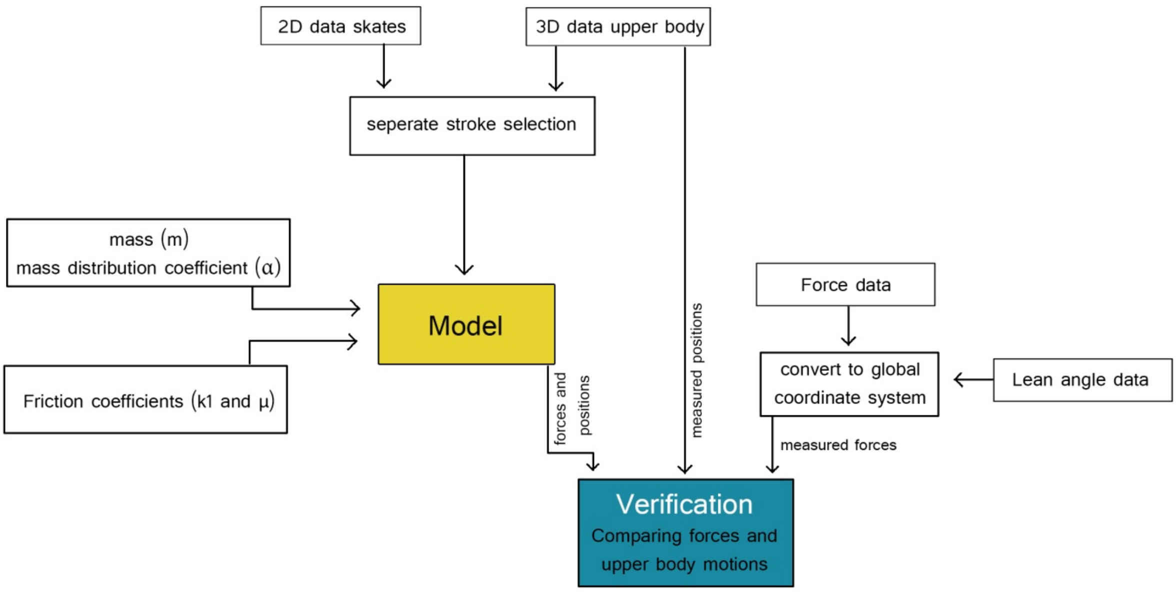

Figure 44 Overview of the variables and steps needed to verify the biomechanical 3D model.

Appendix B Instrumented Skate

This appendix describes the working principle of the measurement skate. In addition, the developments on the instrumented skates and its consequences for this research are described.

B.1 Working principle of the measurement skate

The measurement 'clap' skate measures the forces in three directions with a force platform. This platform consists of two Kistler three component piezoelectric sensors (KISTLER Force sensor with integrated Electronics, type 9602). The measurement skates are based on the dimensions of a normal speed skate frame.

The sensors have two different measurement ranges: Range 1: -5-5 kN and Range 2: -1000 – 1000 N with a sensitivity of approximately 1 and 5 mV/N respectively. The weight of the instrumented skates are approximately 36% higher compared to standard speed skates (about 1.4 kg)(Fintelman 2011).

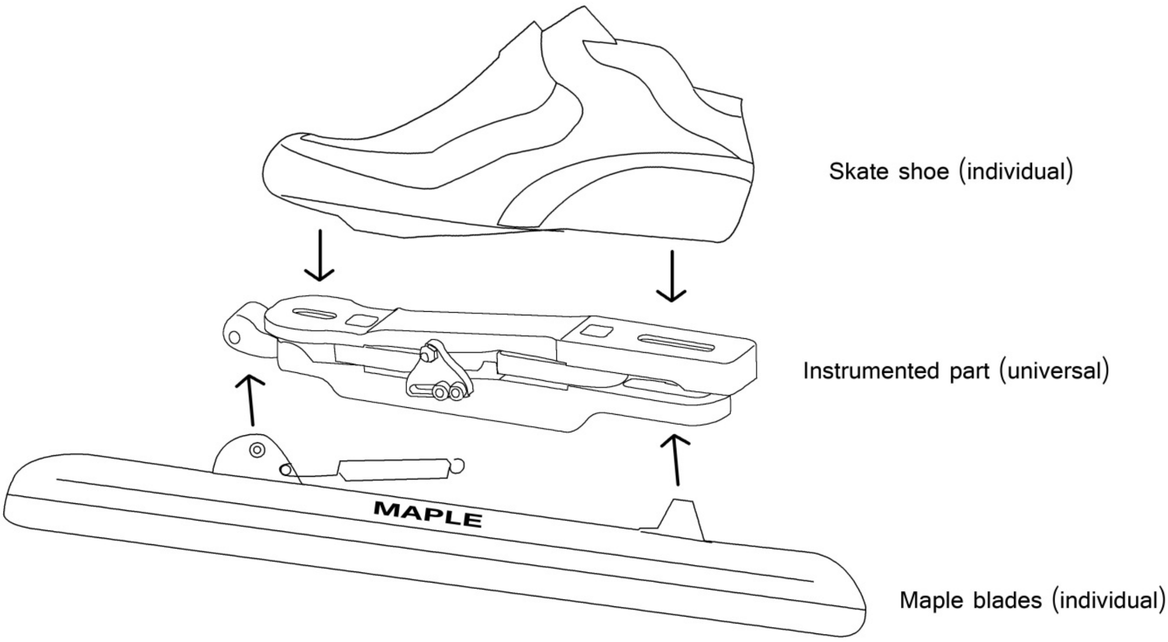

Figure 45 Assembly of (from top to bottom) the skate shoe, the measurement platform and the blade.

B.2 Developments of the instrumented skates

The newest development is a wireless system, integrated in the instrumented skate. This wireless system sends the coded measurements to a dongle in a laptop, where the code is decoded by the software (developed in Labview).

In order to install the wireless components, the measurement skate had to be disassembled. Disassembly requires new calibration of the sensors and adjusted preload. Due to pressure of time, the developers decided to only entail this preload (at 10kN), the calibration was postponed to after the data collection measurements for this research.

B.3 Consequences of the developments for the data collection research.

The instrumented skate did not perform in the most optimal way. The developments of the instrumented skates brought along the following problems and consequences for the data collection research:

1. Insufficient time to prepare the measurements, due to a pressured time schedule during the experiments before closing of the ice rink until the next winter season.
2. The measurement skate was un-calibrated;
3. Due to a design error in both the hardware and the software (of the wireless components) it was impossible to measure the lateral forces. Additionally the skate was only capable of measuring positive forces (in spite of preload);
4. The instrumented skates were only made available the last four possible measurement days.
5. The range of the wireless system was insufficient to measure the whole ice rink.
6. The buffer of the skates filled up very quickly as soon as the skates were out of reach, which resulted in software and hardware crashes and lost data.
7. The sample frequency of the measurement skate is not exactly 100 Hz, differed between the skates and lacked a synchronization signal (timestamp).

Appendix C Ode Solver and Coordinate projection method

In this appendix the steps taken by the Ode solver and the Coordinate projection method are visualized, see Figure 46.

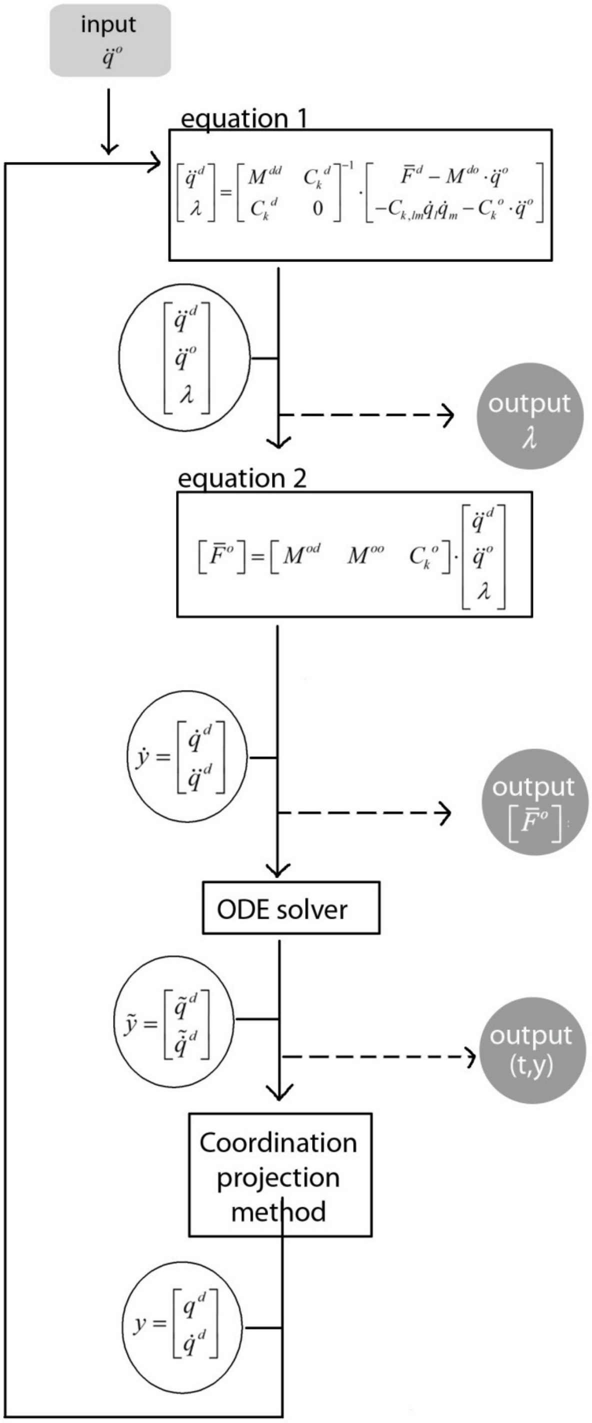

Figure 46 Steps taken in order to solve the differential equation.

Appendix D
Selected measurement systems

A literature study performed on finding accurate kinematic data of skaters on an ice rink, let to a couple of possible options to measure 3D kinematic data of skaters on an ice rink. These systems were selected based on the requirements and an applied Harris Profile. For further details on the selection I refer to (Kruk 2013). The four systems that performed best in the Harris Profile are:

- Local Position Measurement system (LPM)
- MVN suit
- Fiducial based tracking system
- Xsens (for lean angle measurement)

In addition to these systems, also the indoor GPS system (iGPS) was a promising option (Appendix E). The system is mainly very accurate in position. In literature it remained however unknown if the system was applicable for sports application.

The next part of this appendix describes the working principles of the measurement systems selected.

D.1 Local Position Measurement system (LPM)

This system consists of transponders which send out electromagnetic waves to the base stations. A main base station first sends out a trigger to the transponder, see Figure 47. This triggers the transponders to send out tagged electromagnetic waves to the other base stations. These signals are combined and the unknown positions are then found by Time-of-Flight (ToF) and triangulation. The same as for other systems, the LPM system needs at least four base stations to calculate the three unknown coordinates (3D-measurements). Although there is the possibility to have 3D measurements using LPM, the vertical accuracy is much smaller than the accuracy in the horizontal plane. Therefore the system will be considered as a 2D measurement system.

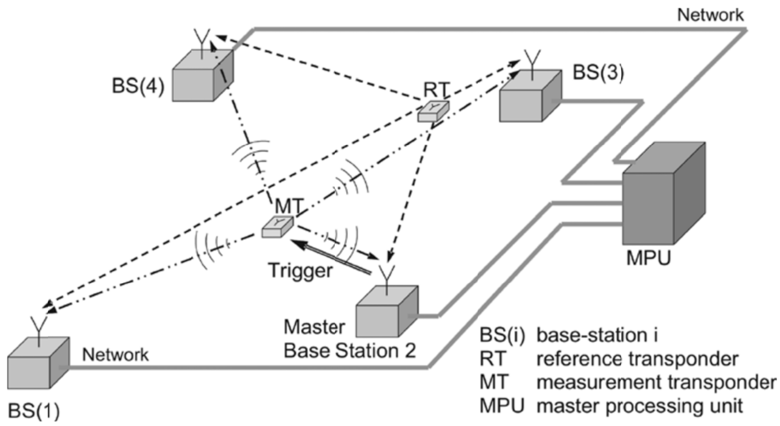

Figure 47 Basic arrangement of an LPM system. The master base station sends out a trigger to the transponder (MT). MT then sends electromagnetic waves to the basestations (BS). All data is collected via a network in the master processing unit (MPU). This figure is adapted from (Andreas Stelzer 2004).

D.2 MVN suit

One of the biggest manufacturers of wireless orientation sensors in the Netherlands is Xsens. On their webpage a lot of examples can be found of the application of the inertial sensor system. Their biggest product applied in the field of sports is the MVN suit (Figure 48): 'MVN BIOMECH is an ambulatory 3D human kinematic measurement system. Using state of the art MEMS inertial sensors, sensor fusion algorithms and validated biomechanical models, highly accurate kinematic data is generated (Xsens 2013)'. The system combines the information from the inertial sensors with a prescribed biomechanical model. In order to obtain secure data, measurements have to be taken of the speed skaters. These measurements are put into the model, which is then used to find the trajectories of the user. Unfortunately there was no MVN suit available for the research of this thesis.

Figure 48 Xsens MVN suit applied in rowing

D.3 Fiducial Based Tracking

Image processing is a method that analyses captured films or photos digitally (in contrast with manually video analysis(Brendle and Hoy 2011)). As opposed to the other measurement methods which are sensor-based, this method is a vision-based method using optical cameras and computer vision algorithms (Akman 2012). Together with inertial sensory systems, it is the most common applied measuring system in sports due to its little immobile and non-invasive technology and its capability to analyse very rapid motion. An example of application is event-detection in sports(Zhong and Chang 2004). Feature-based tracking algorithms use interest points in the frames to track the object. In case of fiducial-based feature tracking known-markers are used to track the object. This is usually more accurate than to detect natural features (e.g. existing corners or edges). 3D positions of the corresponding 2D marker features can be measured with very high accuracy. Negative point of marker-based tracking is that the markers must be put precisely in place before the experiment (grid set-up) and that occlusion of markers may occur.

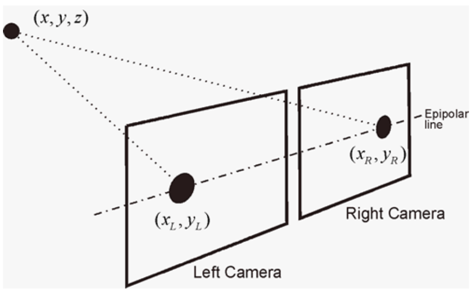

Figure 49 Stereo Vision for Fiducial based tracking

D.4 Inertial sensors (Xsens)

Inertial sensory systems use the tri-axial accelerations of the target; the speed and position can be found by integration of these accelerations. The system usually consists of an accelerometer, which wirelessly transmits 3D accelerations to the computer, and a gyroscope, which measures angular velocities (how fast an object turns); sometimes the inertial sensory system is supplemented with a magnetometer, to determine the heading. The system doesn't have a base station and is therefore the most mobile of all options. Additionally the system is capable of detecting very rapid motion(Zohlandt, Walk et al. 2012). A drawback is the drift which occurs due to integration of the data. Therefore the system is restricted to track only short-term movements. Still inertial measurement sensors are often used in the kinematic analysis in sports, due to that the system is superior in the measurement of fast dynamic movements and is non-invasive for the user. The system is for example already applied in the field of gymnastics (Zohlandt, Walk et al. 2012) and swimming (Lee, Burkett et al. 2011).

D.5 Indoor GPS (iGPS)

Indoor GPS makes use of the optoelectronic working principle. In contrast to what the name may indicate, the (physical) working principle is entirely different from the GPS system. The system has a transmitter which uses laser and infrared light to transmit position information from the transmitter to the receiver. This is a one-way procedure. This means that there is practical no limit to the scalability of the system. Each transmitter sweeps two fanned laser beams throughout the working area around its axis, see Figure 51. The centre of the two fan-shaped laser beams are separated by a certain angle and inclined by an certain angle. An infrared strobe pulse is emitted at the start of every other rotation (Depenthal 2010; Mosqueira, Apetz et al. 2012). Each sensor in the working volume receives the signals from the visible transmitters. The arrival time of the strobe and the two fans is measured by the sensor, see Figure 50. The measured delay between the fan beams is then used to estimate the position and the elevation of the sensor in space, knowing the tilt angles and the rotational speed of the fans, see Figure 51.

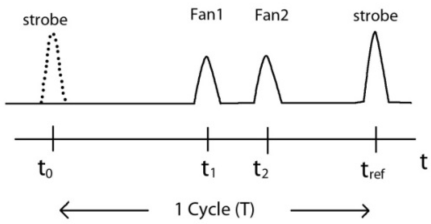

Figure 50 iGPS signal sequence of a transmitter. The sensor detects the fan1 and the fan2 beam with a certain time delay depending on the elevation of the object and the position of the object.

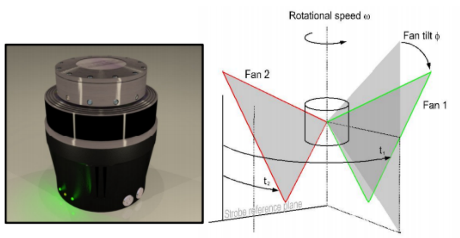

Figure 51 An iGPS transmitter (left) and a schematic representation of the rotating fan beams and their relative timing to the strobe (right), adapted from the report of NPL(Hughes, Forbes et al. 2012).

Appendix E Pilot study iGPS

This appendix describes the first pilot study on the use of iGPS

E.1 Introduction.

The literature study employed to select the kinematic measurement systems, eliminated the iGPS system initially from selection based on the cost requirements and the unknown specifications on performance in a true dynamic environment (Kruk 2013). The developer of the system, Nikon metrology, is however very interested in the applicability of the system in sport environments. At the start of 2013, Nikon ran a test with the iGPS system, measuring the performance of cars on the ice. This new perception let to new possibilities and insights for measuring ice skating. Therefore in consultation with Nikon, it was decided to run a first test with the iGPS system. The main goal of the test was to establish the workability with the measurement system and to get a rough indication on the accuracy of the system.

E.2 Research set-up and method

The pilot test took place in an indoor sports hall at the TU Delft Sports Centre. A set-up was established with four iGPS transmitters (Figure 52);a measurement bike (TU Delft), was used to measure accelerations and speed; additionally the bike was equipped with an iGPS sensor. The participant cycled through the transmitter area, while the Surveyor software sampled the iGPS data (100 Hz).

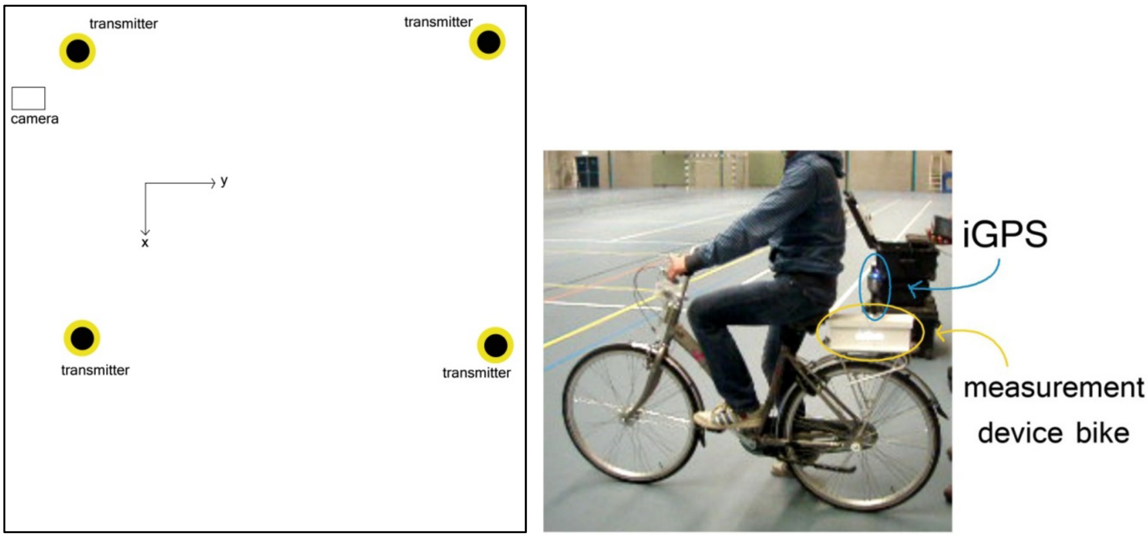

Figure 52 Left:set-up iGPS test; Right: measurement bike equipped with an iGPS sensor.

E.3 Results

E.3.1. Sensor

Nikon proposed two different sensors:

1. I5is (see Figure 53, left)
   This sensor is the latest sensor of the iGPS system. This sensor is completely wireless. It is capable of measuring lean angles, due to the fact that there are two sensors on top of each other.
2. I4is (single detector) (see Figure 53, right).
   The old sensors are smaller but need a wired component which contains the battery and the amplifier.

Figure 53 Indication of the sensor sizes. Left the new I5is wireless sensor, right the I4is wired sensor.

E.3.2. Position data

In Figure 54 the position data obtained by the iGPS sensor(I5is) on the measurement bike are drawn. Conspicuous are the gaps in the data. The point in time and the length of the gaps are given in Table 25.

Table 25 time gaps in the iGPS data from the sensor on the measurement bike.

Global Time [s]	Time Gap [s]
14.73	0.07
17.29	0.28
20.04	1.84
24.96	1.02
33.56	1.61

If we take into account only the straight part of the trajectory, we may assume that the height (z-position) of the iGPS sensors remains constant. In Table 26 and Table 27 the values are given for the straight parts in terms of vertical height (z) position of the iGPS sensor.

Table 26 Overall score for the frames 1:4000 (it was assumed that the height has to stay the same)

Average z-position [m]	Std z-position [m]	Max error [mm]	Min error [mm]
0.8767	0.0063	20.2	-12.7

Table 27 Straight part as given in Figure 54 (time 24.96:33.55)

Average z-position [m]	Std z-position [m]	Max error [mm]	Min error [mm]
0.8745	0.0071	18.0	-14.9

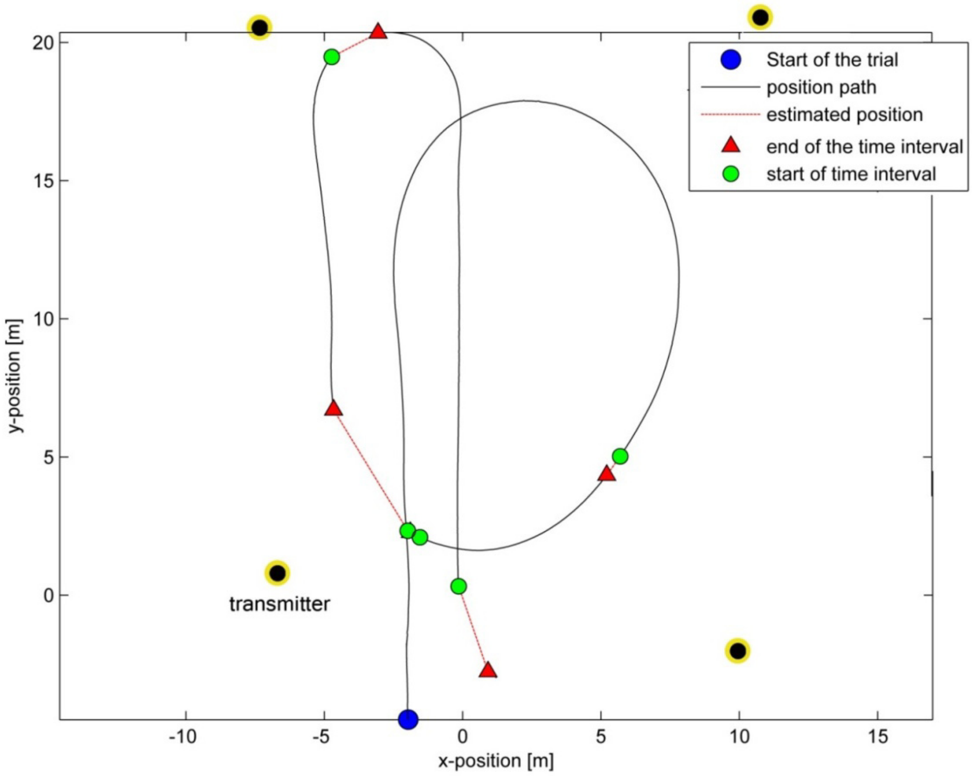

Figure 54 The position data obtained by the (I5is) iGPS sensor on the measurement bike.

E.3.3.   Velocity data

The measurement bike measured the velocities of the bike during the trials. In Figure 55 the velocities are plotted. The first striking fact is that the bicycle trial seems longer than the iGPS trial. Analysis of the data teaches that this is due to sudden resets in the iGPS data. These resets cause the timestamp to return to zero, therefore leaving the length of the time gap unknown, see the yellow triangles in Figure 56. The values of the velocities differ among themselves, however there is no knowing whether the measurement bike or the iGPS system is correct.

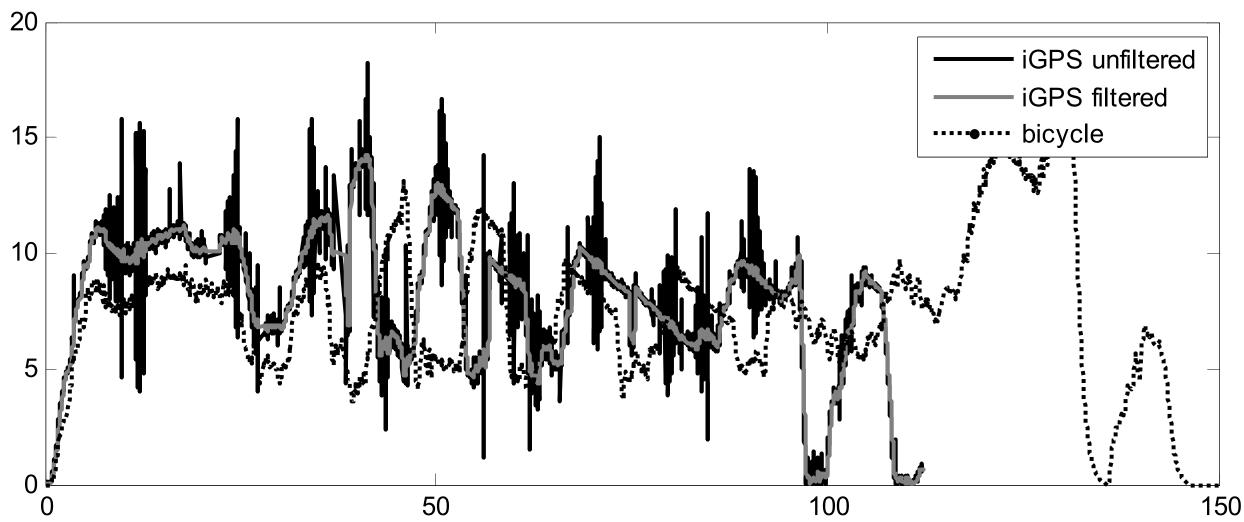

Figure 55 Filtered and unfiltered velocity data of the iGPS sensor and the velocity data of the bicycle.

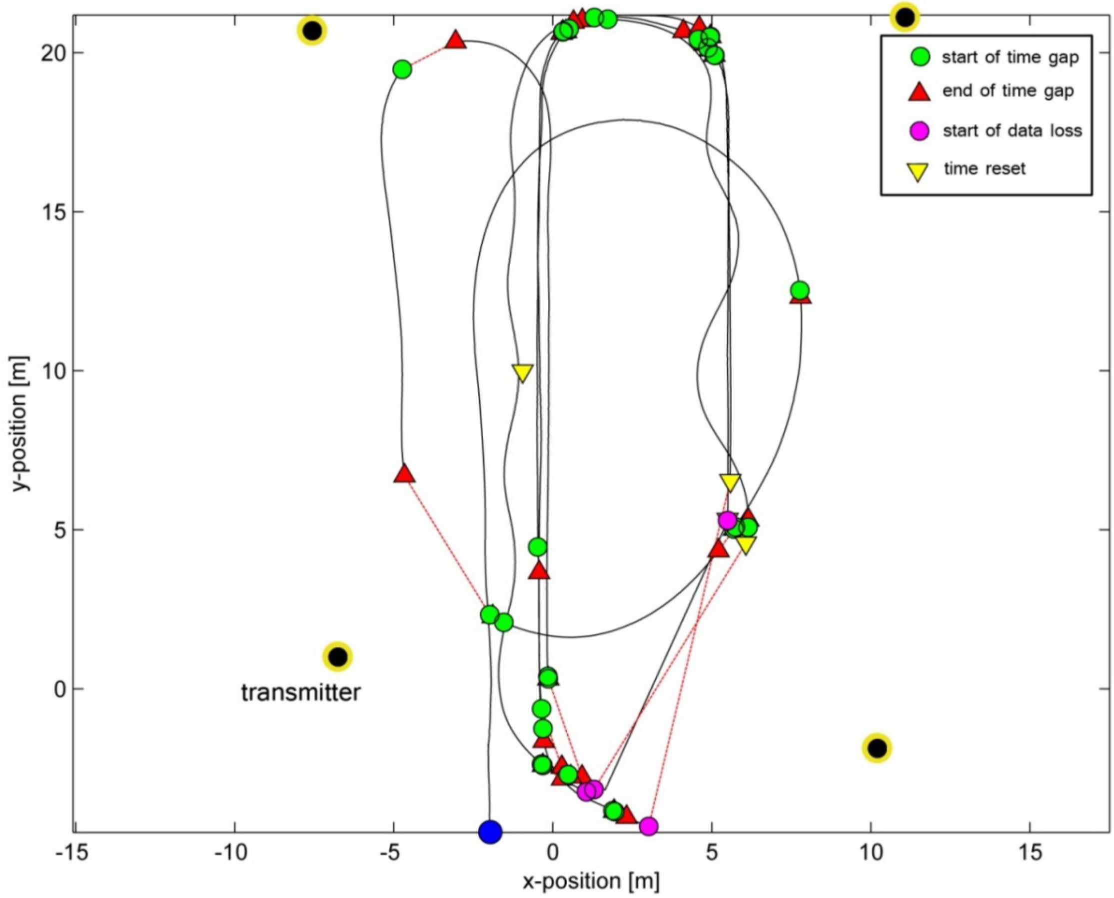

Figure 56 Measured data including the gap indicators and reset points.

E.4 Discussion

Since the iGPS I5is sensors are quit large and heavy, for the purpose of ice skating the I4is sensors are better applicable, see Figure 53 .

The main issue found are the gaps in the data,ranging from 0.07 to 1.84 seconds. A smaller gap is easily fixed by use of interpolation, however larger gaps should be prohibited. Cause of the data gaps are a line-of-sight problems. These problem might be resolved by adding transmitters, or adjusting the set-up. Second issue is the fact that the system seems to reset itself a couple of times. The drawback of the reset is that the timestamp goes back to zero and therefore the length of the occurred time gap is unknown. This is unacceptable when measuring kinematic data, certainly when there are several measurement systems involved. In order to prevent this trouble, a global clock should be installed.

E.5 Conclusion

For the ice skating research, the i4is sensors should be utilized. Gaps occur in the data as soon as the sensor loses line of sight. Therefore more transmitters should be placed and the arrangement of transmitters should be optimized. To increase synchronization feasibility, a global clock, should be installed to prevent the system from resetting. This timestamp has been incorporated into the software after this pilot study.

Appendix F Development Image Processing

This appendix describes the development of the image processing set-up. Since this is the only system that is completely new and undeveloped for ice skating research, the whole procedure is described. The set-up is depending on the required characteristics and the available equipment.

F.1 Variables

In fiducial based tracking there are a number of variables that can be changed in order to adjust the configuration (the independent variables, Table 28). The requirements for the set-up can be expressed in terms of the dependent variables, Table 29. In order to fulfil the requirements, the independent variables need to be adjusted.

Table 28 Independent variables

Variable	Unit	
Focal length (f)	[mm]	Distance from the lens to the sensor, when focused on a subject at infinity.
F stop (fstop)	-	The focal length divided by the diameter of the lens. For example, a 200mm f/4 lens will be 50mm wide.
Sensor size (sscd)	[m]	Size of the sensor of the DSLR.
Pixel size	[µm]	Pixel size of the camera.
Objectsize	[m]	Size of the object that needs to be tracked.
Working distance (s)	[m]	Distance between the object and the camera.

Table 29 Dependent variables

Variable	Unit	
Depth of field (DoF)	[m]	Distance between the nearest and farthest objects in a scene that appear acceptably sharp in an image.
Far limit DoF (D_F)	[m]	Furthest point at which the image is acceptable sharp.
Near limit DoF (D_N)	[m]	Nearest point at which the image is acceptable sharp.
Field of view (FoV)	[m]	Describes the extent of a given scene that is imaged by a camera.
Object Pixel Size	[pix]	Size of the object in pixels on the sensor.

F.2 Requirements

The fiducial based tracking system needs to capture the 3D kinematics of the speed skater on the ice rink. The system designed in this section is implemented in the ice rink of Thialf, Heerenveen.

F.2.1 Object pixel size

The object pixel size is an important variable when it comes to the analysis of images. The object pixel size determines the robustness of the system. The requirement for the set-up is therefore that the object pixel size needs to be at least 5 pixels.

F.2.2 Field of view

The field of view describes the extent of the given scene that is imaged by a camera. When the camera is not moved, this field of view should cover the whole ice rink. However in case the cameras are moved or turned, the FoV is less important, since the FoV will move along with the object.

F.2.3 Depth of Field

The depth of field determines the area (in depth) that yields a sharp picture. The Depth of field is determined by the far and near end of the depth of field. In case of the ice rink, we can define the relationship between these variables. We assume we first want to measure the straight part, using a turning camera. We can then define the relationship between the far and near end of the DoF, see Figure 57:

(F.1.1) $$D_{f\_necessary} = \sqrt{2500 + (D_n + 10)^2}$$

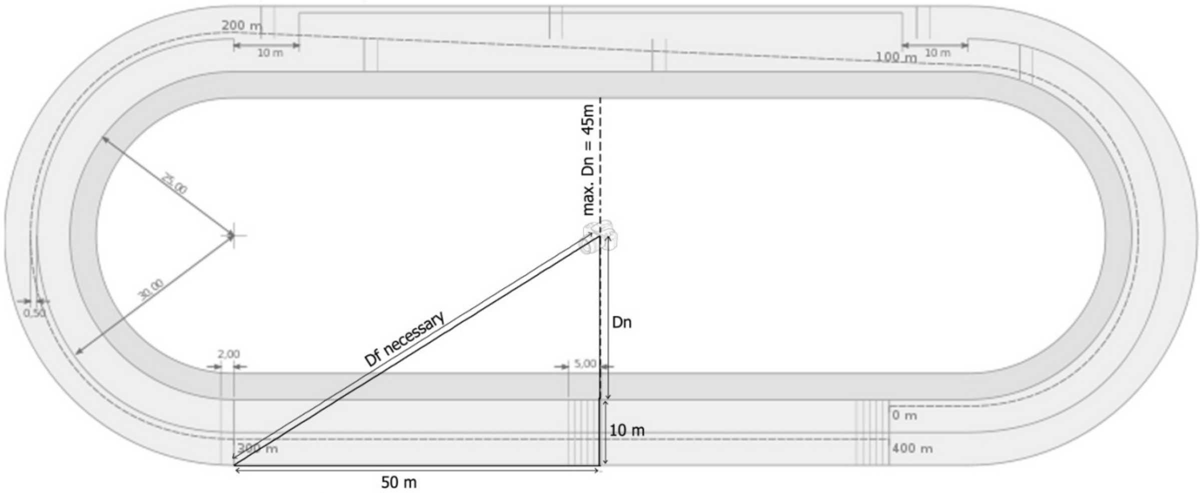

Figure 57 Relation between the far and the near end of the DoF.

F.3 Available equipment

F.3.1 Camera properties

The company DVC machine vision offered a pair of cameras to use in the position accuracy study. The cameras available were Basler aviator cameras, with the specifications as given in Table 32.

Table 30 Camera specifications of the Basler Aviator cameras

Camera	Sensor	Sensor Size	Pixel size	Framerate
avA1600-	Kodak KAI-	2/3''	[5.5, 5.5]	55 fps
avA1900-	Kodak KAI-	2/3''	[5.5, 5.5]	51 fps

F.3.2 Lens properties

Using the specifications of the available cameras, the lens options can be determined. We first determine the restriction based on Figure 57:

(F.1.2) $D_f > D_{f\_necessary}$, while $D_n < D_{n\_\max}$

Where D_{n_max} = 45 meter, due to the size of the ice rink. And D_N and D_f are specified as

(F.1.3) $$D_N = \frac{sf^2}{f^2 + Nc(s-f)}$$

(F.1.4) $$D_F = \frac{sf^2}{f^2 - Nc(s-f)}$$

Where N is the lens f-stop, c is the circle of confusion, f is the focal length and s is the distance at which the camera is used.

Results of possible lens properties, based on the restrictions, are summarized in Table 31. The lens f-number (the f-stop) is an indication of the amount of light available for the sensor. Since the image capturing will be done inside, a large diameter (so a small f-stop) is preferable. Additionally the $D_{f\_necessary}$ should be small, since the object pixel size will decrease when the distance between the camera and the object increases. This reasoning in combination with the available lenses, led to the decision to use a 50 mm f1/1.4 lens.

Table 31 Possible lens properties based on the requirements and given restrictions.

Lens f-number	focal length [m]	Df_necessary	Far limit (Df)	Near limit (Dn)	Working distance (s)
1.40	0.03	58.22	61.58	19.83	30
1.80	0.03	56.61	60.65	16.55	26
2.00	0.03	55.96	57.96	15.13	24
2.80	0.03	54.58	63.17	11.88	20
4.00	0.03	53.37	55.94	8.66	15
5.60	0.03	52.68	66.40	6.60	12
1.40	0.04	63.34	65.00	28.89	40
1.80	0.04	60.71	61.69	24.43	35
2.00	0.04	59.75	60.35	22.71	33
2.80	0.04	57.41	60.64	18.20	28
4.00	0.04	55.34	55.54	13.72	22
5.60	0.04	54.09	58.34	10.64	18
8.00	0.04	53.11	60.29	7.92	14
11.00	0.04	52.50	64.27	6.01	11
1.40	0.05	69.07	70.15	37.65	49
1.80	0.05	65.71	67.49	32.64	44
2.00	0.05	64.46	66.58	30.68	42
2.80	0.05	60.73	61.47	24.47	35
4.00	0.05	57.91	59.13	19.21	29
5.60	0.05	55.94	58.55	15.09	24
8.00	0.05	54.39	57.06	11.40	19
11.00	0.05	53.38	54.27	8.70	15
16.00	0.05	52.66	75.60	6.52	12
1.80	0.06	70.60	70.85	39.84	51
2.00	0.06	69.12	69.91	37.72	49
2.80	0.06	64.60	65.50	30.91	42
4.00	0.06	60.76	61.09	24.53	35
5.60	0.06	58.23	61.51	19.84	30
8.00	0.06	55.96	57.86	15.14	24
11.00	0.06	54.62	60.64	11.97	20
16.00	0.06	53.37	55.64	8.67	15
22.00	0.06	52.70	60.80	6.66	12
2.00	0.07	74.15	74.78	44.76	56
2.80	0.07	68.54	68.70	36.89	48
4.00	0.07	64.02	64.83	29.98	41
5.60	0.07	60.65	62.40	24.32	35
8.00	0.07	57.84	60.36	19.08	29
11.00	0.07	55.94	58.67	15.09	24
16.00	0.07	54.35	59.36	11.31	19
22.00	0.07	53.36	57.11	8.63	15
2.80	0.08	72.77	72.92	42.87	54

4.00	0.08	67.63	69.38	35.54	47
5.60	0.08	63.35	64.96	28.90	40
8.00	0.08	59.75	60.29	22.72	33
11.00	0.08	57.47	59.30	18.33	28
16.00	0.08	55.34	55.39	13.73	22
22.00	0.08	54.13	55.83	10.73	18
4.00	0.085	69.14	69.79	37.75	49
5.60	0.085	64.62	65.36	30.94	42
8.00	0.085	60.78	60.90	24.56	35
11.00	0.085	58.30	60.12	19.99	30
16.00	0.085	55.98	57.49	15.17	24
22.00	0.085	54.62	60.07	12.00	20
5.60	0.1	69.07	70.12	37.66	49
8.00	0.1	64.46	66.53	30.69	42
11.00	0.1	61.09	63.65	25.10	36
16.00	0.1	57.91	59.02	19.22	29
22.00	0.1	55.99	56.92	15.21	24
22.00	0.2	69.19	69.53	37.83	49

F.3.3 Object size

In order to fulfil the requirements of the Object Pixel size of 5 pixels, the object size, which is the fiducial size can be determined. The variables that influence the object pixel size are (in addition to the camera properties), the focal length and distance between the object and the camera. The object pixel size of 5 pixels, should be maintained at every position on the rink. The furthest found position necessary ($D_{f\_necessary}$) is therefore the boundary value for the choice of the fiducial size. In Figure 59 the object position is plotted against the focal length. From this we can conclude that in the situation of a focal length of 50 mm, a fiducial with the a minimum size of 4 cm is required, in order to have an objectpixelsize of 5 pixels at the maximum distance of 70 meter. The pixelsize of a 4cm marker differs along the track, which can be seen in Figure 58.

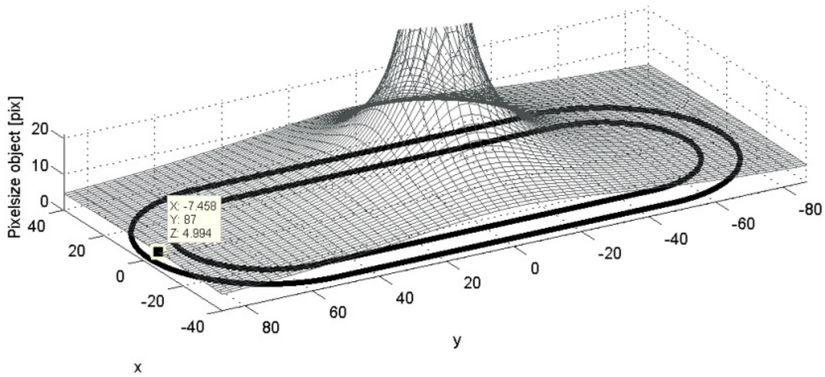

Figure 58 Grid of the objectpixelsize dispersal along the track.

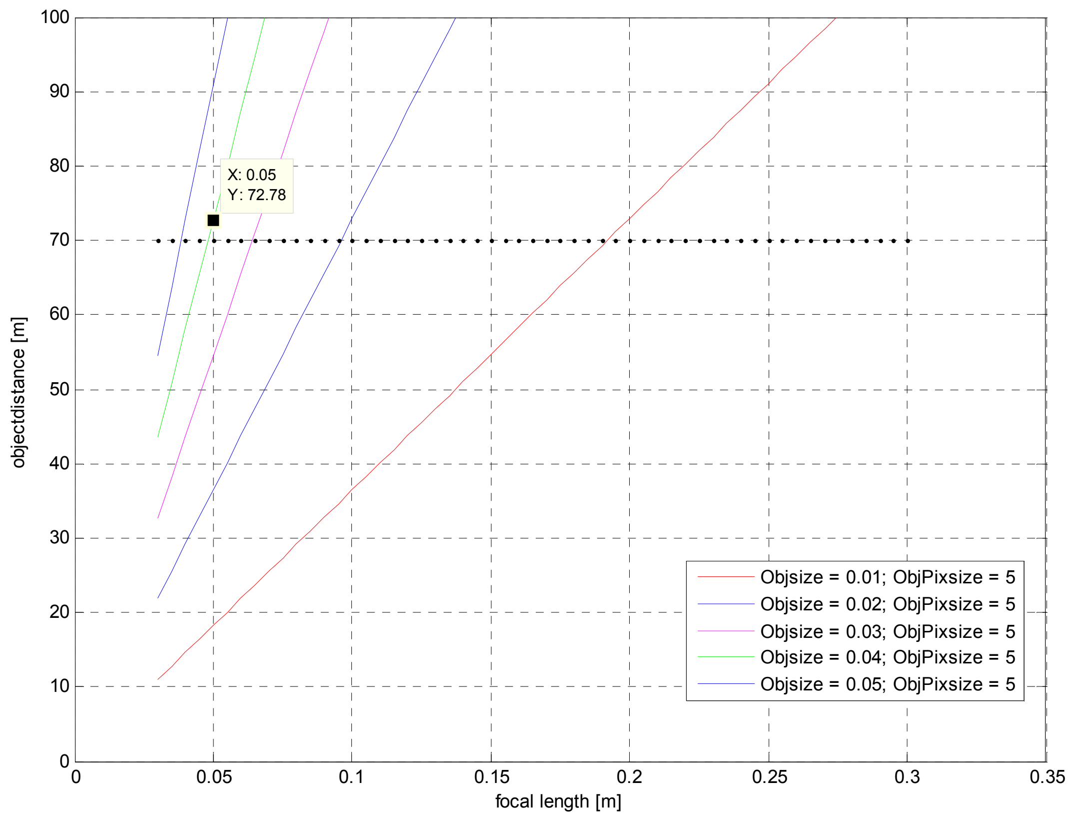

Figure 59 Necessary objectsize at different object distances against the used focal length, with the requirement of a objectpixelsize of 5 pixels.

F.4 Research set-up

F.4.1 Field of View

The camera specifications together with the lens specifications, determine the field of view of the camera. The field of view is increased by a decreasing focal length, see Figure 60.

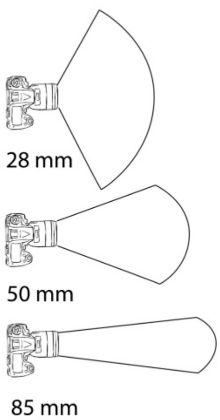

Figure 60 Field of view of the cameras based on the focal length of the lens.

In order to determine the field of view at a specific point in space, we use the formulas

(F.1.5) $$M = \frac{f}{f - s}$$

(F.1.6) $$FoV = \frac{sccd}{M}$$

In which f is the focal length, s is the working distance and sccd is the sensor size in m. The FoV obtained is either the width or the height of the field of view, depending on the parameter given as sccd (the width of the sensor determines the width of the FoV, the height of the sensor determines the height of the FoV). So the FoV is increased by either increasing the working distance, increasing the sensor size or decreasing the focal length.

Using this formula to obtain the FoV for our situation, we obtain a field of view of 23.15 meters width and 15.5 meters high at the working distance of 49 meters. In Figure 61 the field of view is shown as beams and the ring with the near and far end of the DoF is shown.

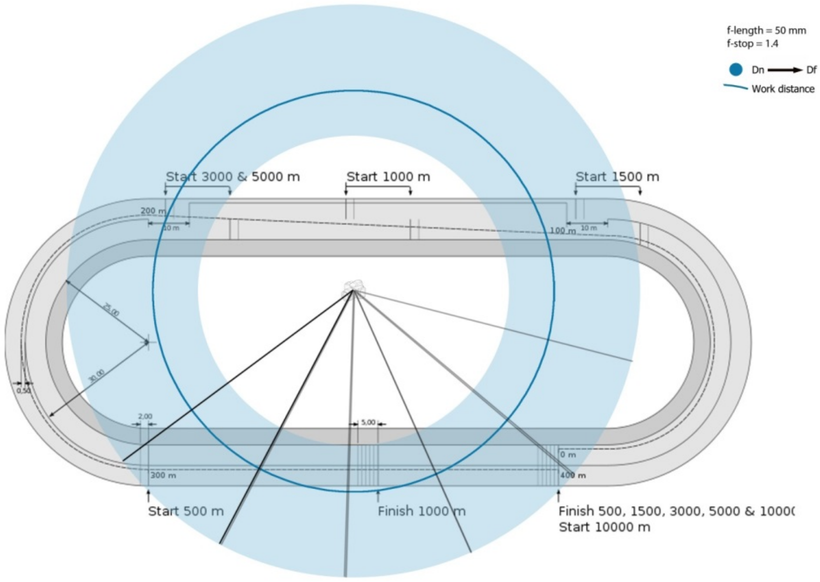

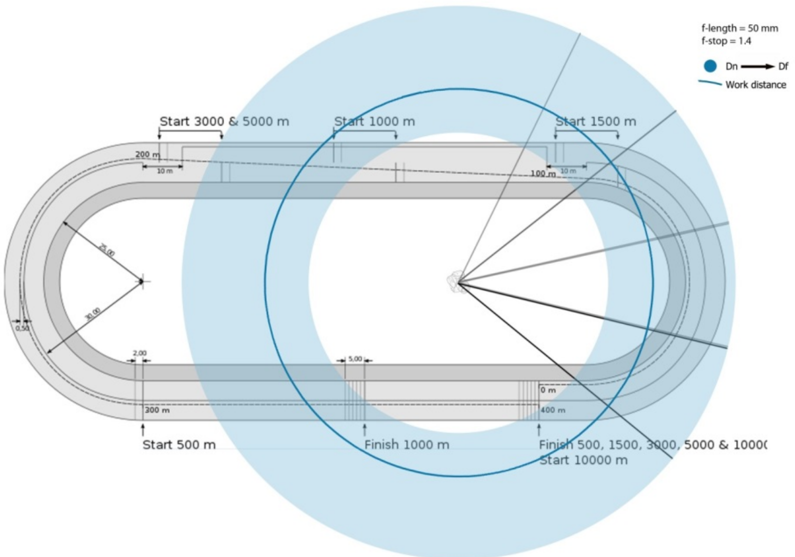

Figure 61The field of view of both camera placements.

F.5 Lean Angle using FBT

The FBT system is capable of tracking lean angles of targets by using deformations in plane. In case of measuring the lean angle of a skate, it is possible to measure the lean angle using a grid. Placing a grid on the skate and the blade of the skate enables us to make triangles out of the intersections. By using three markers of the grid, the angle can always be measured by means of deformation, see Figure 62. If the grid from the picture is tilted by an (lean) angle α, the deformation shown in the front view (camera view) is deformation d.

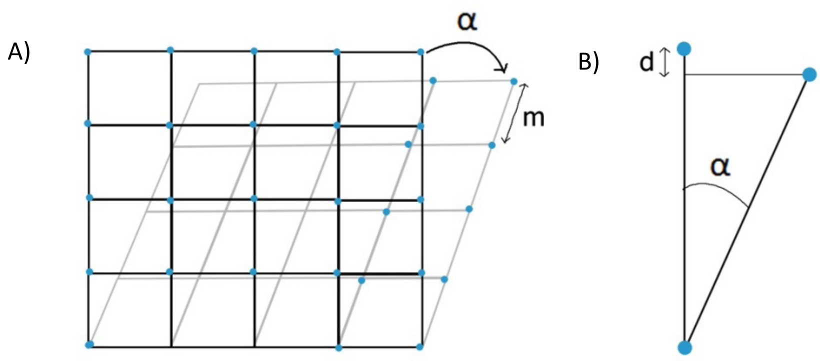

Figure 62 A) Grid that could be placed on the skate. B) Angle at which the grid is moved.

(F.1.7) $$d = m - m\cos(\alpha)$$

The minimum lean angle needs to have an accuracy of 2.5 degrees. In the graph of Figure 63 the marker distance is plotted versus the shown displacement in the camera view plane when the minimum lean angle of 2.5 degrees is applied. This graph shows that the displacement will be really small when a realistic marker distance (m) is applied.

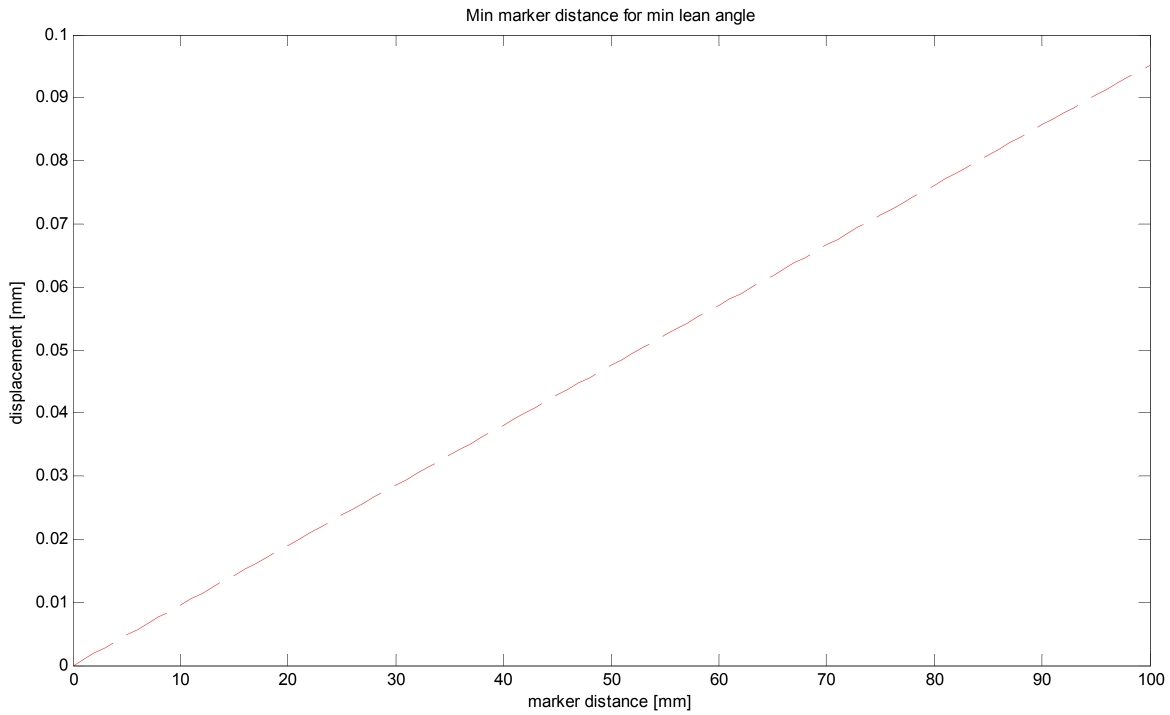

Figure 63 Marker distance versus displacement in the camera view.

In order for the cameras to notify the displacement, we know that the displacement at least has to be around 10 mm for a distance of 30 m. In order to then find an accuracy of 2.5 degrees in lean angle, we can conclude from Figure 64 that the marker distance has to be around 100 m, which of course is an unreal distance.

Therefore we may conclude that it is not possible to find an accurate enough lean angle with the FBT in the volume of an ice rink.

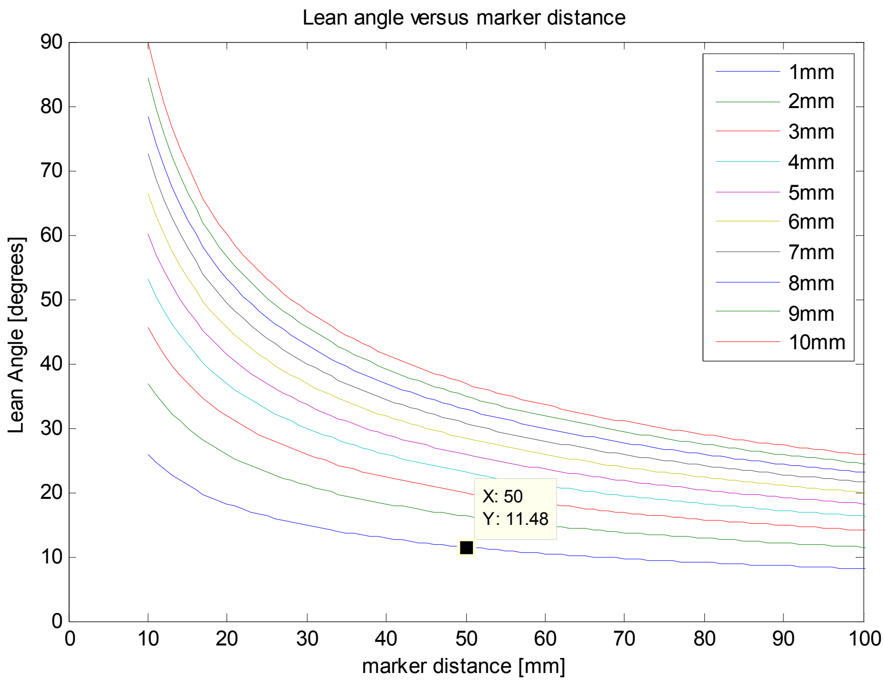

Figure 64 The Lean angle is given as function of the marker distance. The different lines indicate the different displacements (d).

F.6 Design of the ficucials

F.6.1 Criteria of the fiducials.

In order to track the speed skater, several criteria for the design of the fiducials can be taken into account, based on (Owen, Xiao et al. 2002):

- An ideal fiducial should support the unambiguous determination of position of the CoM (3D) and skates (2D) and orientation of the skates (roll or lean angle) relative to a calibrated camera.
- The fiducial should not favour some orientations over others.
- The fiducial must be a member of a set of images that are unlikely to be confused such that a large space or set of objects can be uniquely marked.
- The fiducial must be easy to locate and identify using fast and simple algorithms.
- Fiducials must function over a wide camera capture range.
- The Fiducials have to create a robust system that can handle some occlusion.

F.6.2 The fiducials

Three kind of fiducials were designed: one with different size of squares in order to determine what accuracy (size of square) is possible in this huge volume; one which is a square marker using large squares; and one that is a round marker, still using a square in the middle. The markers were made in different colors, such that the right marker could be chosen during the field test (Figure 65).

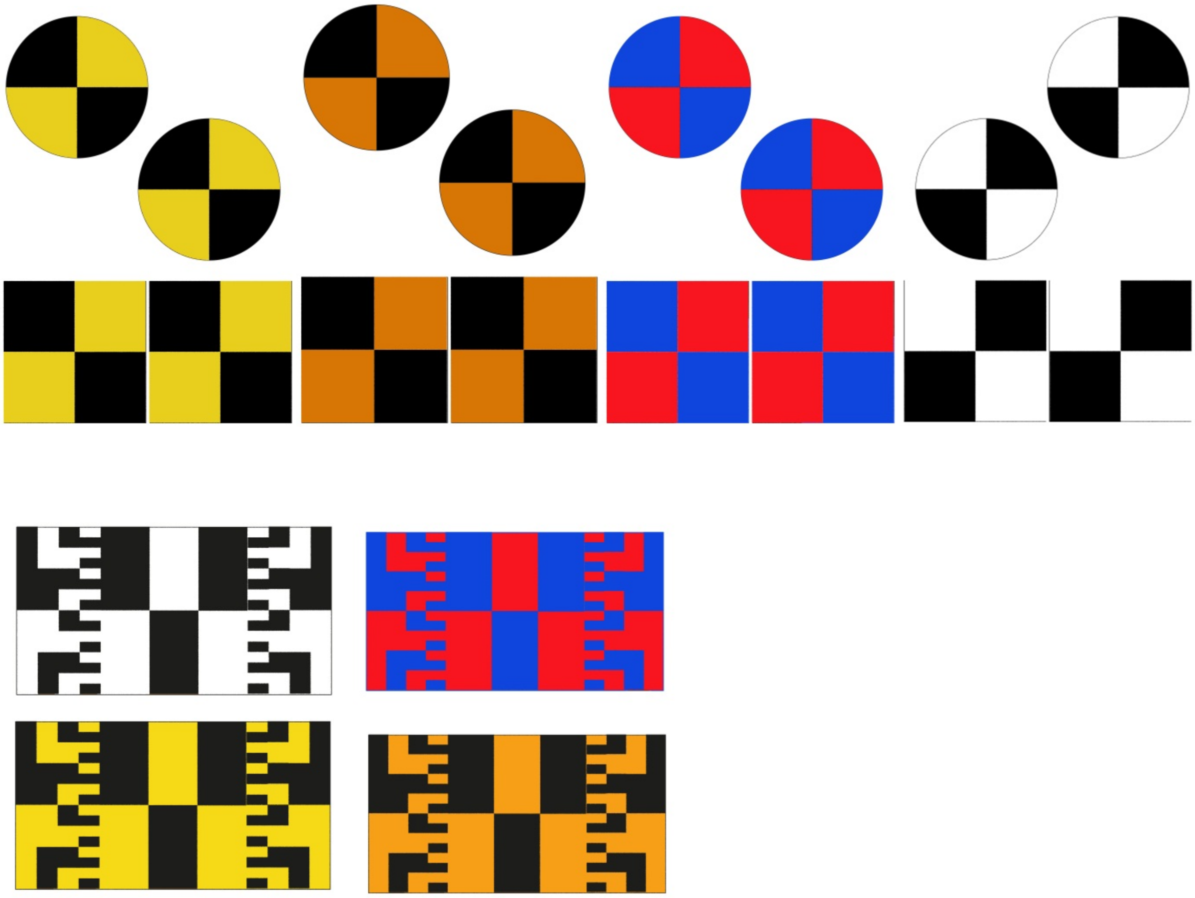

Figure 65 Fiducials designed and printed for the ice skating research. The upper markers were just to track position, the lower markers could indicate what the accuracy of the position measurement was. The markers were all printed in different colors, such that the right color could be chosen during the research.

Appendix G
Results for the image processing measurement system.

The procedure and design of the FBT measurement system is incorporated in Appendix F. This appendix describes the outcome and recommendations concerning the FBT measurement system.

G.1 Outcome of FBT system

The FBT was the only measurement system in this test that was completely undeveloped at the start of this thesis. The system has captured all trials and tests. The first step in determination of positions based on FBT is the calibration of the measurement system. This was done using a large checkerboard pattern, as shown in Figure 66. MATLAB has an integrated image processing toolbox in order to calibrate the captured calibration photos. This tool was used to calibrate both cameras. The projection errors obtained for both cameras by this tool are given in Figure 67.

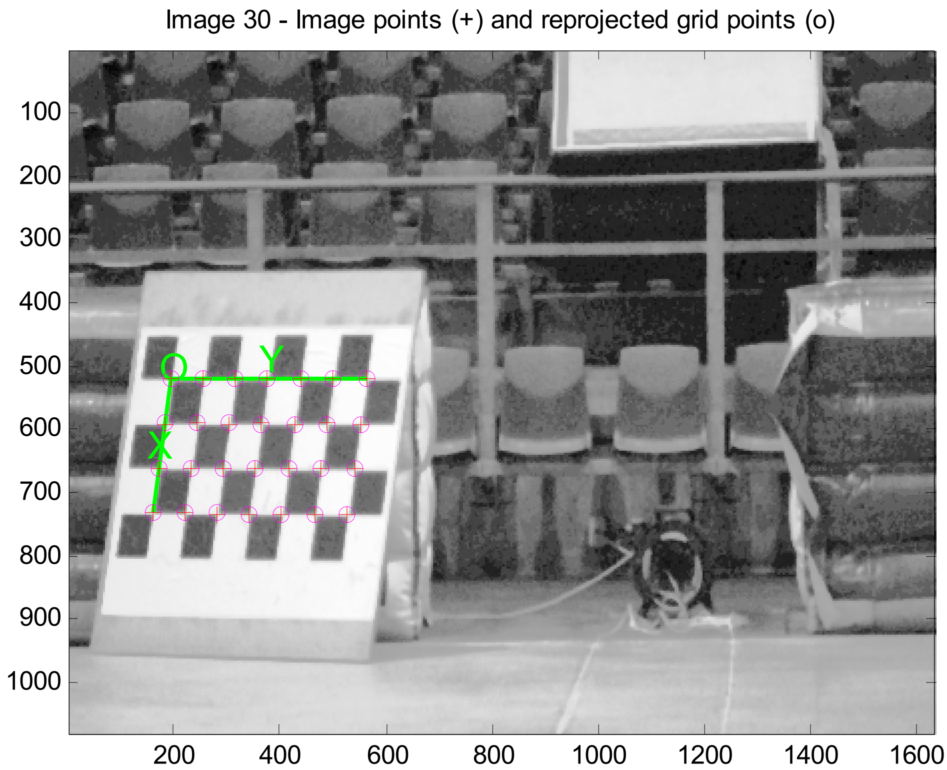

Figure 66 Checkerboard pattern and angle determination points provided by MATLAB for the FBT calibration.

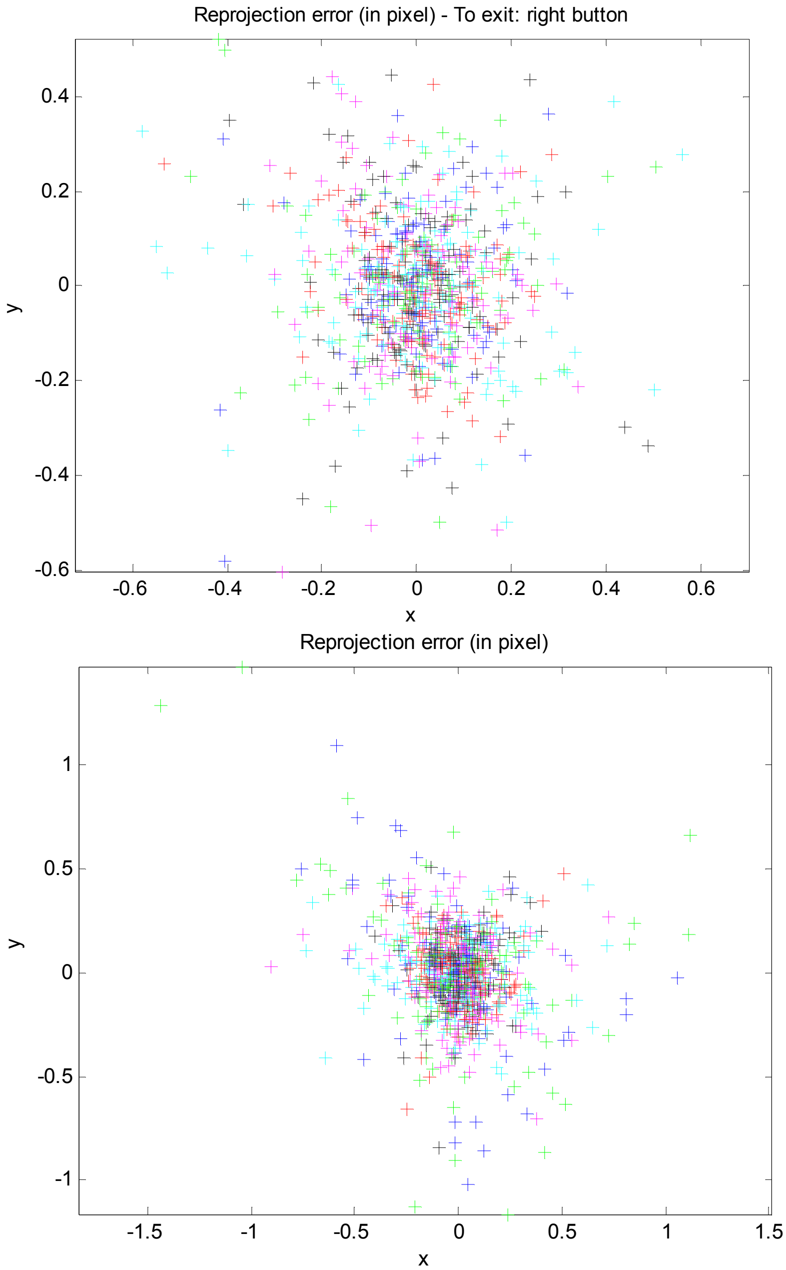

Figure 67 Reprojection error of both the right and left camera qfter calibration of the cameras.

G.2 Decision on the FBT measurement system

Although the calibration of both cameras show a promising result, combining both cameras into stereo vision results in large errors. The cause of this problem is still unknown. Since the error obtained by the iGPS system proved to be very small in the test and due to the fact the developing the FBT measurement system and solving the bugs would require many working hours, it was chosen for this thesis the leave the further development and evaluation of the FBT system for future research.

G.3 Recommendations

All data needed to establish the accuracy of the FBT measurement system in static and dynamic (skate) tests are available in the digital appendix. These data can be used for further analysis by improving and optimizing the image processing algorithm.

Appendix H
Static measurement research protocol

In this appendix the measurement method and protocol is described for the static test.

H.1 Research set-up

The research set-up is described in A.1.1. Figure 68 offers some additional set-up information.

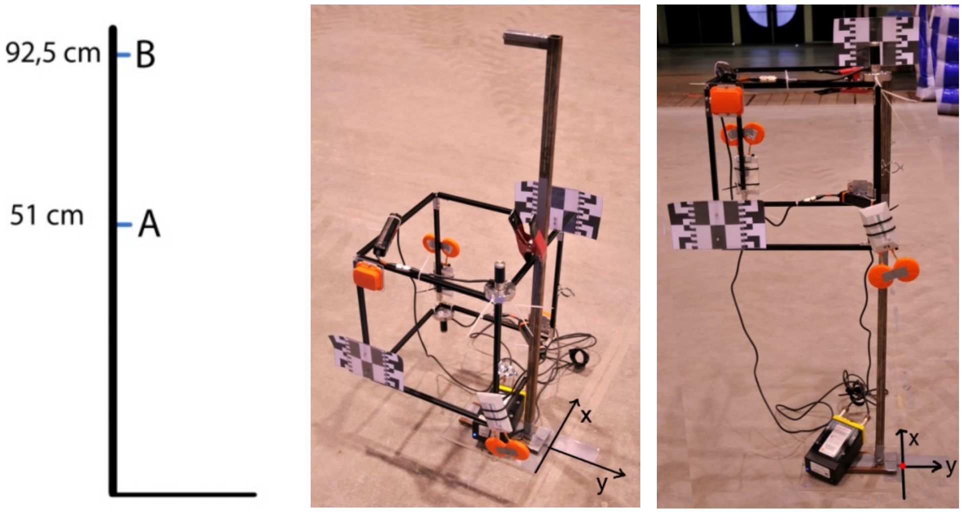

Figure 68 Left: Different height positions of the measurement cube. The top of the cube is placed on this position. Left: Orientation of the measurement cube on the ice rink. 1. is the measurement cube in height position A, 2. is the measurement cube in height position B.

H.2 Fiducial based tracking set-up

The cameras used in this test are specified in Table 32. The set-up determination can be found in Appendix F (Figure 70). The cameras were placed on a tripod with an attached dual mount rig (Figure 69). The accuracy determining black and white fiducials were chosen, since the background of the rink was blue.

Table 32 Camera specifications of the Basler Aviator cameras

Camera	Sensor	Sensor	Pixel size [µm]	Framerate
avA1600-50gm/gc	Kodak KAI-02050	2/3''	[5.5, 5.5]	55 fps
avA1900-50gm/gc	Kodak KAI-02150	2/3''	[5.5, 5.5]	51 fps

a.
b.

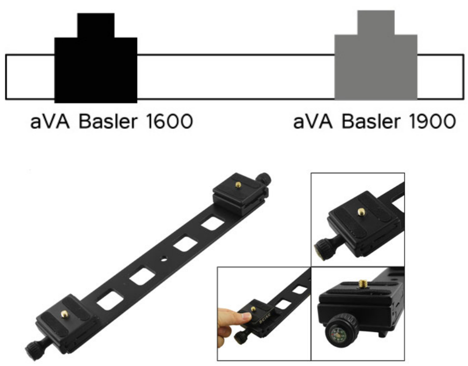

Figure 69 a. Camera placement on the dual mount rig on the tripod. B. the dual mount rig

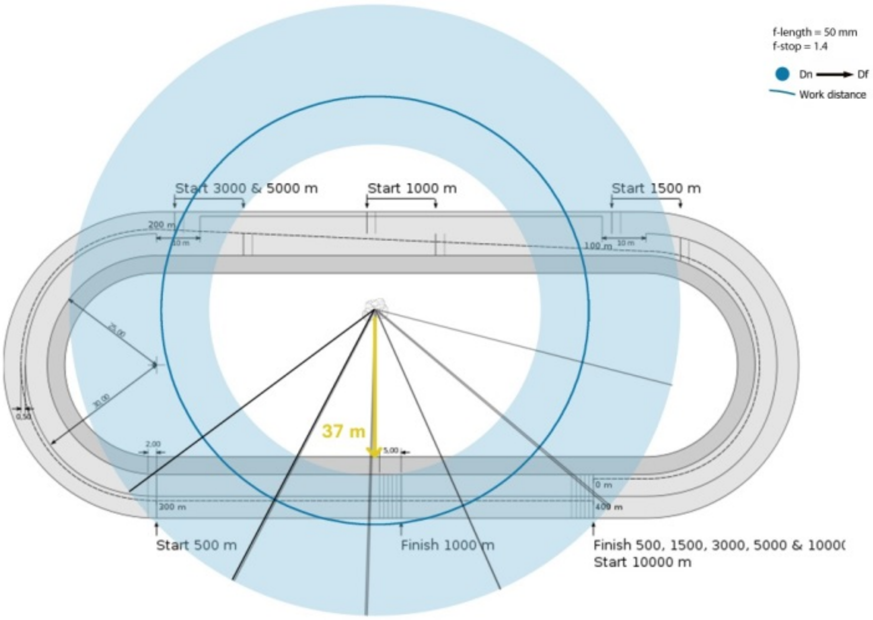

Figure 70 Camera set-up for the Fiducial Based tracking system.

H.3 Indoor GPS set-up

The Nikon transmitters were all placed on tripods for this test (Figure 71). The transmitter height was therefore 1.2 m. Eight transmitters were used. The transmitters were placed in such a way that both the straight part and the curve could be covered (Figure 71). The Nikon iGPS system used single detectors (I4is) (Figure 53).

.

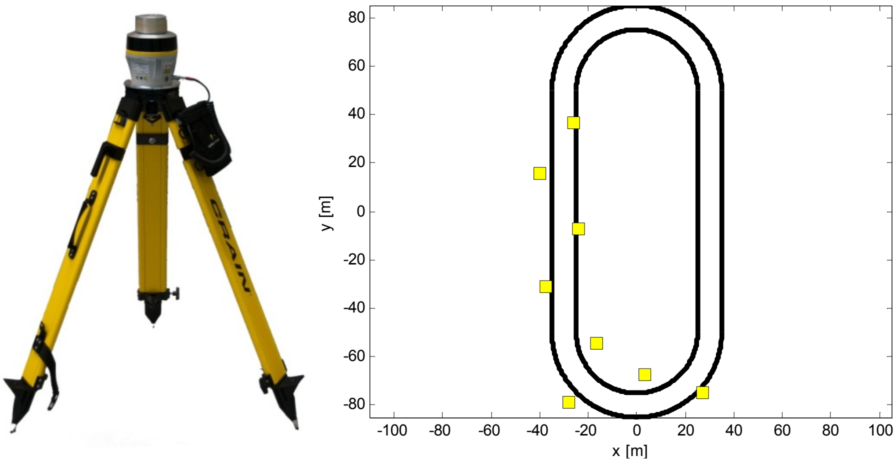

Figure 71 Nikon iGPS transmitter on tripod and their placement. The dimensions of the ice rink are indicated with the black line, the yellow squares are the iGPS transmitters.

H.4 LPM set-up

Thialf (Heerenveen) is the only ice rink equipped a LPM system (Inmotio). The system consists of 12 base stations which are connected by a fiber optical network with a central master processing unit. In this unit the position evaluation and final object tracking is done. The software of LPM itself exports the data to the wanted sample frequency. The data is then exported to Excell.

Appendix I Dynamic measurement research protocol

In this appendix the measurement method and protocol is described for the dynamic test.

I.1 Research set-up

The research set-up is described in section A.2.1. Figure 72 and Figure 73 offer some additional set-up information.

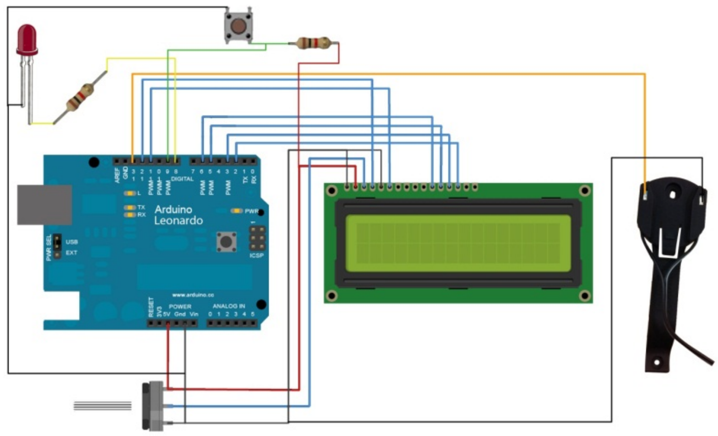

Figure 72 Arduino datalogger; components used: Arduino Leonardo, LED, cycling computer, 10kΩ resistance, push botton, potentiometer, LCD screen, Arduino SD shield.

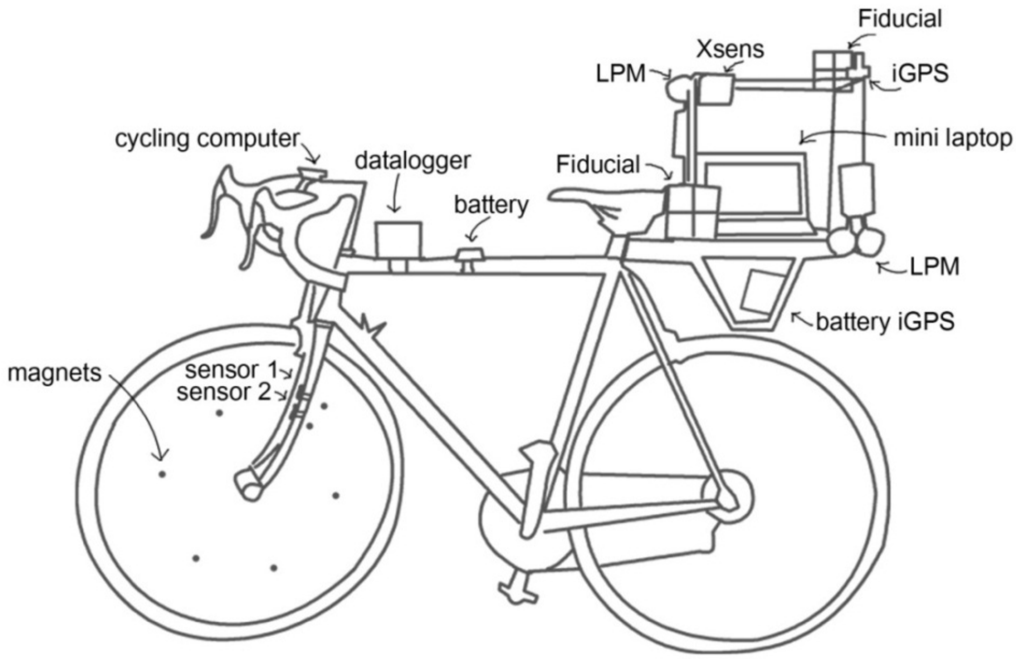

Figure 73 Equipped bicycle as used in the dynamic experiments .

I.2 Test protocol

Straight part protocol

1. For means of synchronisation the bike is moved back and forth in order to obtain a recognizable data point in the data of the cycling computer and the other measurement systems, see Figure 74.

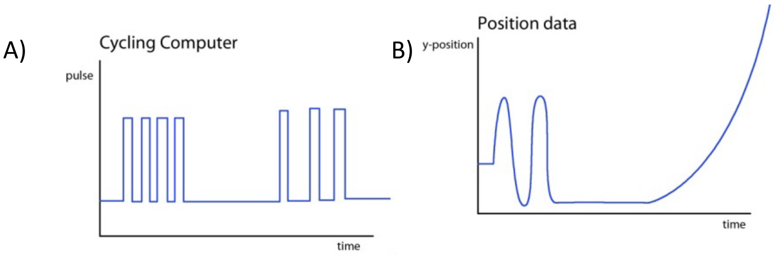

Figure 74 Synchronisation in the first time stamps. A) The Cycling computer gives short pulses; B) the position data show the forward and backward movement.

2. The cyclist gets on the bike and cycles at a speed X.
3. The cyclist makes three rounds at this speed.
4. Only the straight part on one side of the rink is used in the data analysis (Figure 75). The cyclist rides along a cord that is placed on the rink to maintain a straight trajectory (see Figure 75).

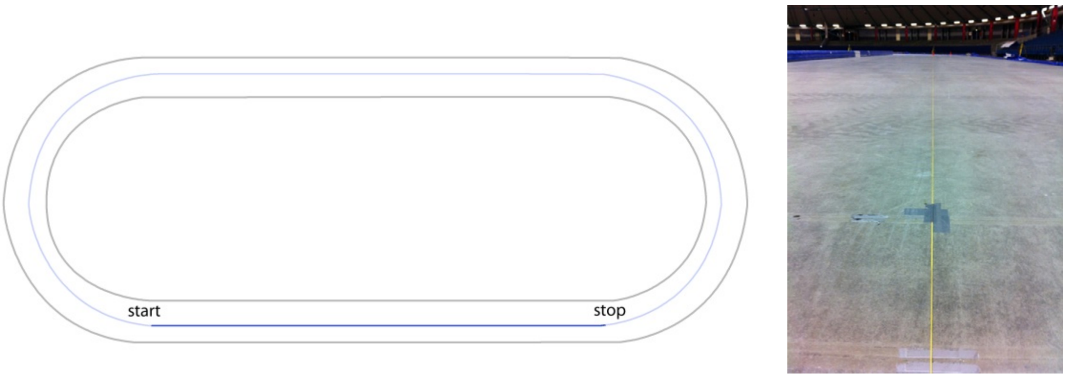

Figure 75 Part of the ice rink that is measured for the straight part measurements; The straight contains a Ccrd for the cyclist to maintain a straight trajectory.

5. Finally the cyclist does one more straight without pedalling (coasting); the speed should go down smoothly and a deceleration should be the result.
6. This protocol is repeated at least 3 times for each speed.

Curve Protocol

The protocol for the curve was the same as for the straight part, with the exception that there is no line to follow, but three cones that indicate the next point of the trajectory.

I.3 Fiducial based tracking set-up

See Appendix H.

I.4 Indoor GPS set-up

The set-up of the iGPS system was according to the set-up described in Appendix H. The transmitter placement is shown in Figure 76 .

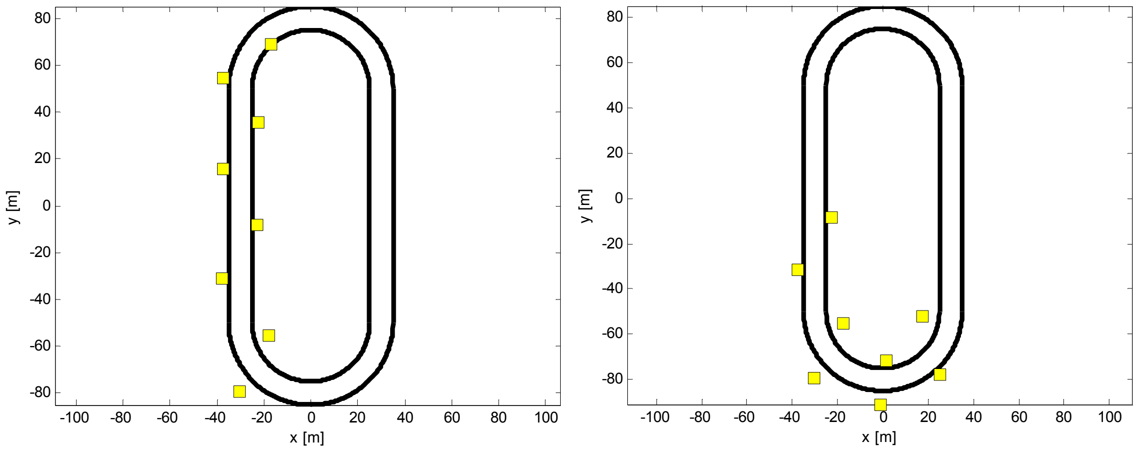

Figure 76 Transmitter positions for the straight measurements (left) and for the curve (right). The dimensions of the ice rink are indicated with the black line, the yellow squares are the iGPS transmitters. All transmitters are placed at the same height.

I.5 LPM set-up

See Appendix H.

I.6 Xsens set-up

The Xsens sensors used in this test are the Mtx and MTi-G 3DOF orientation sensors. The sensors consist of an accelerometer (full scale +/-50 m/s^2, 3d gyroscope (full scale +/- 300 deg/s) and 3d magnetometers (full scale +/- 750 mGauss). The system fuses the sensor information to calculate 3d information. Finally all data is internally filtered with a Kalman filter. All USB cables of the Xsens sensors were connected to the mini laptop, the sensors were running on the Xsens software during this test.

Appendix J Dynamic research results

This appendix contains extended results from the dynamic measurements.

J.1 Removing outliers

The method used in this report for removing the outliers is by use of the z-scores of the distribution, which are simply a way of standardizing the data-set. The data sets are first converted into z-scores using formula (J.1.1).

$$z_i = \frac{X_i - \overline{X}}{s} \tag{J.1.1}$$

Where X_i represents a single data point, $\overline{X}$ is the mean of all data points and s is the standard deviation. This z-score is used to count how many data points fall within important limits. If we take the absolute value of the z-score (i.e. we ignore if the z-score is positive or negative), then we expect that the z-score for only 5% of the points is higher than 1.96, and 1% to have absolute values greater than 2.58 (assuming a normal distribution). We expect none to be greater than 3.29, if this is the case, this data point is assumed to be an outlier and removed from the data set(Field; 2005). In order to remove the outliers, 5 iterative steps are taken.

J.2 LPM Dynamic relative position accuracy results

Table 33 Relative position variables for the LPM system at 15 km/h.

Relative 15 km/h Linear	Mean [mm]	STD [mm]	Max abs error [mm]
Test 1.1	648.4	158.3	381.5
Test 1.2	616.8	150.9	381.6
Test 1.3	601.0	146.5	305.8
Test 2.1	611.0	168.8	433.0
Test 2.2	616.2	156.5	467.5
Test 2.3	636.5	106.3	311.0
Test 3.1	570.7	92.2	251.5
Test 3.2	623.9	76.5	157.1
Test 3.3	626.0	102.0	278.3
All tests	616.7	128.7	329.7

Table 34 Relative position variables for the LPM system at 25 km/h.

Relative 25 km/h Linear	Mean [mm]	STD [mm]	Max abs error [mm]
Test 1.1	619.8	135.8	313.5
Test 1.2	605.6	127.9	328.6
Test 1.3	611.7	136.1	298.2
Test 2.1	619.0	110.9	251.7
Test 2.2	599.3	153.9	370.4
Test 2.3	581.9	134.5	311.2
Test 3.1	655.1	145.0	324.0
Test 3.2	619.6	130.3	344.2
Test 3.3	619.6	112.7	267.0
All tests	614.6	131.9	312.1

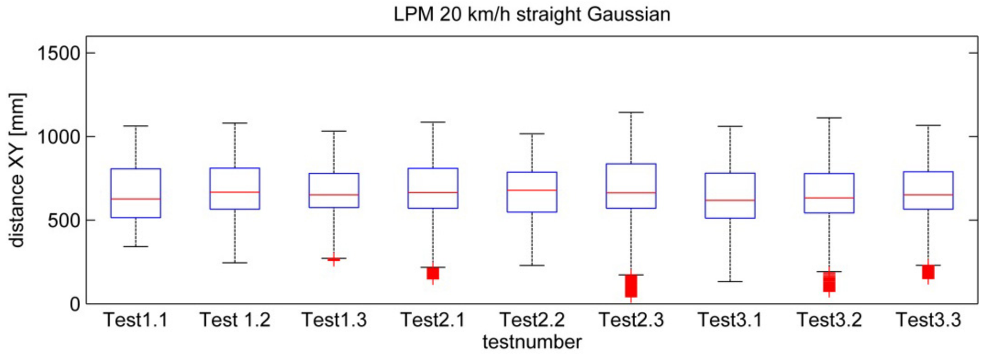

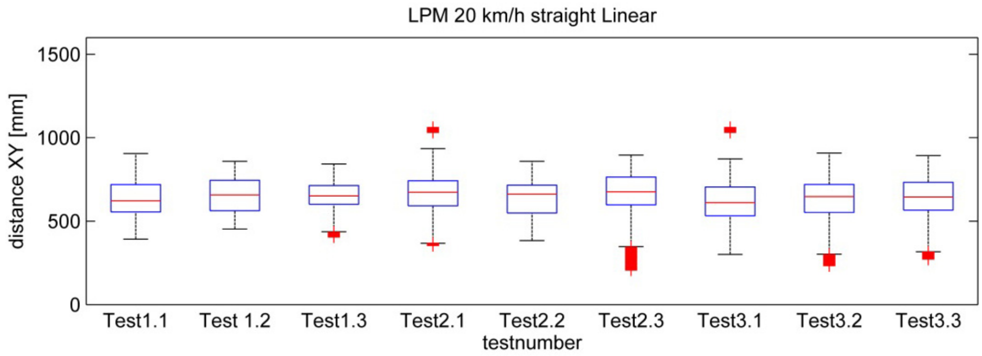

Figure 77 Boxplot indicating the relative distance between sensor 1 and sensor 2 (2D diagonal). This test was performed at the straight part of the rink with a speed of 20 km/h. The upper graph shows the data that is filtered with a Gaussian filter, the lower graph shows the results of the data filtered with a Linear filter.

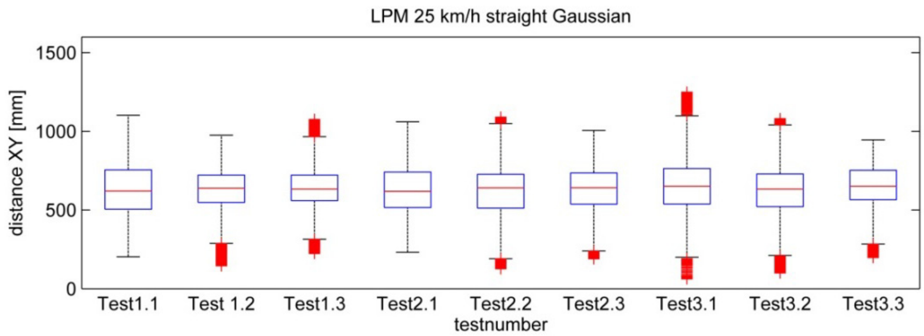

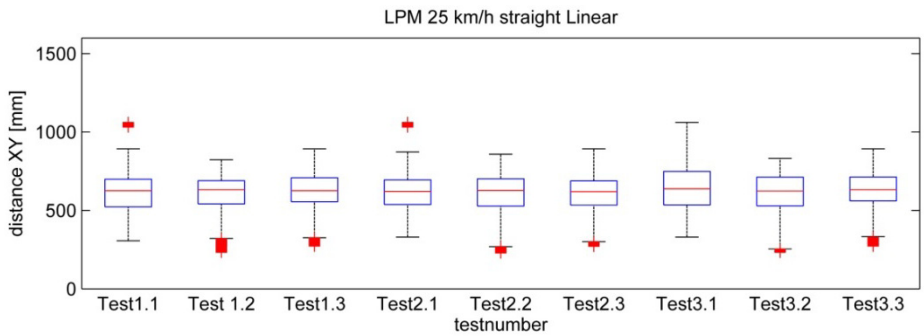

Figure 78 Boxplot indicating the relative distance between sensor 1 and sensor 2 (2D diagonal). This test was performed at the straight part of the rink with a speed of 25 km/h. The upper graph shows the data that is filtered with a Gaussian filter, the lower graph shows the results of the data filtered with a Linear filter.

J.3 iGPS Dynamic relative position accuracy results

Table 35 Data output from the iGPS system for the dynamic straight trials. The relative position between the two sensors, the 3D diagonal, is given.

Relative Position	Mean [mm]	STD [mm]	Max error (abs) [mm]
15 km/h			
Test 1.1	567.3	0.89	3.0
Test 1.2	567.3	1.08	4.3
Test 2.1	579.9	1.5	5.6
Test 3.1	567.2	1.35	4.3
Test 3.2	567.1	1.35	4.3
All tests	569.8	1.2	4.3
20 km/h			
Test 1.1	566.6	1.26	4.4
Test 1.2	566.99	1.35	3.9
Test 2.1	602.4	1.57	5.0
Test 2.2	601.3	1.61	5.3
Test 2.3	601.6	1.55	5.0
All tests	587.8	1.5	4.7
25 km/h			
Test 1.1	567.0	1.86	6.4
Test 1.2	567.0	1.7	6.2
Test 1.3	566.9	1.53	5.0
All Tests	567.0	1.7	5.9

J.4 LPM dynamic relative velocity accuracy results

In addition to the position data, there is the velocity data obtained from the LPM software. The relative velocity is the difference between both sensors, which should be zero. The results show that the relative velocity differs over -0.5 m/s to 0.5 m/s, using a Linear filter.

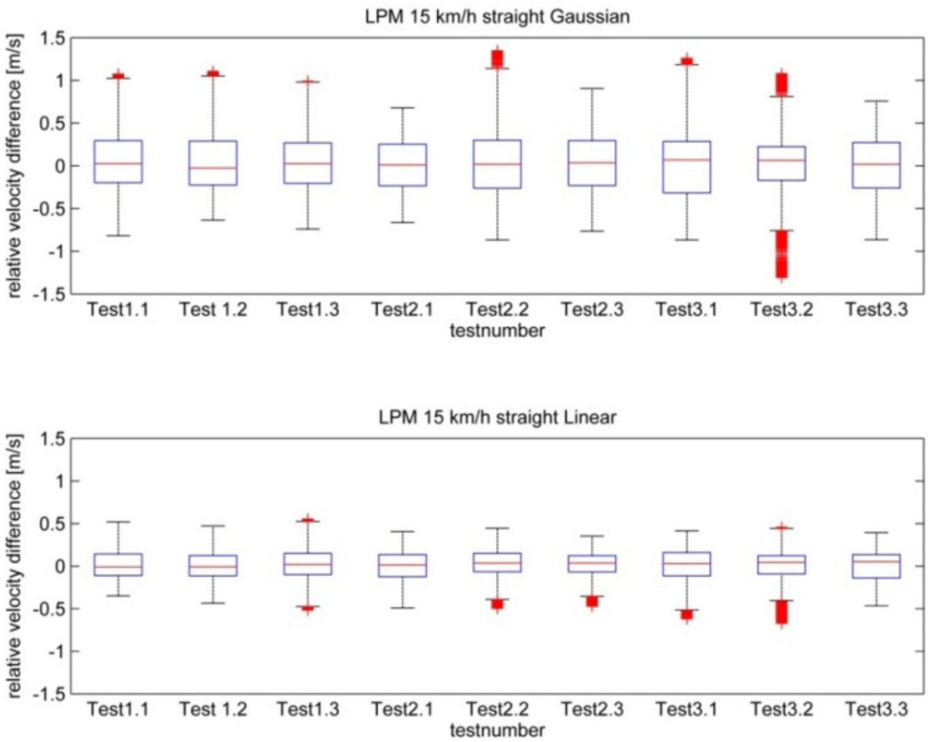

Figure 79 Boxplot indicating the relative velocity between sensor 1 and sensor 2. The relative velocity between the sensors should be zero. This test was performed at the straight part of the rink with a speed of 15 km/h. The upper graph shows the data that is filtered with a Gaussian filter, the lower graph shows the results of the data filtered with a Linear filter.

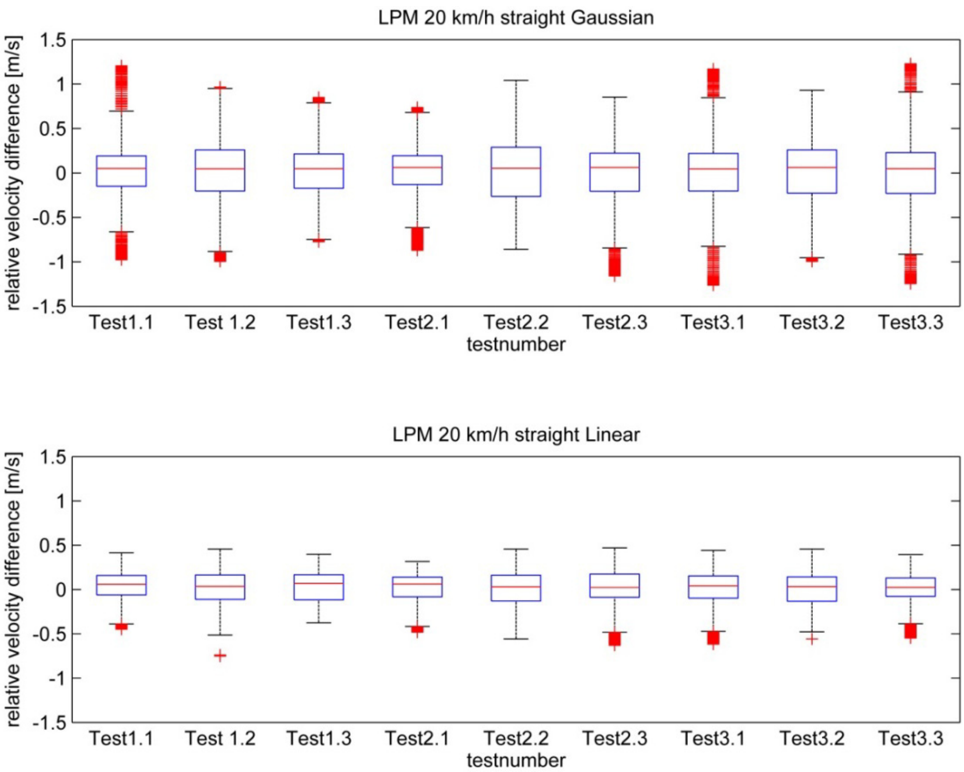

Figure 80 Boxplot indicating the relative velocity between sensor 1 and sensor 2. The relative velocity between the sensors should be zero. This test was performed at the straight part of the rink with a speed of 20 km/h. The upper graph shows the data that is filtered with a Gaussian filter, the lower graph shows the results of the data filtered with a Linear filter.

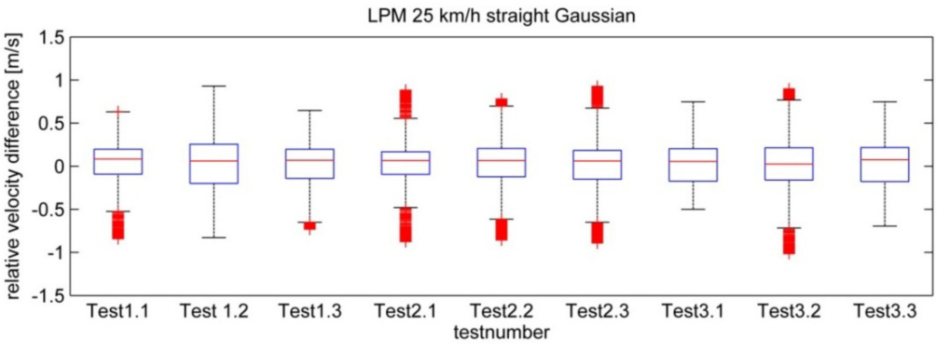

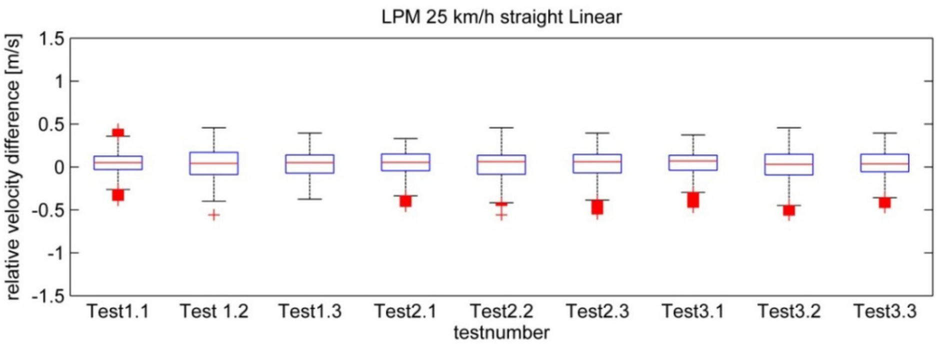

Figure 81 Boxplot indicating the relative velocity between sensor 1 and sensor 2. The relative velocity between the sensors should be zero. This test was performed at the straight part of the rink with a speed of 25 km/h. The upper graph shows the data that is filtered with a Gaussian filter, the lower graph shows the results of the data filtered with a Linear filter.

J.5 iGPS dynamic relative velocity accuracy results

The iGPS software doesn't provide speed, so therefore the speed is simply calculated using the formula (J.1.2).

(J.1.2) $$V_{iGPS\_sensor\_x,k} = \sqrt{\left(\frac{y_k - y_{k-1}}{t_k - t_{k-1}}\right)^2 + \left(\frac{x_k - x_{k-1}}{t_k - t_{k-1}}\right)^2}$$

The outliers are eventually removed. The result is shown in Figure 82 and in Table 36 . The relative velocity for the iGPS system has a maximum error of about 1.5 m/s, which is approximately the same as for LPM, however the distribution of the iGPS results are different.

Table 36 mean, standard deviation and maximum error of the relative velocities for iGPS. The tests of 15 km/h and 20 km/h are averaged over 5 trials; the test of 25 km/h is averaged over 3 trials.

Relative Velocity	Mean [m/s]	STD [m/s]	Max error (abs)
15 km/h	0.00076	0.32	1.00
20 km/h	-0.0026	0.314	1.00
25 km/h	-0.0133	0.46	1.46

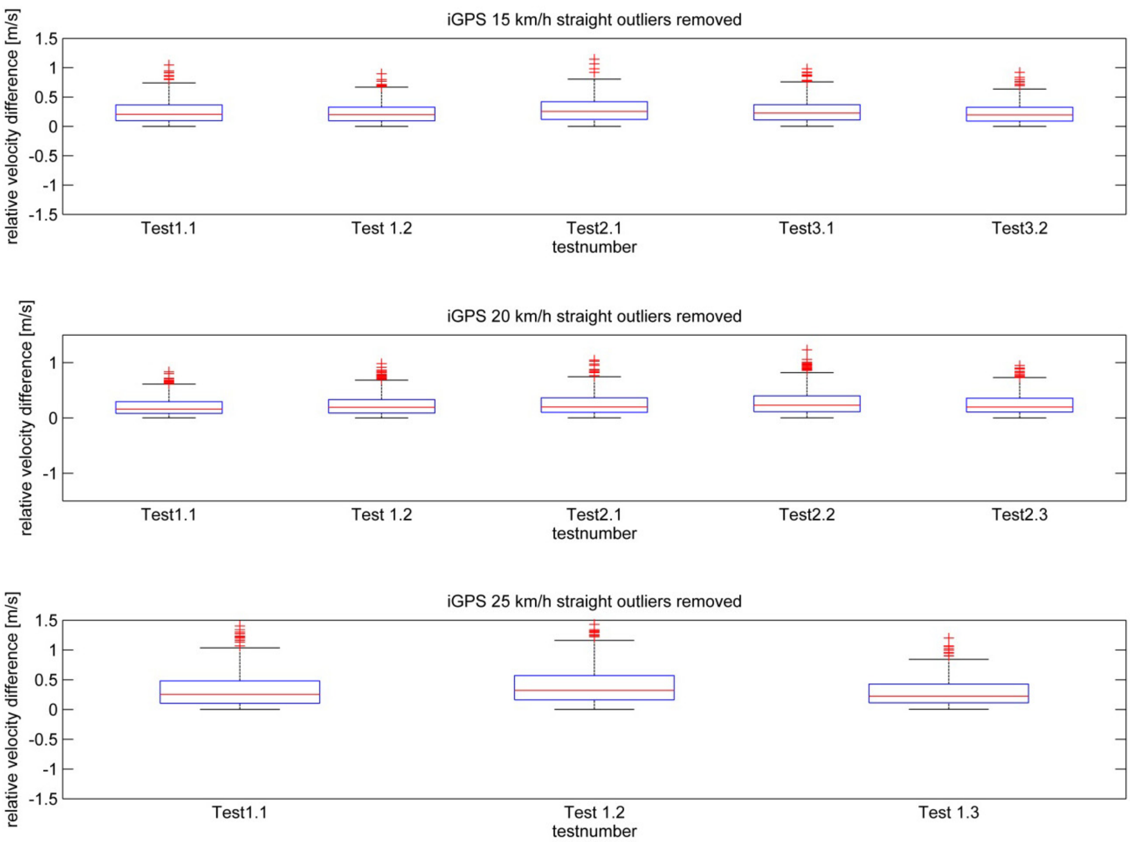

Figure 82 Boxplot indicating the relative velocity between sensor 1 and sensor 2. This test was performed at the straight part of the rink with a speed of 15 km/h, 20 km/h and 25 km/h. The outliers are removed from these data.

Table 37 results for the relative velocity of the different tests for iGPS.

Relative Velocity	Mean [m/s]	STD [m/s]	Max error (abs) [m/s]
15 km/h			
Test 1.1	0.0035	0.35	1.05
Test 1.2	-0.0103	0.28	0.89
Test 2.1	0.0017	0.36	1.14
Test 3.1	-0.0012	0.32	0.98
Test 3.2	0.0101	0.28	0.91
All tests	**0.00076**	**0.32**	**1.00**
20 km/h			
Test 1.1	0.0018	0.26	0.83
Test 1.2	-0.0104	0.30	0.97
Test 2.1	7.65e-4	0.32	1.05
Test 2.2	-0.006	0.38	1.22
Test 2.3	8.18e-4	0.31	0.95
All tests	**-0.0026**	**0.314**	**1.00**
25 km/h			
Test 1.1	-0.01	0.45	1.41
Test 1.2	-0.02	0.55	1.78
Test 1.3	-0.01	0.38	1.19
All Tests	**-0.0133**	**0.46**	**1.46**

J.6 iGPS sampling rate data

Table 38 The table indicates N = number of samples with no outliers, OR = number of outliers that are removed, Time, Distance measured and the Time divided by the number of samples.

iGPS	N	OR	Time [s]	Distance [m]	Time/N [Hz]
15 km/h					
Test 1.1	511	23	16.2	68.5	31.5
Test 1.2	533	26	16.91	70.2	31.5
Test 2.1	224	14	17	70.5	13
Test 3.1	680	14	19.75	84	34.4
Test 3.2	611	28	20.1	84.6	30.4
20 km/h					
Test 1.1	306	14	12.1	71.7	25.3
Test 1.2	525	3	15.2	84.9	34.5
Test 2.1	471	16	15	83.0	31.4
Test 2.2	376	18	15.8	73.6	23.8
Test 2.3	451	20	15.5	84.4	29.1
25 km/h					
Test 1.1	267	15	12.0	68.2	22.2
Test 1.2	248	13	12.3	69.8	20.2
Test 1.3	366	16	11.5	80.3	31.8
Additional Tests					
Test 2.1	381	10	11.9	84.8	32
Test 2.2	320	14	13.1	71.5	24.4
Test 2.3	62	2	6.8	47.3	9
Test 3.1	397	13	12	84.9	33
Test 3.2	285	10	13	72.2	22
Test 3.3	261	12	10.4	70.5	25

Appendix K
Roller-skate measurement research

K.1 Research set-up

The purpose of this test was to determine the functioning of the systems in case of an ice skate movement, concerning occlusion, gaps and functionality. This test was conducted for iGPS and FBT. The sensors were placed on a pair of (roller) skates and on the upper body of the skater (three iGPS I4is single detectors (30Hz) and three Fiducials for FBT)(Figure 83). The backpack contained the battery of the iGPS system. The participant skated three to five rounds at a speed of around 25 km/h (straight and curved part were measured separately). No synchronisation was needed in this test. In the analysis of the skate measurement the focus is on the qualitative result of the measurements. In other words, how many gaps there are in the data. The fiducial based tracking set-up is given in Appendix I. The set-up of the iGPS system is shown in Figure 84 .

Figure 83 Skater equipped with three sensors of iGPS and three fiducials.

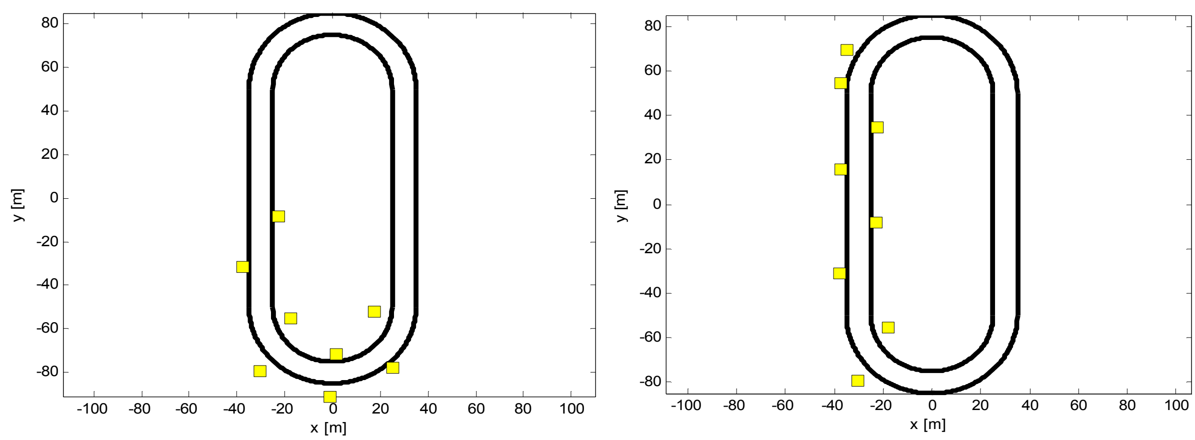

Figure 84 Transmitter positions for both the curve (left) and the straight measurements (right).

K.2 Results

K.2.1 iGPS

The results for the first test are shown in Figure 85 - Figure 89. The results show that there are many gaps in the signal, especially for the upper body and the right skate.

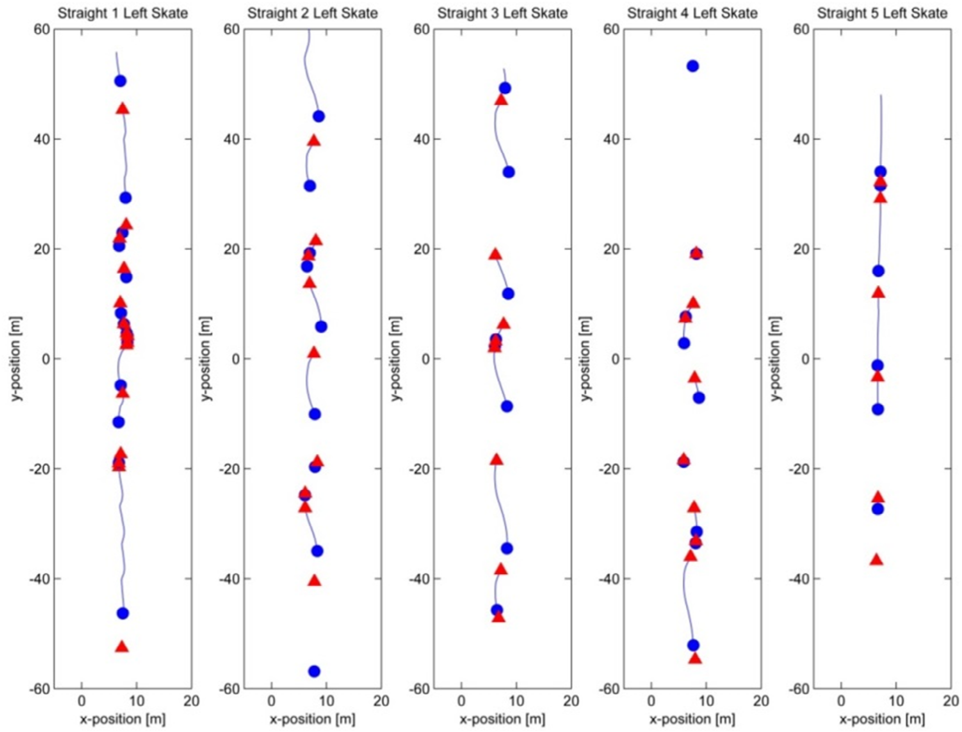

Figure 85 Test 1: Position of the Left skate over time for the 5 straight parts. The red triangles indicate the start of a gap, the blue rounds indicate the end of a gap.

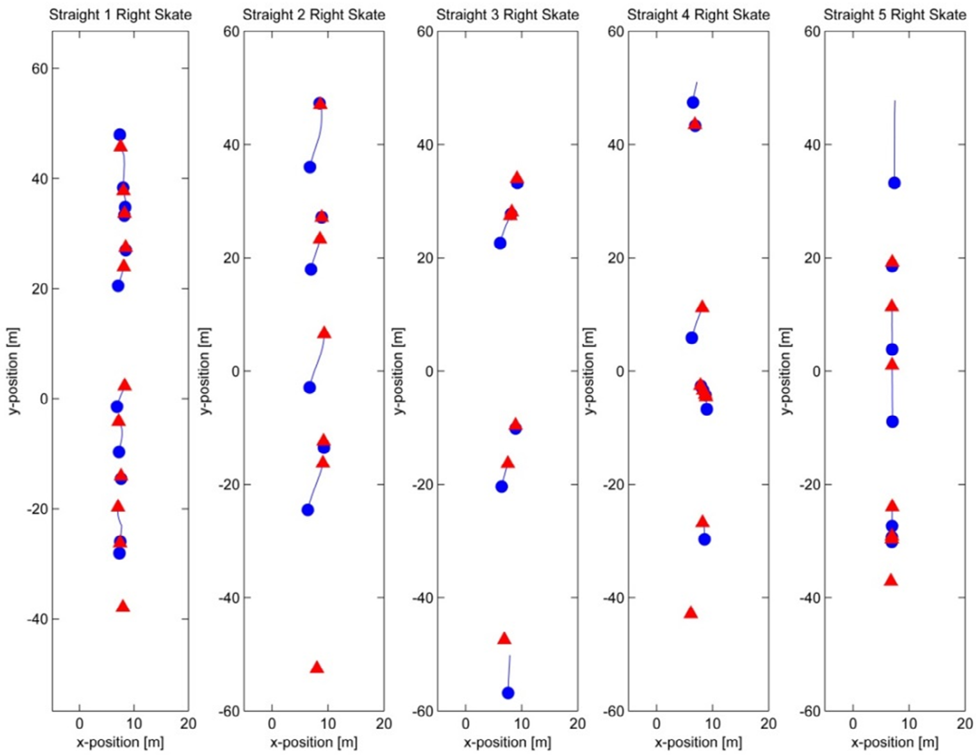

Figure 86 Test 1: Position of the Right skate over time for the 5 straight parts. The red triangles indicate the start of a gap, the blue rounds indicate the end of a gap.

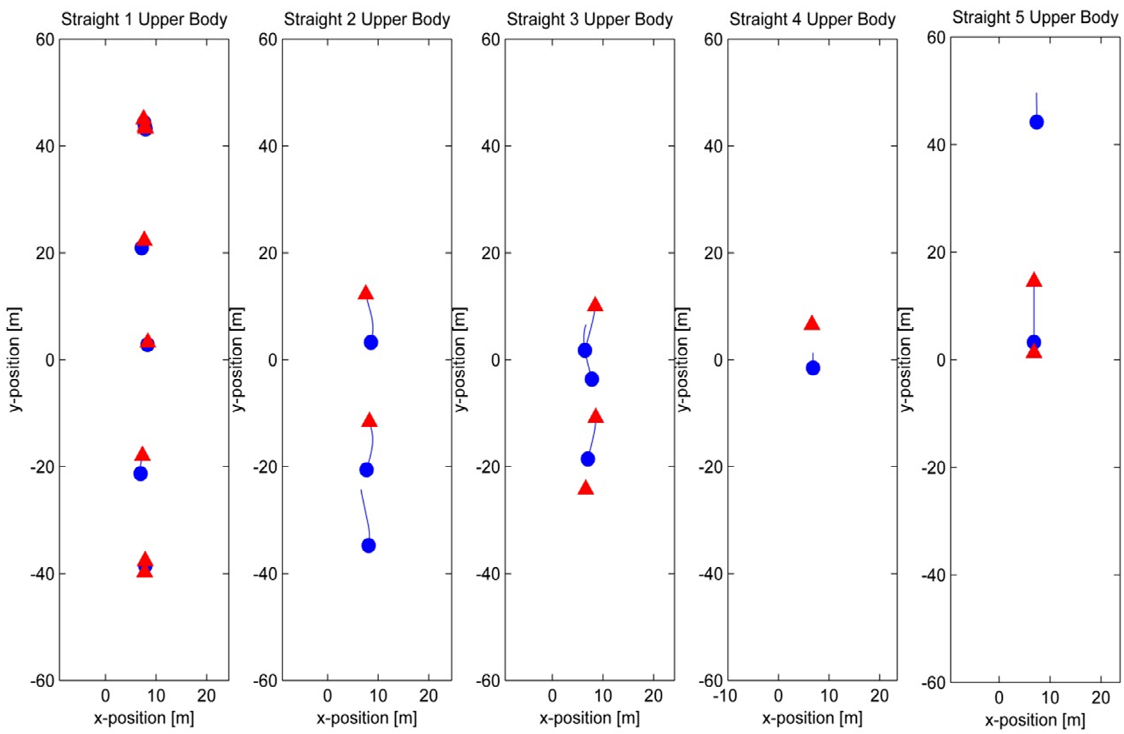

Figure 87 Test 1: Position of the Upper body over time for the 5 straight parts. The red triangles indicate the start of a gap, the blue rounds indicate the end of a gap.

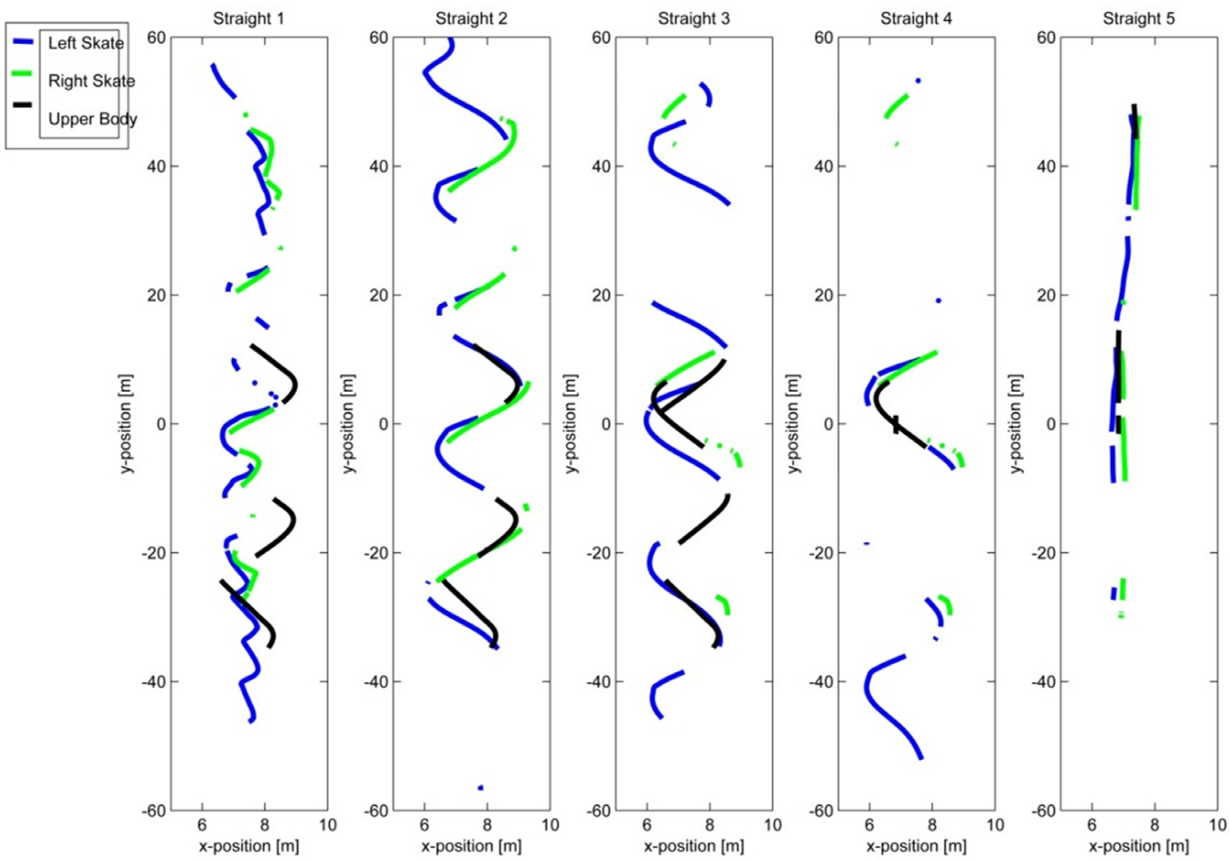

Figure 88 Position of all three sensors during the first test.

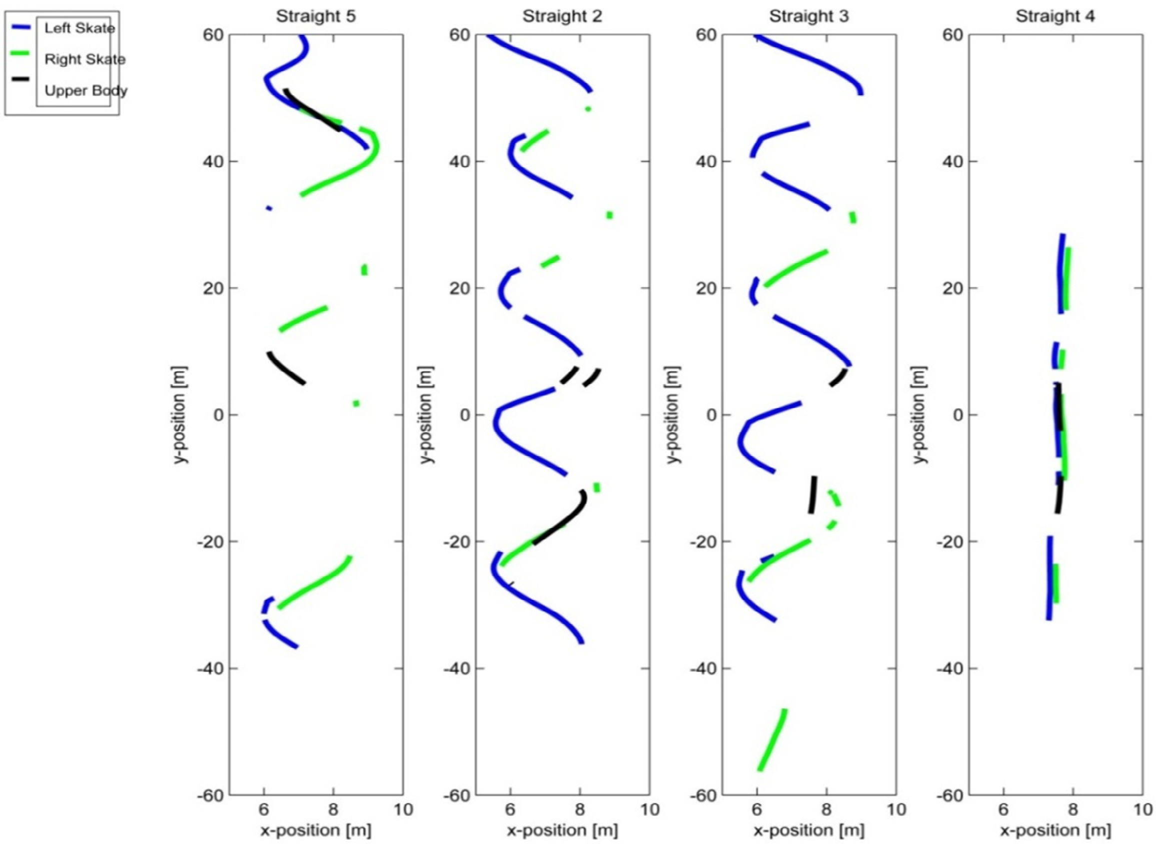

Figure 89 Position of all three sensors during the second test.

K.3 Discussion

There are many gaps in the iGPS data for the skate test. A possible explanation for the bad results is the fact that the line of sight of the iGPS system might have been occluded by the fiducials on the skates and the backpack. In addition to that, the transponders were positioned at the same height (1.2m) around the rink; alternation of the transmitter height might improve the signal. Recommendations were given as shown in Appendix L.

Appendix L
Optimization of the iGPS system

In collaboration with Nikon metrology Leuven, the requirements for optimization of the iGPS system were discussed. The results of this conversation are given in this appendix.

Optimizations for the iGPS system on behalf of the ice skate research

Consultation Nikon - 7 June 2013

Present at the meeting

TU Delft	**Nikon Metrology**
Eline van der Kruk (MSc student)	Darian Butt (Product Owner, Canada)
	Michiel Meyaert (Application Engineer, Leuven, Belgium)

Problems and solutions

a. Transmitter placement
    a. The sensor is sensed too late by the transmitters along the straight part. Therefore is would be beneficial to place some transmitters before the straight, so the sensor is sensed during the full straight part of the rink. Possibly there is an option for more transmitters.
    b. The transmitters were place along the rink during the first measurement, however the 'crash barriers' occluded the line of sight for the sensors at the feet. If the transmitters can be placed on the ice, the line of sight would be improved.
    c. The transmitters need to be placed at different height positions in order to have a clearer line of sight of the feet. Problem could occur that the reflection of the ice interferes with the signal, so that has to be monitored carefully.

b. Synchronisation of the sensors
    a. The sensors need to be better synchronised. This is possible in the new software of Nikon. This new version will therefore be used in the new tests.

c. Alignment of the coordinate system
    a. In the first test we saw that the alignment of the coordinate system wasn't completely perpendicular to the straight of the rink. Only a few degrees of difference in alignment leads to a large deviation of the straight line at the other side of the rink. Alignment should therefore be done more accurate.

d. Fixation of the sensors
    a. The sensors need to be attached to the skater in a comfortable way. Also the line of sight can be improved with a better sensor placement. It might be beneficial to fix the sensors at the tip of the skate and the CoM sensor at the top of the back. Additionally we need to find an improved way of fixating the battery to the skater, so the backpack becomes redundant.

e. Inertial sensors
    a. In the next experiments, an inertial sensor will be used to measure the lean angle of the skate. This same inertial sensor might be used to:
        i. Fill gaps if necessary
        ii. Sample at a higher frequency (using the iGPS data as reference)

f. Speed
    The sensors have been tested before at the speed of 50 km/h. The speed should therefore not give too much problems during the measurements.

Next measurements

Preferably the measurement are done on an empty ice rink, in order to place the iGPS transmitter on the ice. Nikon is available on the following dates:

- 4 - 5 July 2013
- 11 - 12 July 2013

TU Delft Delft University of Technology

Challenge the future

Appendix M iGPS Skate research

The goal of the research is to establish if the proposed optimizations can improve the performance of the iGPS system in terms of robustness and to find the best suitable set-up for data collection for the verification of the 3D biomechanical model, taking into account the recommendations as formulated before (Appendix L).

M.1 Method

The measurement was performed on an ice hockey rink in Leuven, Belgium. Four iGPS transmitters were placed along a straight part of the ice hockey rink. The following recommendations (Appendix L) are examined:

1. Improved synchronisation of the sensors;
   The new Nikon software is used
2. Positioning and fixation of the sensors;
   The sensors are placed at the tip of the skate, see Figure 90. The sensor at the back is placed on a belt at the height of the umbilicus (belly button). The battery is fixed at shoulder height.

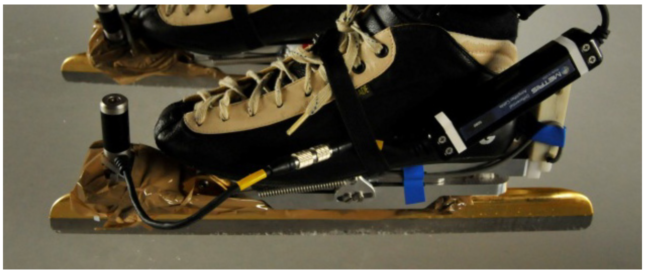


Figure 90 Positions of the sensors

3. Improving the line of sight;
   The transmitters will be placed on the ice (instead of behind the border).
4. Positioning of the transmitters;
   The positioning of the transmitters will be the variable in this experiment. In the experiments the height of the transmitters will be alternated, see Figure 91:
   A. All transmitters at CoM height
   B. Alternated heights of the transmitters
   C. All transmitters at foot height

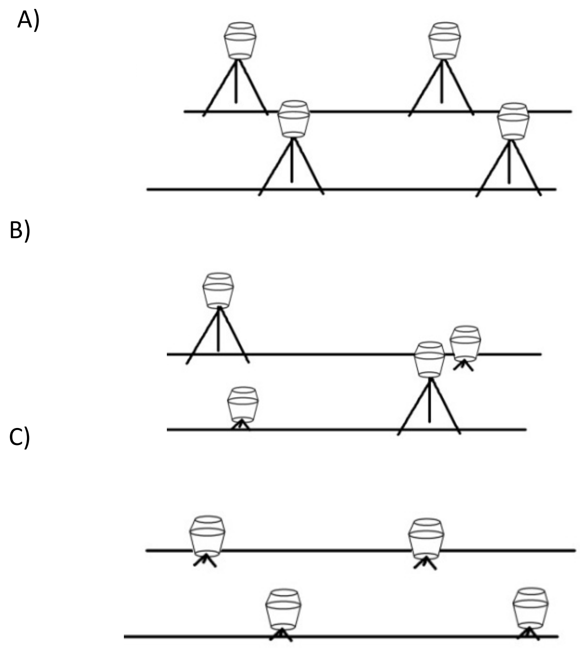

Figure 91 Transmitter positioning

M.2 Set-up

The transmitters are placed in either arrangement A,B or C (Figure 91) at the positions given in Figure 92. The participant is equipped with three iGPS single detector sensors (Figure 90). Due to a broken amplifier only two sensors could be connected to the iGPS system (Table 39). The output variables (metrics) are given in Table 40. The participant skates round, the area of interest is the straight part (Figure 92). A straight part is defined as the part where the y-coordinate <3 [m]. The placement of transmitters on the ice could lead to noise from ice reflection. This will mainly influence the sensors on the skate. Ice reflection can be determined by considering the z-position data of the skates. In case of reflection we expect to see misplaced data points that are scattered in a random pattern.

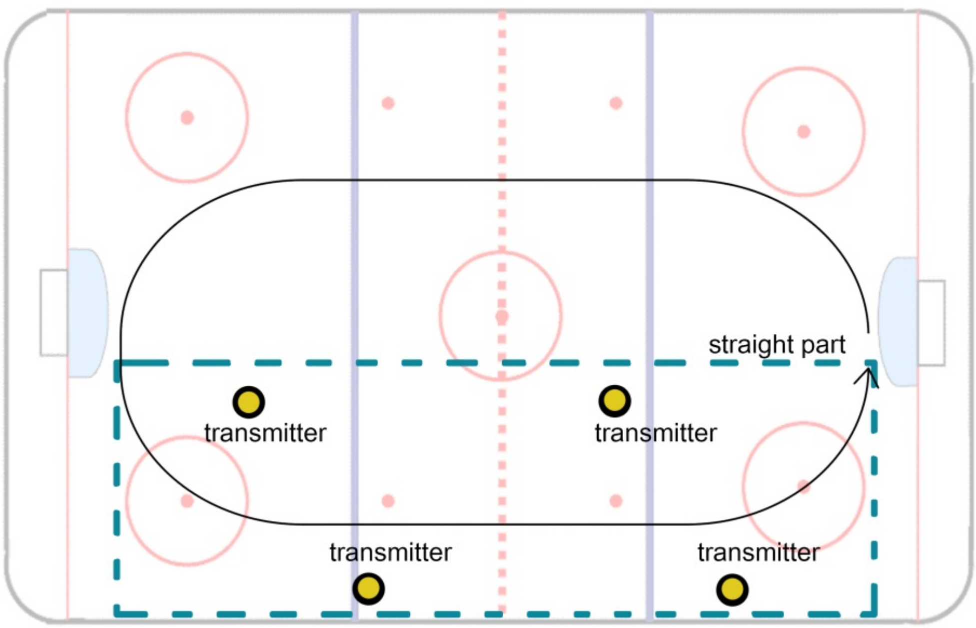

Figure 92 Transmitter positions on the ice hockey rink in Leuven

Figure 93 Picture of the research set-up in Leuven

Table 39 Sensor combinations used in the different trials

Arrangement	Trial	Left Skate	Right Skate	CoM
A	TEST-A	X	X	
A	TEST-B	X	X	
B	TEST-D	X	X	
C	TEST-F	X		X
C	TEST-G	X		X

Table 40 Metrics as used in this research

Variable		Description	Unit
Number of Straight	NS	Number of straights in this trial	[-]
Total Time	TT	time measured by iGPS on the straight part	[s]
Number of Gaps	NoG	number of gaps on the straight part	[-]
Time Gaps	TG	Total time of the gaps	[s]
Average Time Gaps	ATG	Total time of the gaps divided by the number of gaps	[s]
Maximum Time	MTG	Maximum Time gap found	[s]
% measured	%M	(TT-TG/TT)*100%	[%]

M.3 Results

M.3.1 iGPS coverage

The results show that for each arrangement the sensor on the left skate performs better than the sensor on the right skate or on the upper body (Figure 94, Figure 95 ,Figure 96). The right skate is blocked by the left skate in the curves. The CoM sensor has an additional impediment in the line of sight (Figure 96), since the participant blocked the sensor with the upper body (poor ice skating posture).

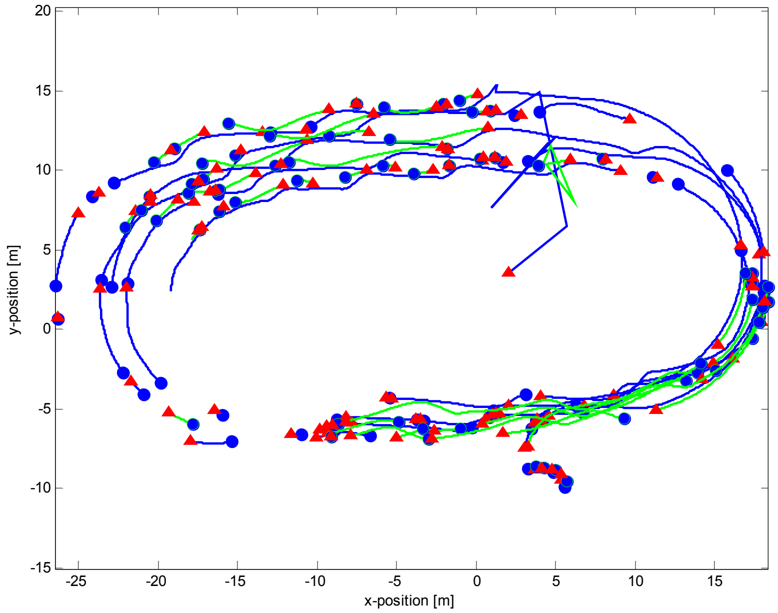

Figure 94 Arrangement A; all transmitters on tripods. The blue line indicates the left skate, the green line is the right skate. The res triangles refer to the start of a gap, the blue dot is the end of a gap. Straight is defined as the part y<3.

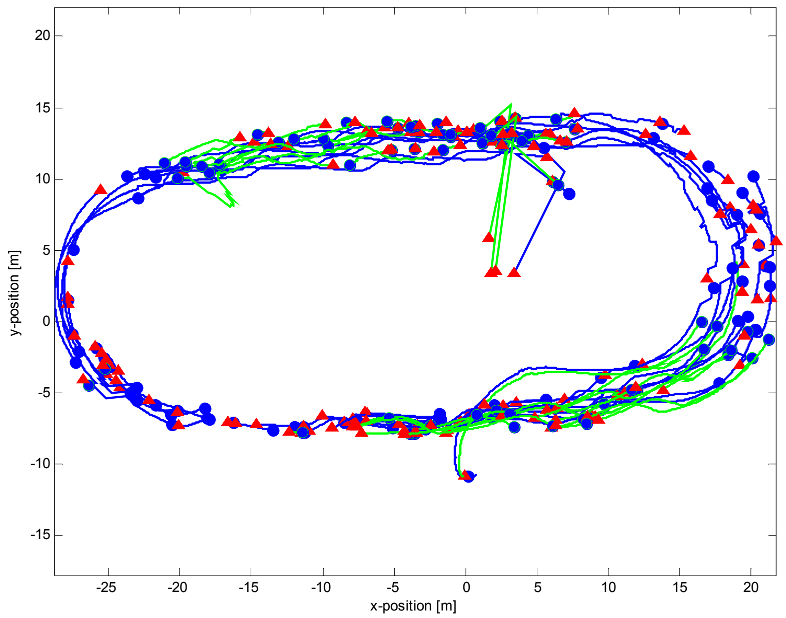

Figure 95 Arrangement B; transmitters on both the ice and tripods. The blue line indicates the left skate, the green line is the right skate. The red triangles refer to the start of a gap, the blue dot is the end of a gap. Straight is defined as the part y<3.

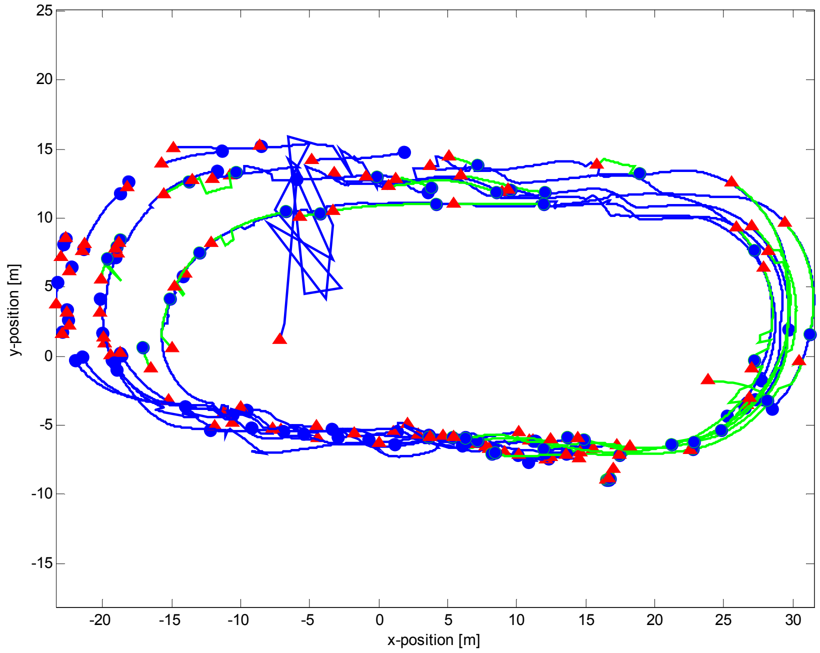

Figure 96 Arrangement C; transmitters on the ice. The blue line indicates the left skate, the green line is the CoM. The red triangles refer to the start of a gap, the blue dot is the end of a gap. Straight is defined as the part y<3.

M.3.2 iGPS gaps

In Table 41 the results are given for the sensor on the left skate. The results given are mean values, taken over several straight parts. The results indicate that arrangement B has the least number of gaps, together with arrangement C. The average time of a gap, the total time of all gaps and the maximum time gap are all lowest for arrangement B, although the results are very close.

*Table 41 Table with the metrics of the sensors for arrangement A,B and C for the sensor on the left skate. The numbers are the mean values taken over several straight parts. NS = number of straight; TT = total time; NoG = number of gaps; TG = total time gaps; ATG = average time of a gap; MTG = maximum time gap; %M = TG/TT*100%.*

Left Skate	NS	TT	No	TG	ATG	MT	%M
A: Tripods	5	12.	8.4	4.9	0.5	2.8	61.
B: Ice +Tripods	8	13.	7.4	4.3	0.5	1.9	67.
C: Ice	7	14.	7.4	5.2	0.7	3.5	63.

The results for the upper body sensor of arrangement C are given in Table 42 The results show however that the part that is measured has an acceptable coverage, in spite of the low positions of the transmitter.

*Table 42 Table with the metrics of the sensors for arrangement C for the sensor on CoM. The numbers are the mean values taken over several straight parts. NS = number of straights; TT = total time; NoG = number of gaps; TG = total time gaps; ATG = average time of a gap; MTG = maximum time gap; %M = TG/TT*100%.*

CoM	NS	TT	No	TG	ATG	MT	%M
C: Ice	7	8.0	4.2	2.3	0.3	1.5	82%

M.3.3 iGPS vertical position

Figure 97 shows the unfiltered z-position data from the left and right skate in arrangement A (all transmitters on tripods). The first thing to notice is that the alignment of the coordinate system is not levelled (indicated by the large sinus wave in the data). Looking at the smaller sinus waves (the parts where the participant was at the straightaway), there is no clear sign of reflection noise in this (unfiltered) data. If this is compared to the data obtained in arrangement C (all transmitters on the ice, Figure 99), we see a clear indication of reflection: the data points are more scattered and staggered. The same holds for arrangement B (see Figure 98.)

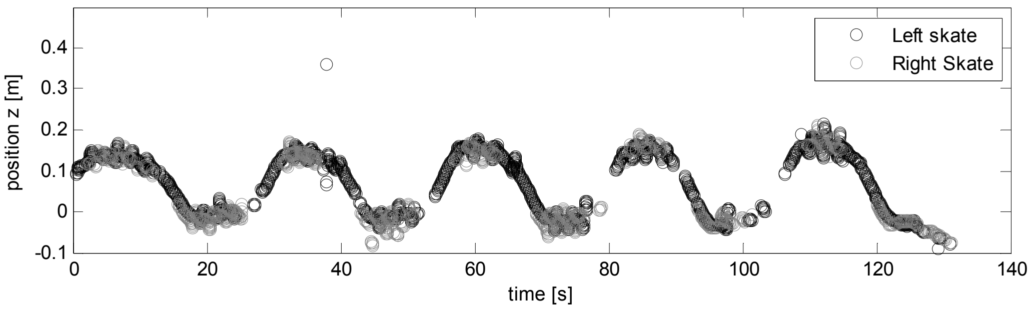

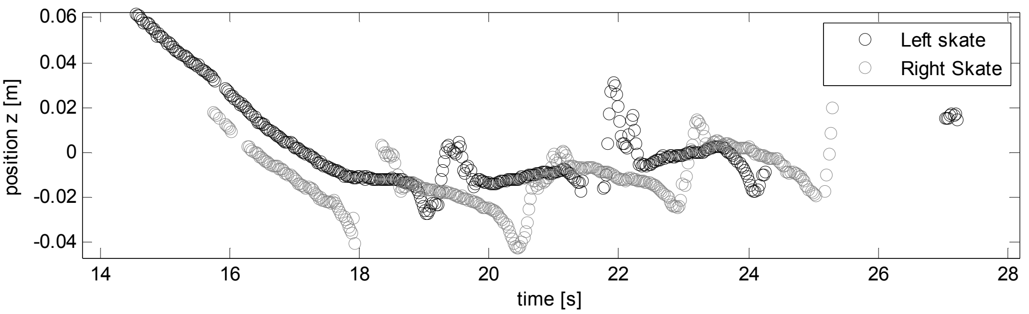

Figure 97 Data points from the sensors on the feet for arrangement A (test-B). The lower graph is a zoomed-in part of the upper graph. Sensor A is the left foot, sensor C is the right foot.

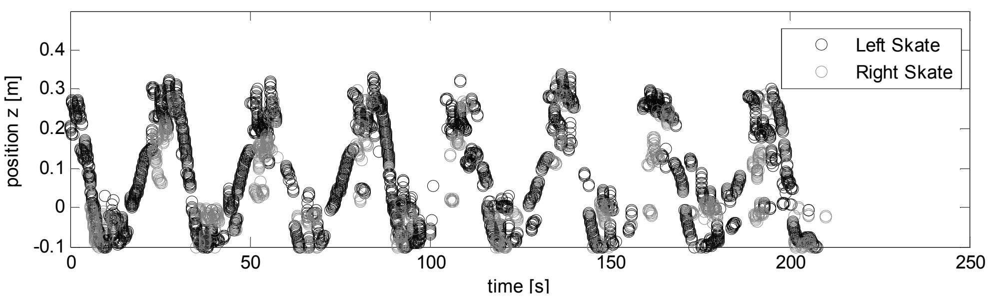

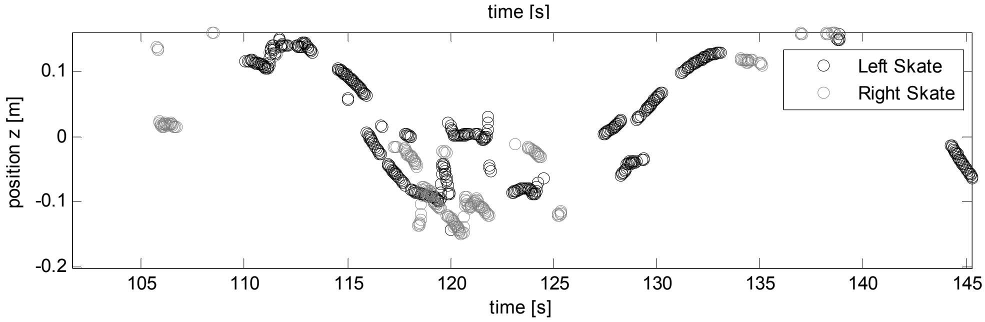

Figure 98 Data points from the sensors on the feet for arrangement B (test-D). The lower graph is a zoomed-in part of the upper graph. Sensor A is the left foot, sensor C is the right foot.

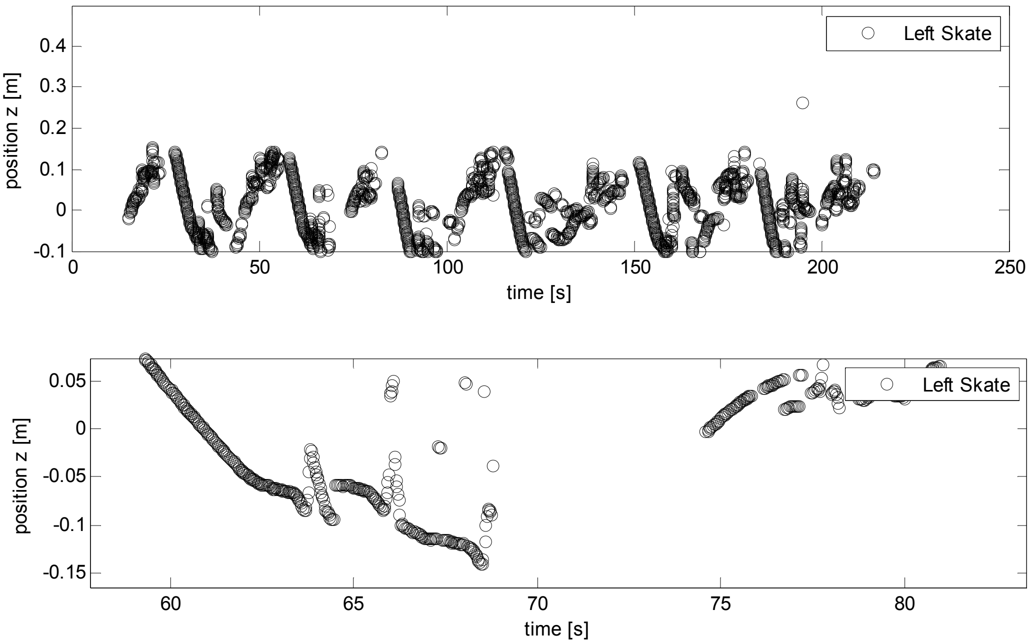

Figure 99 Data points from the sensors on the feet for arrangement C (test-F). The lower graph is a zoomed-in part of the upper graph. Sensor A is the left foot, sensor C is the CoM.

M.4 Discussion

In the results there are two main problems to consider; first the slow localization of the sensor after loss of signal. In order for the system to work consistently for the true data collection, the sensor needs to be localized before entering the measurement area. Since a loss of signal (or loss of line of sight) is inevitable at a large ice rink with a limited number of transmitters, a possible solution is to place transmitters before the start of the straight-part measuring area, in order to localize the sensor before it enters the straight part. The second problem are the gaps in the data. The gaps indicate that the system is not a true optimal system for measuring the ice skating movement for training or feedback. The system is however very accurate (section 0) and is therefore the most optimal system to collect data for the verification of the dynamic model. The gaps were reduced by transmitter placement on the ice (instead of along the border). However, for the skates there is still only about 67% of the data points covered. In data collection for the verification of the model, this is a limited problem, as long as there is opportunity to measure a whole stroke and interpolation is feasible.

The results show that the sensor at the upper body (aside from the localization) has a coverage that is higher than the one of the sensor on the skate, even when all transmitters are placed at the height of the skates (see Table 42). This is mainly due to the less occluded sensor at the upper body. This sensor is less often covered by the participant's movements. Also (in contrast to the skates), this sensor is less dynamic in its movements. Additionally the upper body sensor suffers less from ice-reflection.

The ice reflection can be of high influence on the performance of the iGPS system. It is therefore important to be aware of this noise. The reflection has main influence on the measurement of the z-position of the skate. Based on the results we may conclude that for the skates the measurement in the horizontal plane is best covered when placing the transmitters on alternated heights, while measurements in the vertical direction (concerning mainly the skates) are optimized in arrangement A, the transmitters on the tripods. With respect to the data collection for the skater model, the 2D measurements of both skates are most important, together with the 3D measurements of the upper body. These measurements are best performed using the configuration with alternated transmitter heights.

M.5 Conclusion

1. Improved synchronisation of the sensors;
   The sensors are indeed optimally synchronised with the use of the new Nikon software
2. Positioning and fixation of the sensors;
   The sensor placement at the tip of the skate is an improvement for the line of sight. In order to attach the sensor to the skate, a new tool is designed, based on the requirements found during this test. In order to improve the line of sight of the upper body sensor, the battery is better placed at the bottom of the back for future research, so the battery is never in line of sight of the sensor.
3. Improving the line of sight;
   Overall it is beneficial to place the transmitters on the ice. However the iGPS system recovers slowly from a loss of signal, therefore it is beneficial to place additional transmitters in front of the straight (in de curve) that can detect the sensors before entering the measurement area.
4. Positioning of the transmitters;
   Concerning the transmitter placement, arrangement B, placing some transmitters at ice height and some at tripods, is the best possible arrangement to collect 2D data of the skates and 3D data from the CoM. This is therefore the arrangement that should be applied in the data collection research.

Appendix N Lean angle research

This appendix describes the research protocol for the lean angle research. The literature review(Ingen Schenau 1982), nominates an inertial sensor to measure the lean angle of the skate of the speed skater. This appendix describes the research whereby the accuracy of the wired Xsens inertial sensor is established and is compared to the wireless ProMove sensor.

N.1 Method

In order to sincerely compare the Xsens with the ProMove system and in order to give an indication of their accuracies, the measurements are done at the ice rink in Thialf, Heerenveen. The environmental problems (temperature, humidity, metal under the ice etc.) were therefore taken into account. The skates are equipped with two Xsens sensors (Xsens MTx , Xsens MTi-G(Xsens 2013) (100 Hz)) linked to a mini laptop and two wireless ProMove sensors (ProMove 3D(Garcia, Chatterjee et al. 1998; ProMove-3D 2013) (100 Hz)). The positions of the sensors are alternated in order to eliminate the position error (Figure 101). The lean angle is captured with an additional Sony Videocam (30fps). The analysis is done with a designed Gui (MATLAB, 2012a) . The video analysis tool GIMP v2.8.6 is used to measure the lean angle based on the video. Caution has to be taken with this measurement tool on account for distortion of the picture. The data was found through the standard export of the Xsens in roll-pitch and yaw angles. The raw data of the ProMove sensors is converted into the roll-pitch-yaw angles by the company ProMove itself.

Figure 100 Lean angle research set-up

Figure 101 Skates equipped with the ProMove and the Xsens sensors. The sensor are alternated placed.

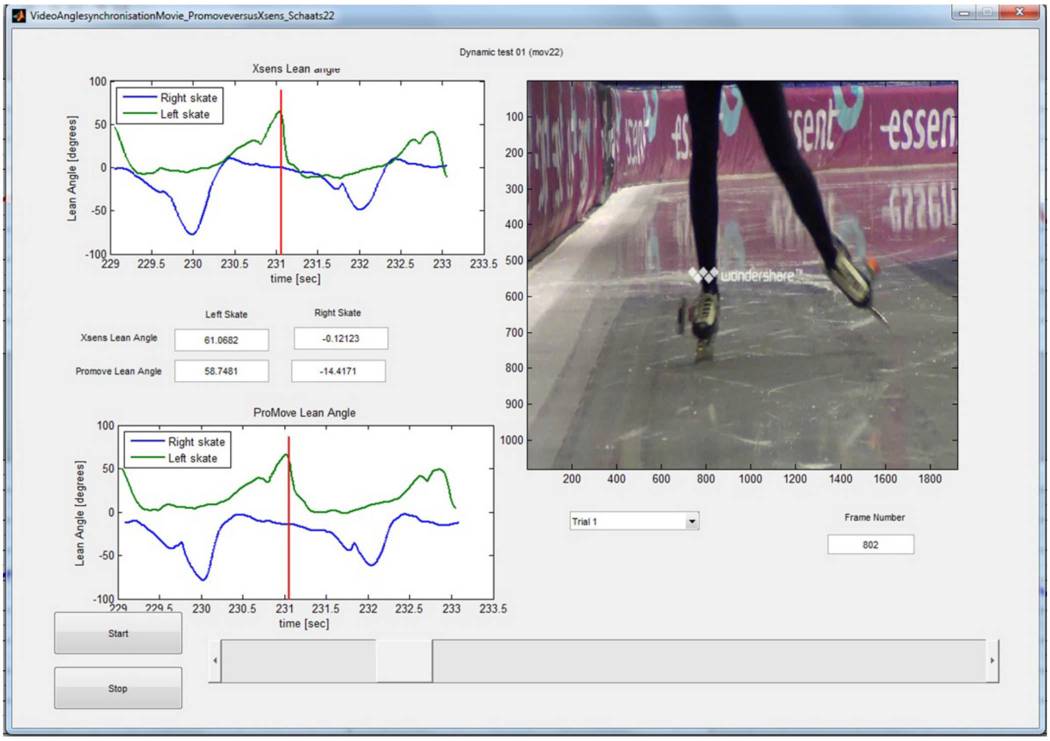

Figure 102 GUI of the lean angle measurement. The GUI indicates the lean angle measured by Xsens (at the top) and the ProMove (bottom) for the left and right skate. The values of the angles is given in the middle. The right part shows the video of the trial, which is synchronized with the red line in the graphs. The frame number indicates the frame number of the video.

Figure 103 Result from the GIMP software to measure angles in a videoframe.

N.2 Research Protocol

1. The video camera is placed on the ice in such a way that the lean angle of the skates is clearly shown on the images.
2. The skater is equipped with a backpack including the mini laptop. The skates are fastened with the Xsens and ProMove switched off.
3. The Xsens sytems are connected to the mini laptop through a USB cable. The MATLAB program which samples the data from the Xsens is run.
4. The Promove sensors are turned on. The camera is switched on.
5. The skater jumps with the skates on two times. This is seen in the Promove and Xsens data and can also be seen on video, so all systems can be synchronized.
6. The calibration of the system : the skater puts his skates in the calibration frame (see Figure 104). The frame keeps the skates upright and in line with the straight of the rink.
7. The skater is released from the frame and skates the straight part up and down a couple of times.
8. All systems are switched off.

Figure 104 Skates in the calibration frame. The frame is aligned with one of the finish lines.

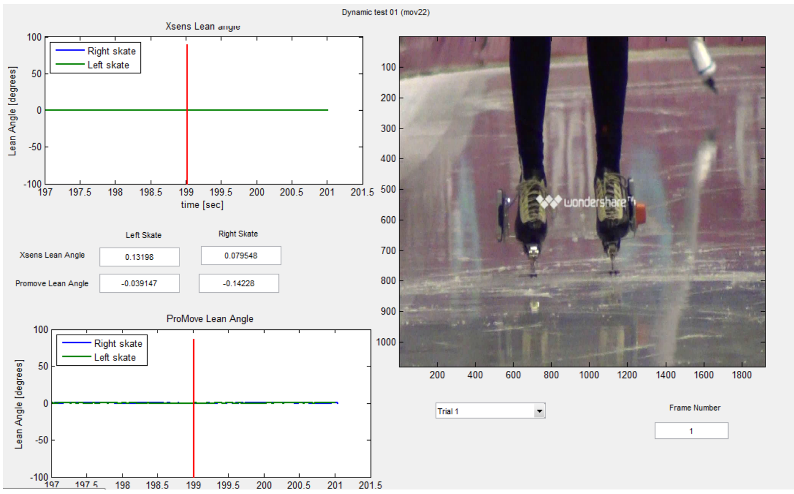

N.3 Results

The results are shown in Figure 105. The difference between the ProMove and the Xsens angles are given in Figure 108.

The overall shape of both plots indicates a drift in one or both of the lean angle measurement systems. It is noted that inertial systems in general suffer from such drift. Figure 108 indicates that mainly the ProMove suffers from drift in this test. The difference between the two systems might therefore be caused by the drift in the ProMove system. The difference between the two systems seems to increase in time in the course of one straight. The drift recovers after each straight part that is skated.

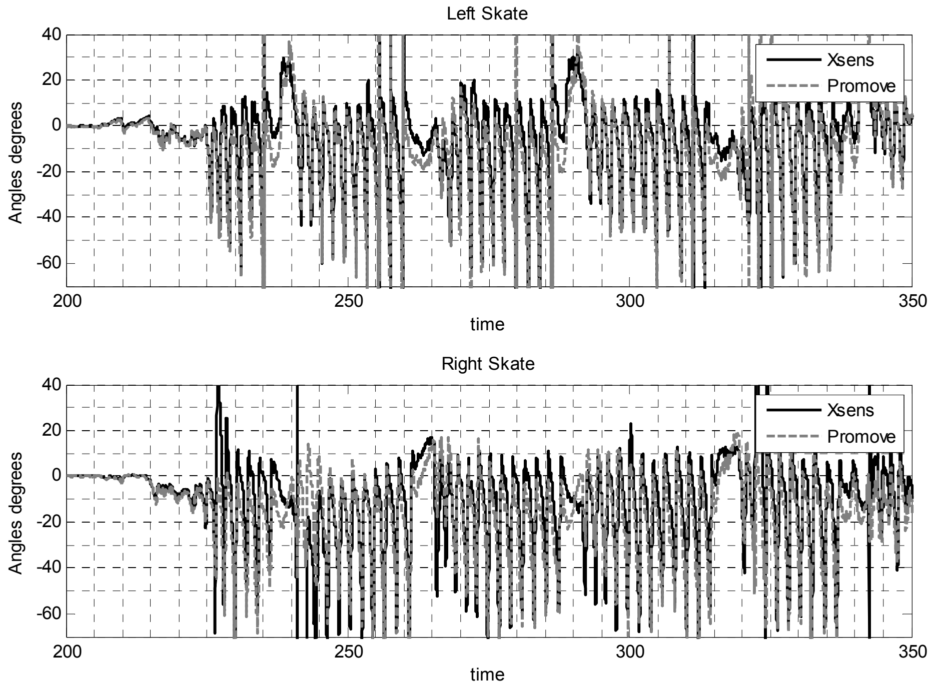

Figure 105 Lean angle results from the Xsens and the Promove sensor for trial 4.

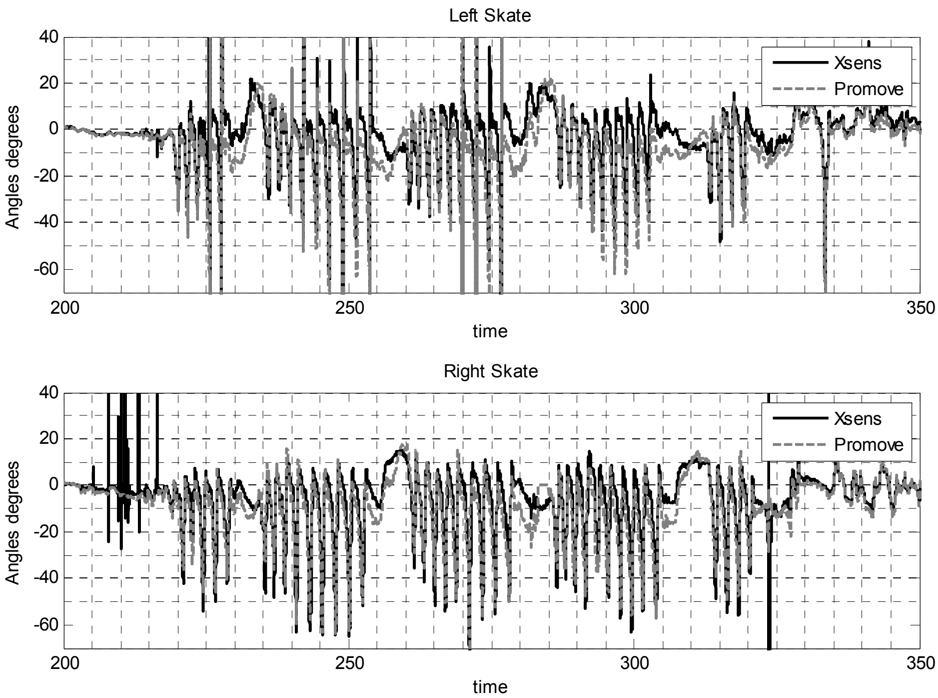

Figure 106 Lean angle results from the Xsens and the Promove sensor for trial 1.

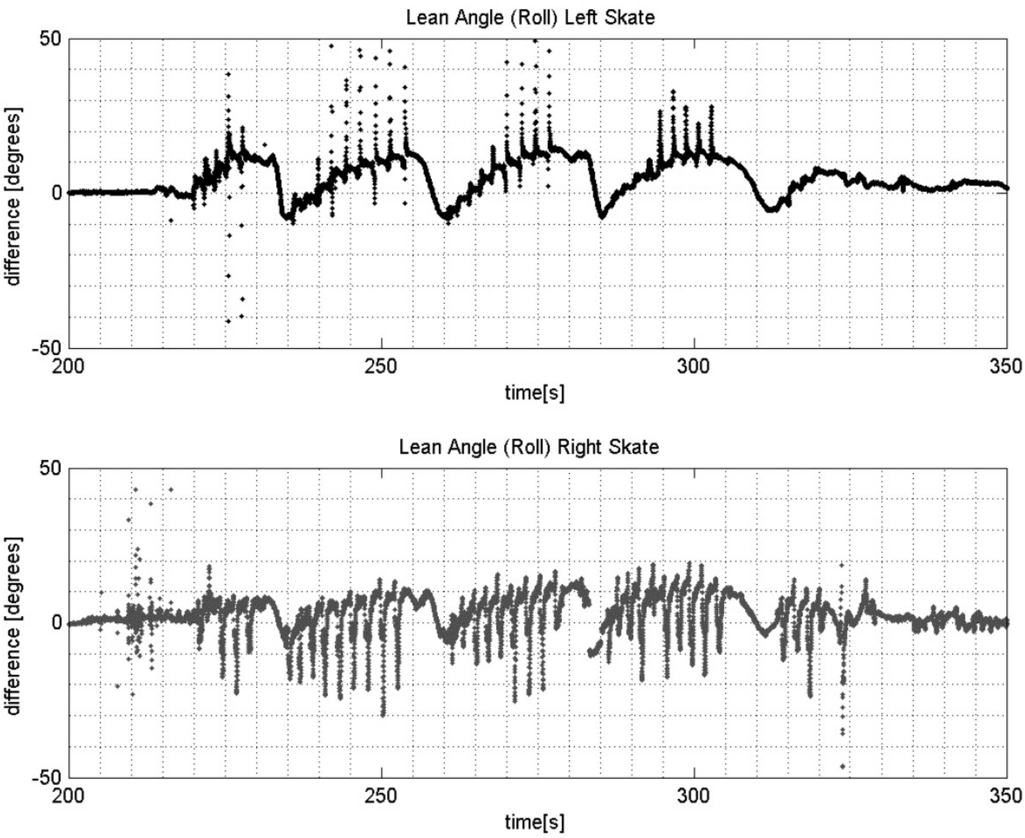

Figure 107 Difference in angle between the ProMove and the Xsens for both the Left and the Right skate for Trial 1.

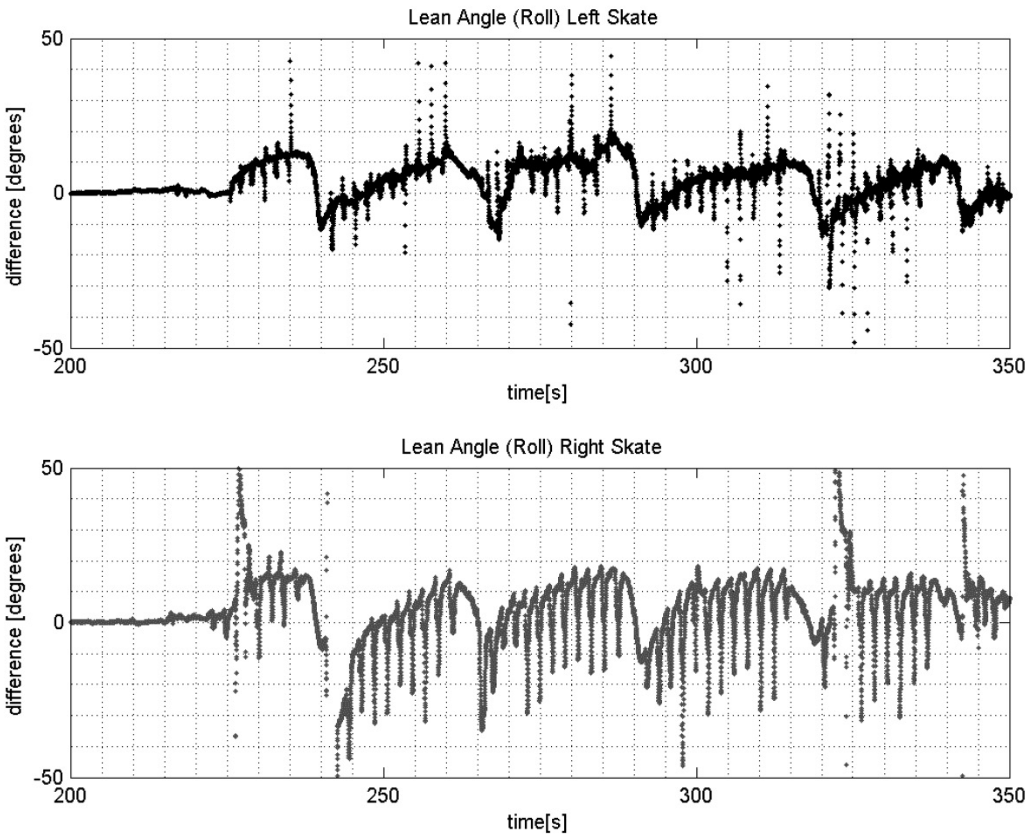

Figure 108 Difference in angle between the ProMove and the Xsens for both the Lef tand the Right skate for Trial 4.

Video analysis

The two parts that are analysed with both the GUI and the GIMP tool are shown in Figure 109 and Figure 110.

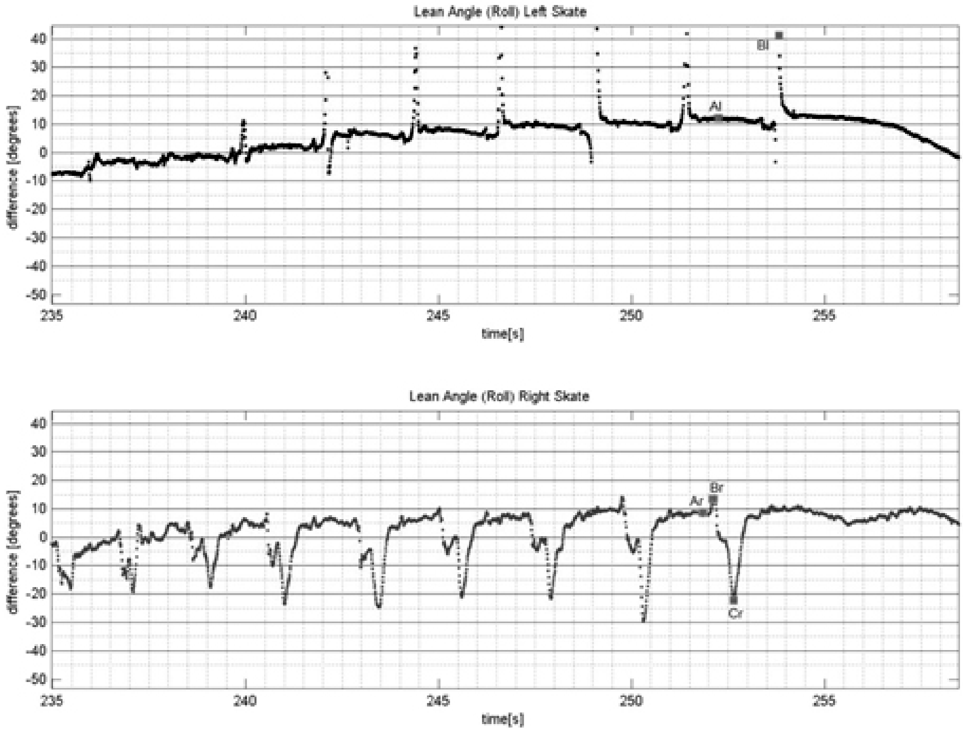

Figure 109 Selected part from the difference plot of Trial 1.

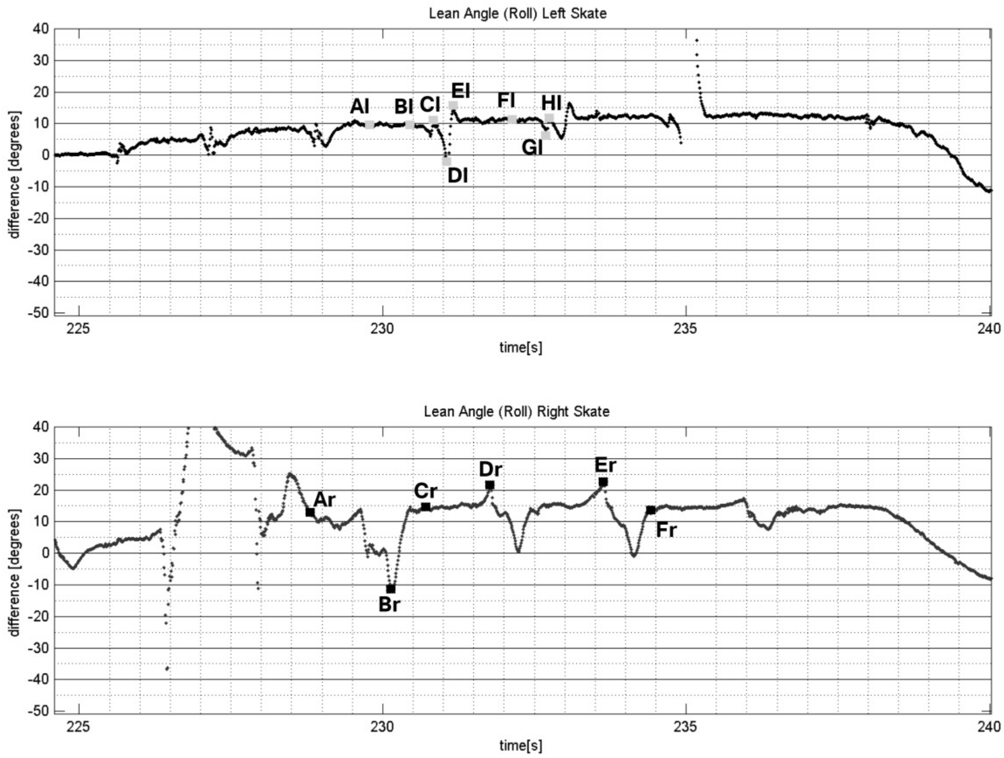

Figure 110 Selected part from the difference plot of Trial 4 (Figure 108).

Trial 4

In Figure 110 several points are selected in time of trial 4. Points Cl, Dl, El, GL, Hl, Br, Dr and Er are peaks in the graphs; Points Al, Bl, Fl, Ar, Cr and Fr are randomly chosen points while the respective skate is active; Each point is analyzed using the values from the ProMove sensor, the Xsens sensor and the video analysis tool. Results are shown in Table 43 . The image regarding the point chosen can be found in Appendix O.

Table 43 ProMove, Xsens and Video analysis results for trial 4

	Time [s]	**Video Frame**	**Skate**	**ProMove [^{0}]**	**Xsens [^{0}]**	**Video analysis [^{0}]**	**Skate phase**	**Best Result**
Al	229.8	770	Left	5.7	-4.0	3.5	Glide	ProMove
Bl	230.4	785	Left	19.0	9.4	6	Glide	Xsens
Cl	230.8	798	Left	52.0	42.8	38	Push-off	Xsens
Dl	231.1	802	Left	58.7	61.1	-*	Reposition	-*
El	231.2	805	Left	17.6	3.6	-*	Reposition	-*
Fl	232.2	828	Left	9.0	-2.1	1	Glide	Xsens
Gl	232.7	843	Left	36.7	30.4	32	Push-off	Xsens
Hl	232.8	846	Left	48	38.4	39	Push-off	Xsens
Il	233.1	853	Left	8.7	-7.0	-	Reposition	-
Ar	228.8	746	Right	-5.8	6.8	4.5	Glide	Xsens
Br	230.2	779	Right	-35.4	-46.8	-*	Reposition	-*
Cr	230.7	797	Right	-13.2	1	-1	Glide	Xsens
Dr	231.8	820	Right	-41.5	-20.6	-33	Push-off	ProMove
Er	233.6	866	Right	-47.3	-25.6	-32	Push-off	Xsens
Fr	234.4	886	Right	-5.1	7.3	-*	Reposition	-*

* The respective skate is inactive.

The points in the repositioning phase and at the end of push-off show an enlarged difference between the sensors. The last column of Table 43 shows the system that is closest to the video analysis measurement. Overall the Xsens performed better in this test.

Trial 1

The points Bl, Br and Cr are peaks in Figure 109. The random points selected are Al and Ar. The images belonging to these points can be found in Appendix O. The results of the measurements are shown in Table 44 . Again the Xsens appears to be most accurate based on the video analysis.

Table 44 Results from the Xsens measurement, the ProMove measurement and the video analysis.

Trial	**Time [s]**	**Video Frame**	**Skate**	**ProMove [^{0}]**	**Xsens [^{0}]**	**Video analysis (Gimp) [^{0}]**	**Skate Phase**	**Best Result**
Al	252.3	848	Left	6.7	-5.1	0	Glide	Xsens
Bl	253.8	885	Left	10.4	-39.6	-*	Reposition	-*
Ar	251.9	838	Right	-27.4	-18.9	-14.04	Push-off	Xsens
Br	252.1	843	Right	-38.1	-24.8	-20.2	Push-off	Xsens
Cr	252.6	856	Right	-10.1	-31.2	-*	Reposition	-*

* The respective skate is inactive.

N.4 Discussion

The results show that there is a difference between the two measurement systems ranges up to 22^0, neglecting the repositioning phases of the skates, since the research is only concerned with the 'active skate'. The video analysis demonstrates that the Xsens is closest to the values measured by the GIMP-tool with an average difference as indicated in Table 12. Remember that these values are based on few selected points from the trials and are based on video analysis, which entails distortion

The required lean angle accuracy for the data collection is 2.5^0. Although the video analysis is not accurate enough to determine the exact accuracy of the Xsens system, the results from this test show that an accuracy of 2.5^0 is out of range for the Xsens measurement system.

Table 45 Differences between the lean angle measured by the MEMS systems and the video analysis GIMP tool

	Tria	ProMove [^{0}]	Xsens [^{0}]
Average difference	1	12.7	4.9
Maximal difference	1	17.9	5.1
Minimal difference	1	-6.7	4.6
Average difference	4	9.7	4.4
Maximal difference	4	15.3	7.5
Minimal difference	4	-14	-12.4

N.5 Conclusion

In this test the lean angle of the skate of a speed skater is measured using an Xsens and a ProMove sensor. The results of both measurements are compared and video analysis is used to determine which measurement is closest to the true value of the lean angle. The results show that the Xsens measurements are closest to the angles found by the video analysis. The required accuracy of 2.5^0 (section 3.2) will not be reached with the wired Xsens system used.

Appendix O
GUI selected frames and points.

This appendix contains the images referring to the points indicated in Figure 109 and Figure 110.

O.1 Trial 4

The images for points Ar to Fr are shown in Figure 111 . The image for points Al to Il are shown in Figure 112 .

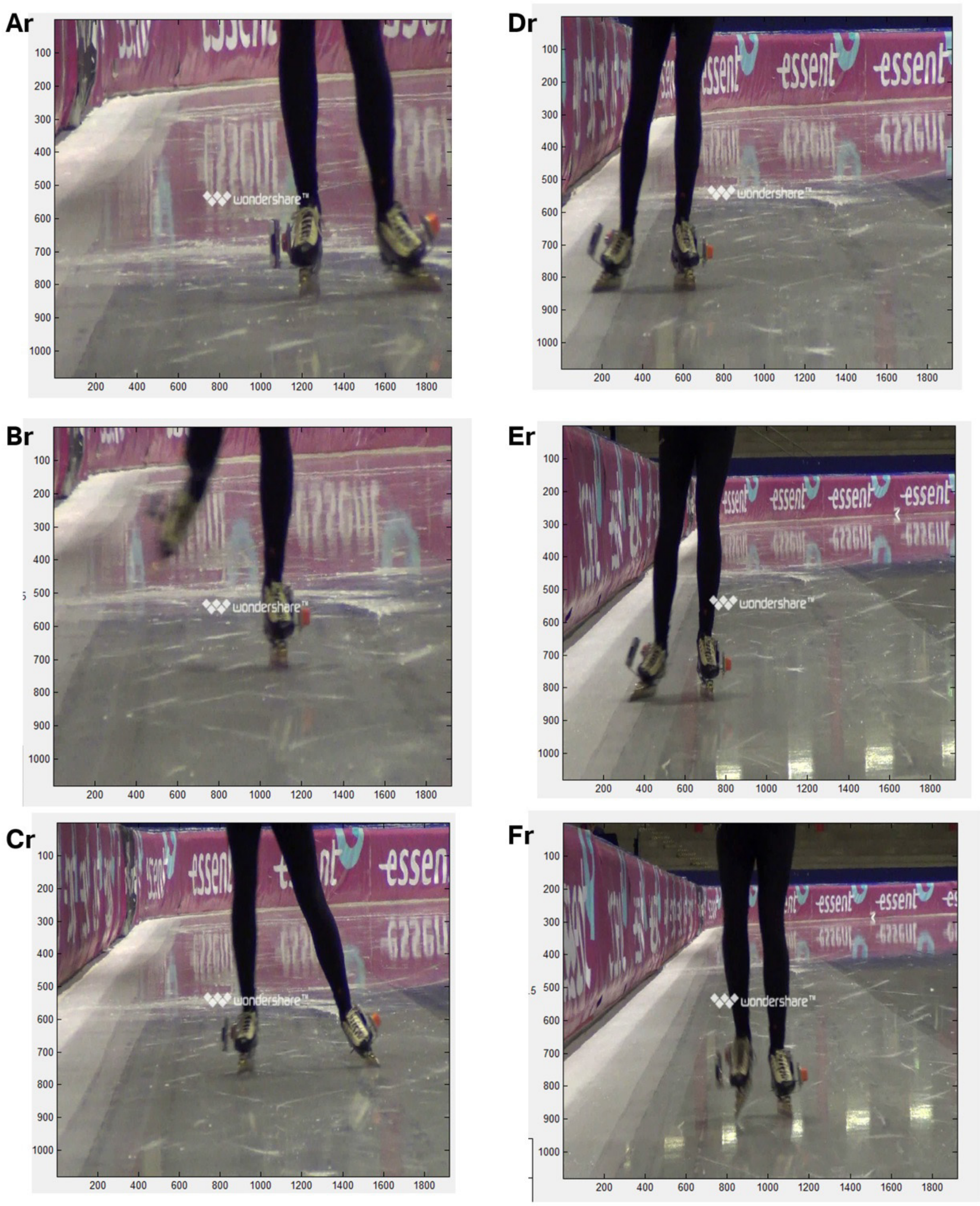

Figure 111 Images of the movements made at the time points Ar to Fr in Figure 110

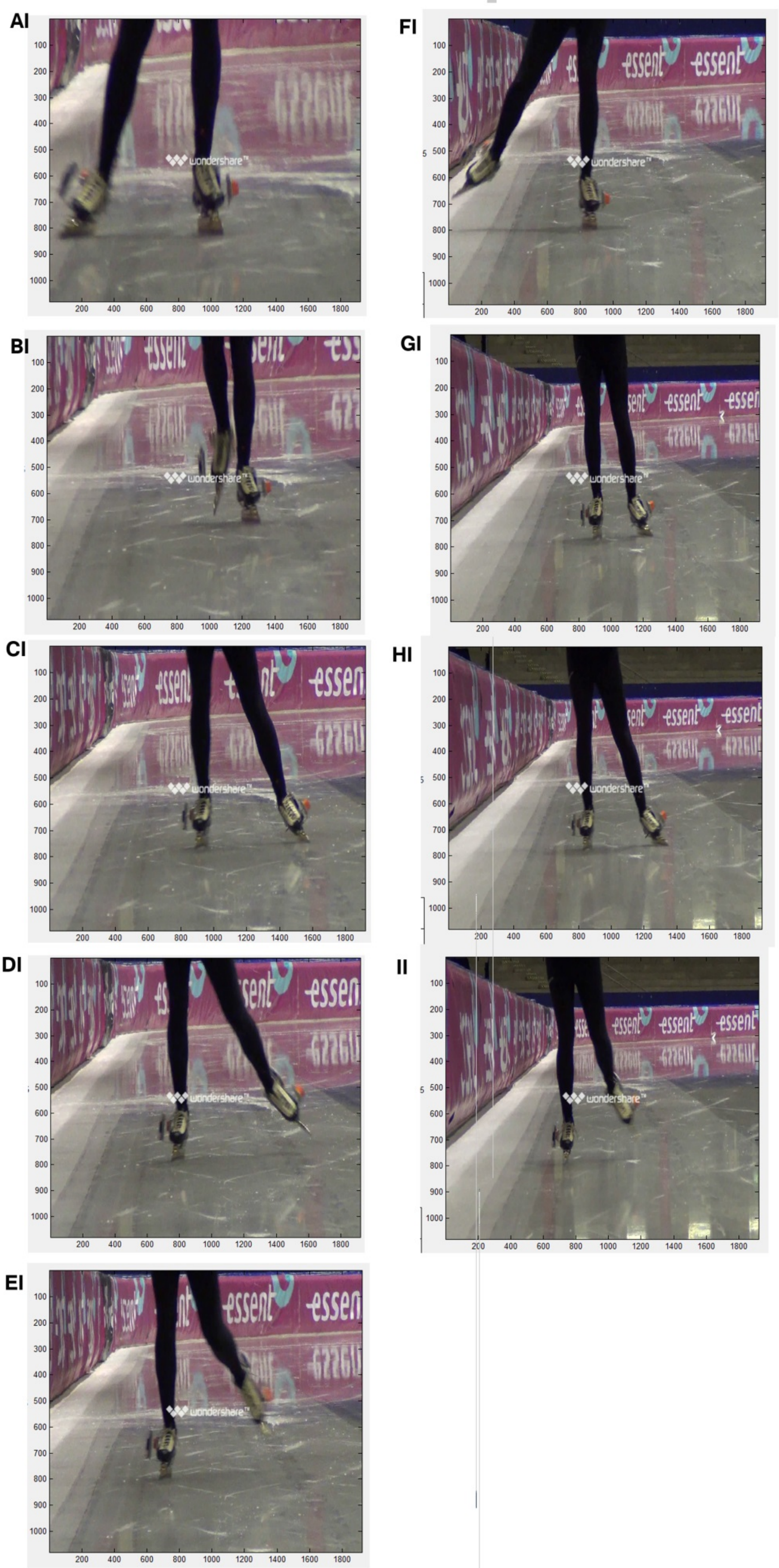

Figure 112 Images of the movements made at the time points AI to II in Figure 110

O.2 Trial 1

The images for points Al, Ar and Br of Trial 1 are given in Figure 113.

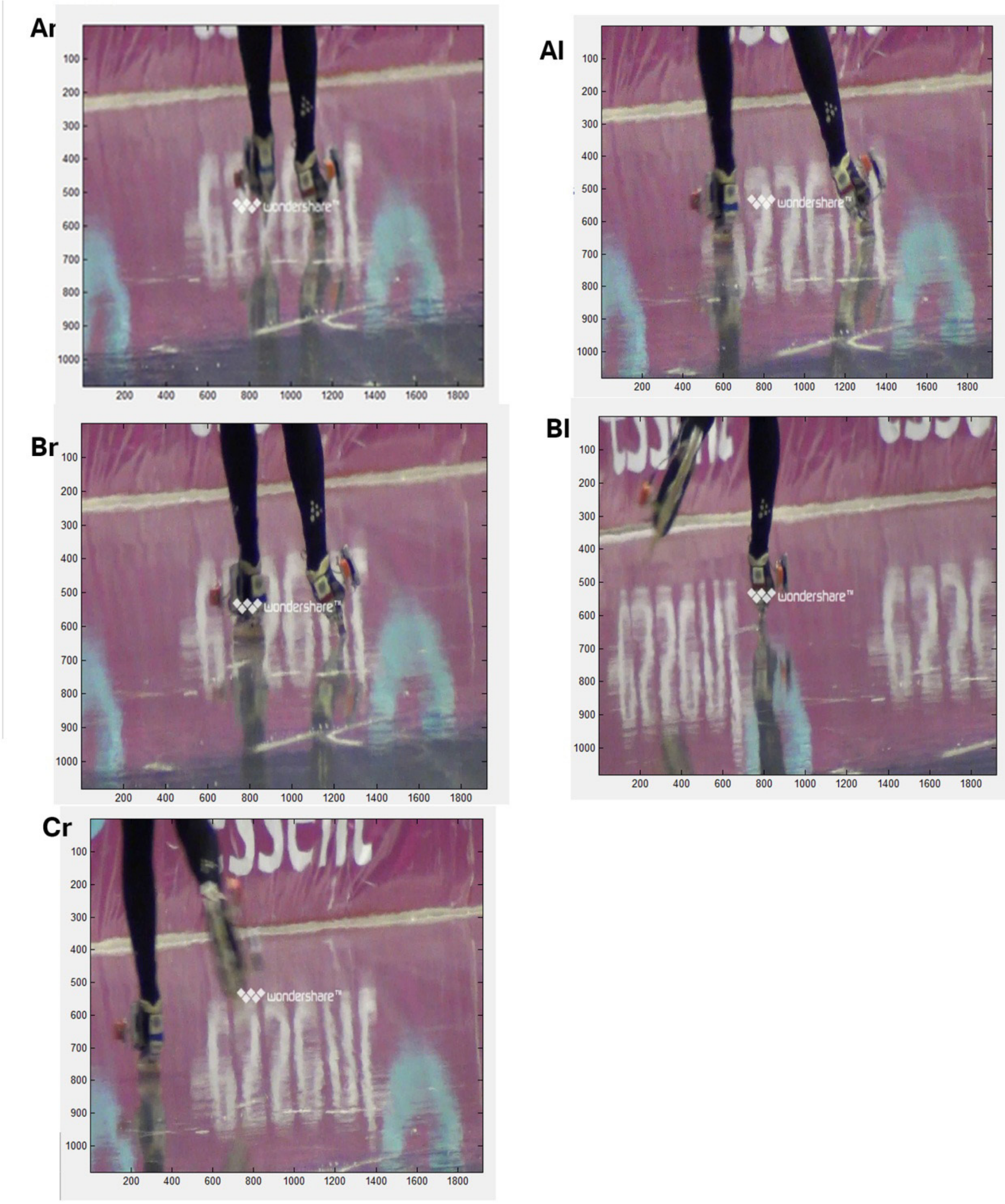

Figure 113 Images of the movements made at the time points Al, Ar and Br in Figure 109

Appendix P
Overview collected data of each trial

This appendix contains the table with an overview of the collected data separated for each straight part, per trial, per participant.

Table 46Overview of the collected data and the usability of it for each participant and trial.

				LPM		iGPS		force data		Xsens
Participant	**Trial (file)**	**Trial**	**straight**	**CoM**	**feet**	**CoM**	**feet**	**Left**	**Right**	
Participant 1	11.1	A	1	X	X	X	X*	X**	X**	X**
Participant 1	11.1	A	2	X	X	X	X	X**	X**	X**
Participant 1	11.1	A	3	X	X	X	X*	X**	X**	X**
Participant 1	11.1	A	4	X	X	X	X	X**	X**	X**
Participant 1	11.2	B	1	X	X	X	X*	X**	X**	X**
Participant 1	11.2	B	2	X	X	X*	X*		X**	X**
Participant 1	11.2	B	3	X	X	X	X*		X**	X**
Participant 1	11.2	B	4	X	X	X*	X*		X**	X**
Participant 1	11.2	B	5	X	X	X*	X*		X**	X**
Participant 1	12.1	C	1			X*	X*	X**	X**	X**
Participant 1	12.1	C	2			X		X**	X**	X**
Participant 1	12.1	C	3				X	X**	X**	X**
Participant 1	12.1	C	4			X*	X	X**	X**	X**
Participant 1	12.1	C	5			X		X**	X**	X**
Participant 2	13.1	A	1	X	X	X*	X		X**	X**
Participant 2	13.1	A	2	X	X	X	X		X**	X**
Participant 2	13.1	A	3	X	X	X	X		X**	X**
Participant 2	13.2	B	1						X**	X**
Participant 2	13.2	B	2			X	X*		X**	X**
Participant 2	13.2	B	3			X	X		X**	X**
Participant 2	13.2	B	4			X	X		X**	X**
Participant 4	66.1	A	1	X	X	X		X**	X**	X**
Participant 3	15	A	1	X		X				X**
Participant 3	15	A	2	X		X				X**
Participant 3	15	A	3	X		X				X**
Participant 3	15	A	4	X						X**

* The data contain many gaps
** The data contain unknown data gaps

Appendix Q
Measurement protocol data collection

This appendix describes the measurement protocol applied for the collection of data to verify the biomechanical model.

Q.1 Protocol

1. Equipped skater (Figure 22) sits on a stool
2. Turn on LPM system and the Dome cameras
3. Turn on Xsens by running the MATLAB file at the minilaptop
4. Turn on the measurement skate:
    a. Lift skate from the floor
    b. Turn both skates on
5. Turn on the High speed (HS) camera and the Lean angle camera (LA)
6. Start synchronization:
    a. HS camera and LA camera both film the skates
    b. Skater lifts left foot from the floor and keeps it from the floor for approximately 10s
    c. Skater stamps on the ground with its skates
    d. Skater lifts left foot from the floor and keeps it from the floor for approximately 5s
    e. The skater stamps on the ground again
    f. Skater lifts left foot from the floor and keeps it from the floor for approximately 10s
    g. Repeat step b-f for the right foot.
7. Xsens calibration: the skates (while still worn) are put into a sharpening table Figure 114 for approximately 10 s. The sharpening table is aligned with the ice rink.
8. Skater is ready to enter the ice
9. HS camera and LA camera are put in position (see Figure 23) and iGPS is turned on
10. The skater skates 3 rounds at his or her preferred speed (three time through the measurement area). The fourth time of passing the measurement area, the skater performs a coasting exercise (no ice skating movement).

> During the skating exercise the LPM and iGPS are synchronized; the HS camera captures the skater when he passes the iGPS transmitter and the LPM sensor (see Figure 23). The light at the back of the skater is an attention point that can be used to recognize the point of passing. The HS camera is also provided with a string that provides a vertical line in the snapshots at the position of the finish line, LPM sensor and iGPS transmitter.

11. The skater leaves the ice and returns to the stool
12. End synchronization: Step 6 is repeated.
13. LPM (+dome cameras), iGPS, the instrumented skate, the HS camera, the LA camera and Xsens are switched off.

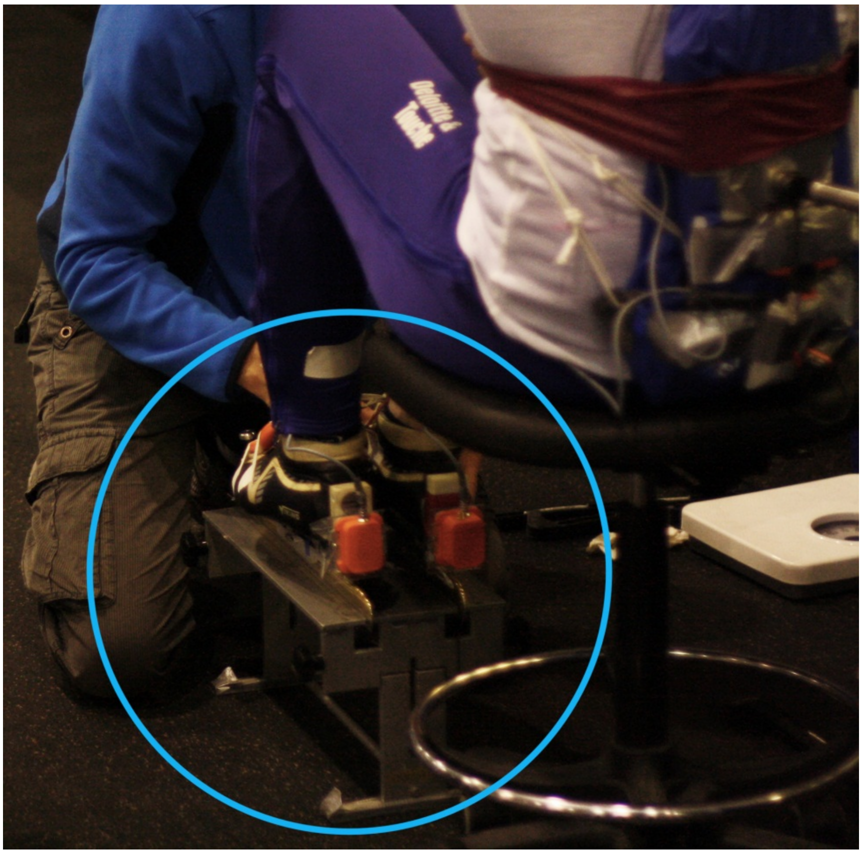

Figure 114 Calibration of the Xsens using a shareping table. The skates are put upright into the sharpening table, the sharpening table is aligned with the ice rink, using the junctions of the rubber mats at the floor.

Appendix R Data gaps.

This appendix describes how the data gaps in the lean angle data and force data were discovered. The time between the start and end synchronisation and the time between the two synchronisation points is known by means of the High speed camera (HS). This knowledge is applied for both measurements.

R.1 Lean angle measurements

In Figure 115 trial 1A with a start and end synchronization is shown; Table 47 shows the time difference between the time measured by the cameras and the Xsens sensors. The time differences between the Xsens and the HS measurements are very large. This could either be due to a deviant sample frequency, or due to data gaps. However we know that the system did sample at 100 HZ, so unknown data gaps occur in the data.

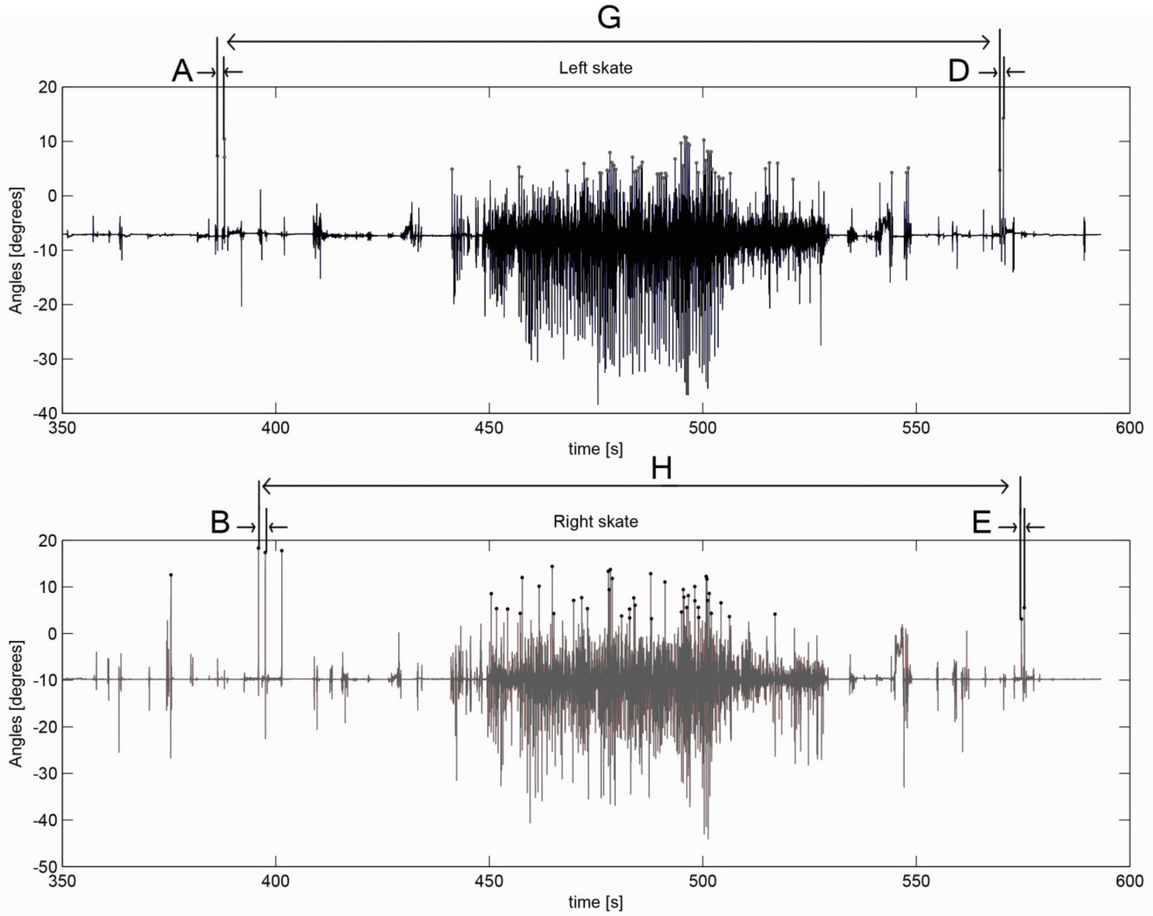

R.2

Figure 115 Acceleration data in z-direction of the lef tand right skate for participant 1A.

Table 47 Values on the time difference obtained by the HS camera and the xsens sensors. Δt is the time for distance i according to the Xsens; # of frames indicates the number of frames the time span holds for the Xsens; Δt HS shows the time measured by the High speed camera for this interval; Δt HS/#frames indicates the possible sample frequency for the Xsens.

Period	Δt (100 Hz)	# of frames	Δt HS [s]	Δt
A	1.62	162	5.2	31.1538
B	1.59	159	5.22	30.4598
D	0.82	82	3.77	21.7507
E	0.68	68	3.17	21.4511
G	183.2	18323	717.0	25.5551
H	178.7	17867	709.4	25.1861

R.3 Force measurements

In Figure 116 trial 1A with a start and end synchronization is shown; Table 48 shows the time difference between the time measured by the cameras and the instrumented skate. Distance G and H show that there is a large time gap between the start and the end of the trial. This could either be due to a different or irregular sampling time or due to time gaps in the data. Distances A,B,E and D can be used to establish the sample frequency. Based on these distances and time differences, we may conclude that the sample frequency is approximately 100 Hz at these points. Therefore the explanation for the time gaps is either an irregular sample frequency or, which is likely the case, data gaps due to the wireless transmission. All trials suffer from the mentioned time gaps.

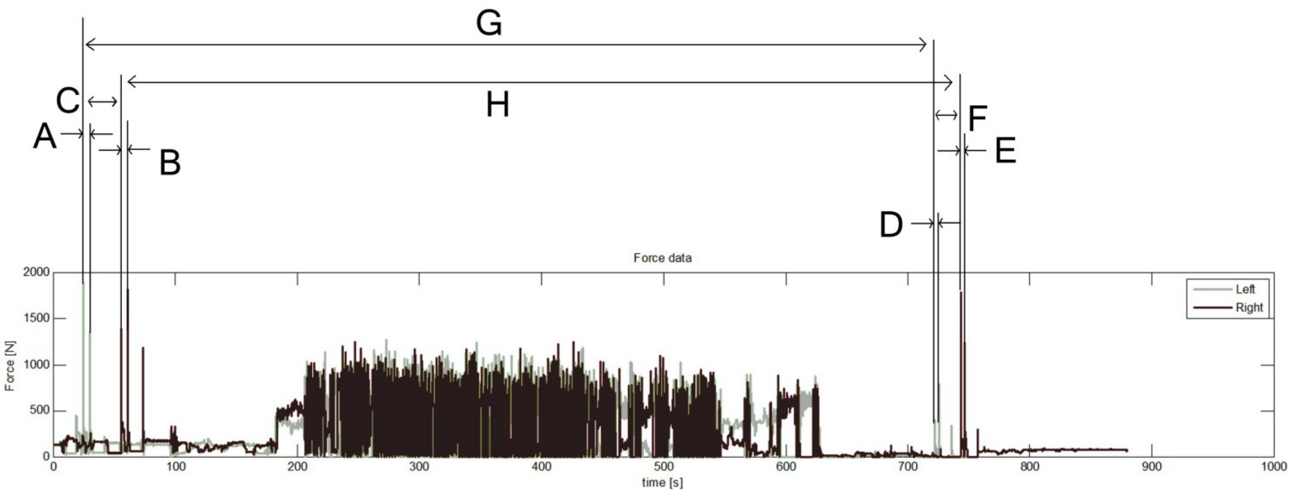

Figure 116 Force data from the right and the left skates with the start and end synchronization peaks.

Table 48 Values on the time difference obtaines by the HS camera and the measurement skate. Δt is the time for distance i according to the instrumented skate; Δt HS shows the time measured by the High speed camera for this interval;

Period	Δt measurement skate	Δt high speed camera [s]	Δt [s]
A	5.04	5.2	-0.16
B	4.94	5.22	-0.26
C	36.28	36.27	+0.01
D	3.88	3.77	+0.11
E	3.08	3.17	-0.09
F	22	23.4	-1.4
G	696.8	717.0	-20.2
H	687.5	709.4	-21.9

Appendix S
Upper body position and skate take-off

In section 4.5.3 the vertical upper body movement was discussed. In this discussion the point where the upper body is lowest was related to the position of the upper body in the horizontal plane. Although limited in data points, Figure 117 illustrates the position of the skates as the upper body is at its lowest point. However exploratory, this point is expected to be the point of take-off of the skate.

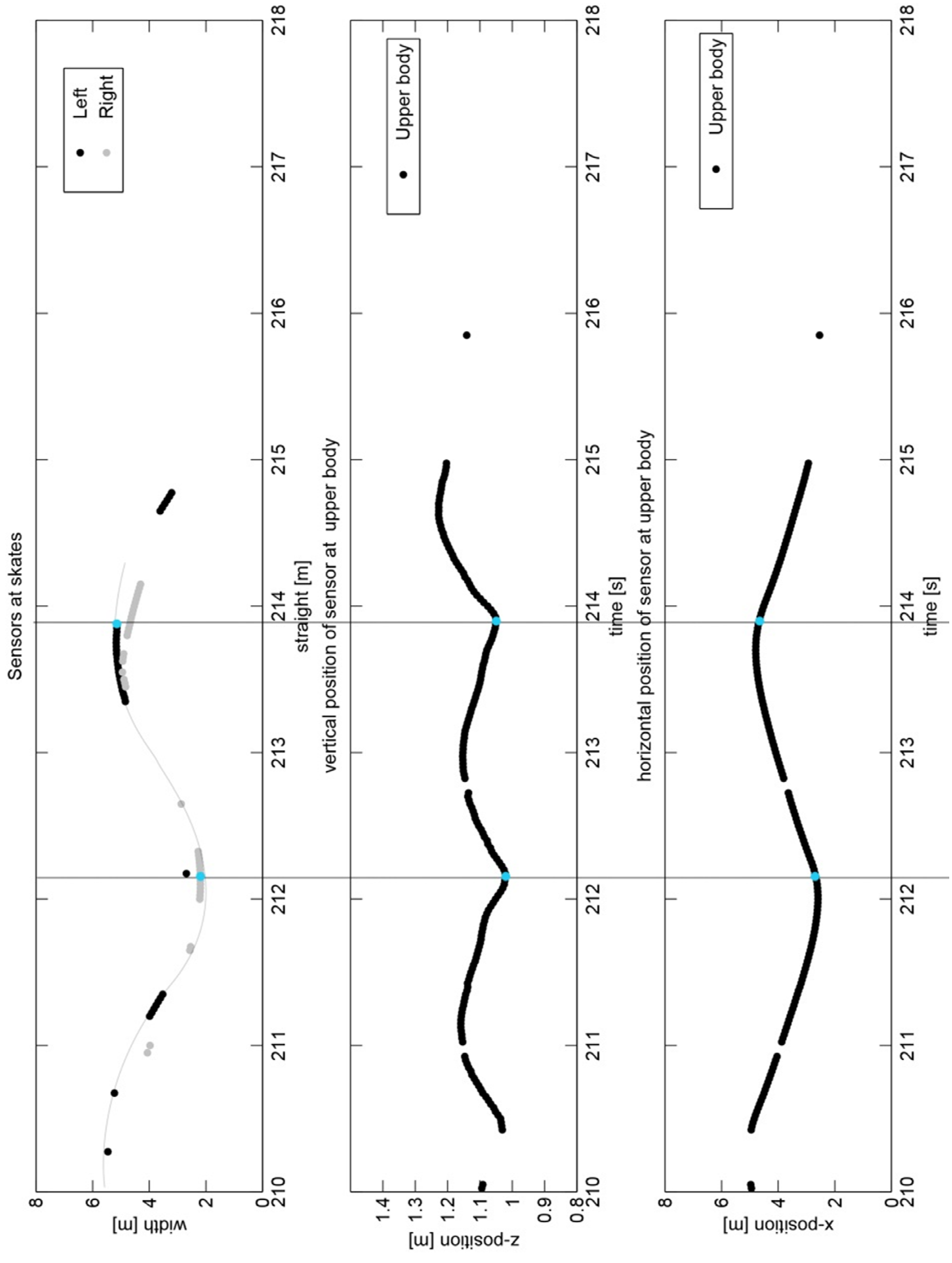

Figure 117 A) lateral position (x) of the sensors at the skates over time; B)vertical position of the sensor at the upper body; C) lateral position (x) of the sensors at the upper body over time; the blue dots illustrate the lowest positions of the upper body.

Appendix T
Convert collected data to input

This appendix describes the formulas used to convert the collected (global) data into the input data (leg extension) needed to run the model.

T.1 Convert the data

1. Data to steer angle

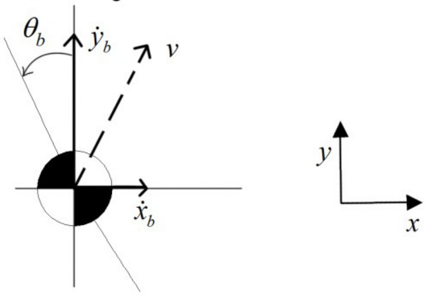

$$\theta_b = -\sin^{-1}\left(\frac{\dot{x}_b}{\sqrt{\dot{y}_b^{\,2} + \dot{x}_b^{\,2}}}\right)$$

2. Left skate - data to leg extension

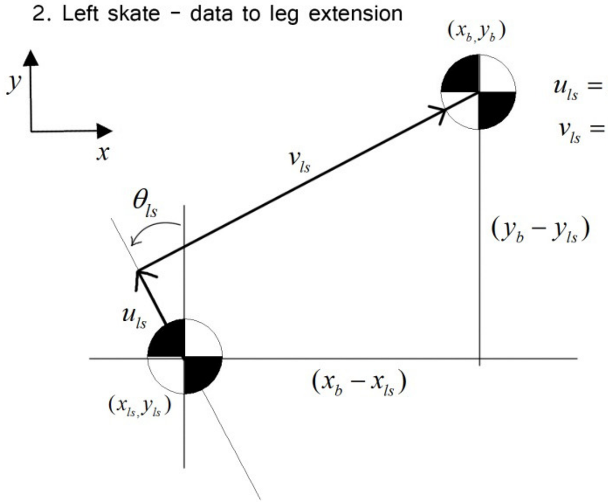

$$u_{ls} = \cos(\theta_{ls})\cdot(y_b - y_{ls}) - \sin(\theta_{ls})\cdot(x_b - x_{ls})$$
$$v_{ls} = \sin(\theta_{ls})\cdot(y_b - y_{ls}) + \cos(\theta_{ls})\cdot(x_b - x_{ls})$$

3. Right skate - data to leg extension

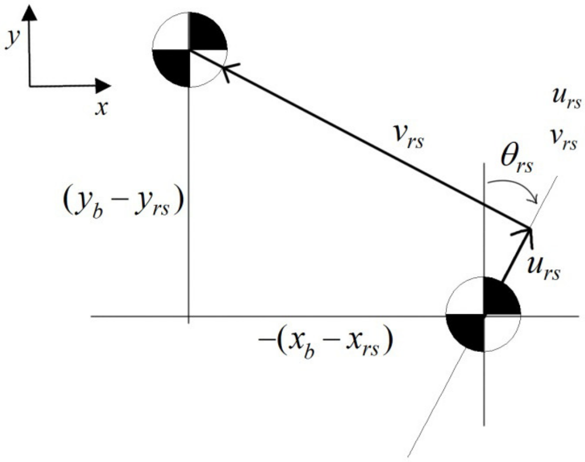

$$u_{rs} = \cos(\theta_{rs})\cdot(y_b - y_{rs}) + \sin(\theta_{rs})\cdot(x_b - x_{rs}$$
$$v_{rs} = \sin(\theta_{rs})\cdot(y_b - y_{rs}) - \cos(\theta_{rs})\cdot(x_b - x_{rs}$$

T.2 Parameterization of the coordination body functions

All measured positions of the bodies need to be numerical differentiated to find the velocities and accelerations. In order to eliminate differential and filtering errors all positions are parameterized. The method used is based on the report of Fintelman, for further elaboration on the method I refer to this report. The used parameterization functions are shown in equation (T.1.1). The fit is cut off at the start and end of the parameterization to prevent mismatched in initial conditions.

$$
\begin{aligned}
&f = c_0 + c_1 t + \sum\nolimits_{k=1}^{5} a_k \sin\left(\frac{t}{T}2\pi k\right) + b_k \cos\left(\frac{t}{T}2\pi k\right) \\
&\dot{f} = c_1 + \sum\nolimits_{k=1}^{5} \frac{2\pi k}{T}\left(a_k \cos\left(\frac{t}{T}2\pi k\right) - b_k \sin\left(\frac{t}{T}2\pi k\right)\right) \\
&f = \sum\nolimits_{k=1}^{5} \left(\frac{2\pi k}{T}\right)^2 \left(-a_k \sin\left(\frac{t}{T}2\pi k\right) - b_k \cos\left(\frac{t}{T}2\pi k\right)\right)
\end{aligned}
\qquad \text{(T.1.1)}
$$

Appendix U Mechanical constants

This appendix gives the tables containing the mechanical constants obtained by use of optimization.

Tables 49 In each run two straight parts were selected. The tables show the results for the whole two straight parts (S1, S2) and for the separate strokes on the straight parts (L1,L2,R1,R2..etc). Optimization was performed minimizing the function (5.2.2) with the fmincon *function in MATLAB. The results show the residuals of the variables (function (5.2.5)). The nomenclature of the tables is:*

Variable	
α	Mass distribution coefficient
k_1	Air friction coefficient
μ	Ice friction coefficient
$mass$	Mass
T_{shift}	Time shift of position data relatively to force data
t_d	Time shift of simulated vertical upper body movement
T	Period of the simulated upper body movement
$J_{\min}$	Minimization criterion (5.2.2)
x	Position residual lateral to skate direction
y	Position residual longitudinal to skate direction
dx	Velocity residual lateral to skate direction
dy	Velocity residual longitudinal to skate direction
F	Local normal Force residual

Test	
Constant upper body	Optimization with a constant upper body position
Data shift	Optimization were the position data could be shifted relatively to the position data.
Upper body motion (constant period)	Optimization with a simulated vertical upper body movement, whereby the simulated motion was shifted relatively to the horizontal motion
Upper body motion (varying period)	Optimization with a simulated vertical upper body movement whereby the simulated motion was shifted relatively to the horizontal motion and the period could vary.
Upper body motion + data shift	Optimization were all optimization parameters could change.

Index	
S1,S2	Straight 1, Straight 2
L1, L2…	First left stroke, second left stroke
R1, R2…	First right stroke, second right stroke

The variables to be optimized are:

Variable	*Constant upper body*	*Data shift*	*Upper body motion (constant*	*Upper body motion*	*Upper body motion +*
α	X	X	X	X	X
k_1	X	X	X	X	X
μ	X	X	X	X	X
T_{shift}		X			X
t_d			X	X	X
T				X	X

Run 26 - Constant upper body

Run 26	L1	L2	L3	L4	L5	L6	R1	R2	R3	R4	R5	R6	S1	S2
α	0	0	0	0	0	0.088	0	0	0	0	0	0	0	0.1478
k_1	0.01	0.01	0.2153	0.2132	0.1561	0.01	0.01	0.01	0.01	0.1971	0.01	0.01	0.2816	0.3133
μ	0.1508	0.0731	0.099	0.1152	0.0054	0.001	0.001	0.001	0.001	0.0481	0.0165	0.001	0.001	0.001
$mass$	77	77	77	77	77	77	77	77	77	77	77	77	77	77
J_{min}	0.0105	0.0141	0.0088	0.0068	0.0031	0.0091	0.0158	0.0225	0.201	0.0137	0.019	0.0185	0.0131	0.0145
x	0.0587	0.042	0.0187	0.036	0.0173	0.0653	0.0677	0.0224	0.0102	0.0281	0.0416	0.0289	0.1672	0.1429
y	0.1634	0.109	0.1051	0.1631	0.0488	0.1992	0.1374	0.155	0.0348	0.0755	0.1646	0.0959	0.2651	0.3002
dx	0.1254	0.0655	0.0637	0.1138	0.0647	0.1016	0.1	0.0654	0.0519	0.061	0.0667	0.0572	0.0712	0.0581
dy	0.7091	0.2152	0.3232	0.7086	0.2587	0.3494	0.4747	0.3794	0.1885	0.3559	0.3525	0.1972	0.2219	0.1691
F	73	83	67	56	34	53	78	93	126	85	95	116	86	74.0000

Run 26 - Data shift

Run 26	L1	L2	L3	L4	L5	L6	R1	R2	R3	R4	R5	R6	S1	S2
α	0	0	0	0	0	0.0761	0	1	0	0	0	0	0	0.1033
k_1	0.2614	0.1996	0.269	0.2571	0.1695	0.01	0.01	0.7	0.196	0.2306	0.01	0.2188	0.2938	0.3258
μ	0.1	0.068	0.1	0.1	0.0113	0.001	0.0203	0.1	0.001	0.0477	0.0257	0.0073	0.001	0.001
$mass$	77	77	77	77	77	77	77	77	77	77	77	77	77	77
T_{shift}	1.67E-04	-0.0125	-0.0066	5.00E-04	0.0012	9.77E-06	0.0143	1.50E-01	-0.0288	-1.48E-02	-0.0178	-0.0348	-0.0188	-0.012
J_{min}	0.0109	0.0109	0.0077	0.0069	0.003	0.0091	0.0118	0.0898	0.0056	0.0071	0.0075	0.011	0.0106	0.0134
x	0.0683	0.0329	0.0148	0.0405	0.0133	0.066	0.0567		0.0193	0.0291	0.036	0.0125	0.1431	0.1427
y	0.1455	0.0611	0.0733	0.1521	0.0682	0.2016	0.1254		0.0602	0.0776	0.1422	0.0293	0.9281	0.4679
dx	0.1163	0.0695	0.0706	0.1108	0.0622	0.1025	0.0973		0.0556	0.0615	0.0541	0.0359	0.0723	0.06
dy	0.6097	0.2075	0.3054	0.6685	0.2752	0.3527	0.5165		0.1907	0.3549	0.3055	0.1205	0.2315	0.1785
F	72	86	62	57	35	53	65		59	64	69	75	75	72

Run 26 - Upper body motion (constant period)

Run 26	L1	L2	L3	L4	L5	L6	R1	R2	R3	R4	R5	R6	S1	S2
α	0	0	0.2346	0.3652	0.3866	0.36	0	0.3881	0	0.3639	0.2592	0	0.0908	0.3904
k_1	0.7	0.01	0.4669	0.5318	0.2461	0.01	0.01	0.01	0.01	0.2333	0.01	0.01	0.3697	0.5199
μ	0.1	0.0998	0.1	0.1	0.0116	0.001	0.0122	0.0085	0.001	0.0704	0.0356	0.0215	0.001	0.001
$mass$	77	77	77	77	77	77	77	77	77	77	77	77	77	77
T_{shift}	0	0	0	0	0	0	0	0	0	0	0	0	0	0
td	0.3107	0.1465	0.1131	0.049	0.1282	0.1775	0.2219	0.1166	0.1217	0.0672	0.2117	0.328	0.1518	0.1743
J_{min}	0.0073	0.0096	0.0073	0.0073	0.006	0.0087	0.0164	0.0229	0.0117	0.0141	0.0193	0.0116	0.0108	0.0141
x													0.1535	0.1198
y													0.4151	0.1519
dx													0.0751	0.0577
dy													0.2429	0.1646
F													77	79

Run 26 - Upper body motion (varying period)

Run 26	L1	L2	L3	L4	L5	L6	R1	R2	R3	R4	R5	R6	S1	S2
α	0.2631	0.2956	0.2757	0.5401	0.5683	0.2337	0.054	0.3213	0.2967			0.1305	0.229	0.305
k_1	0.3002	0.2564	0.2624	0.5489	0.0512	0.0332	0.1279	0.2313	0.2476			0.1554	0.2563	0.2632
μ	0.0772	0.0233	0.1	0.1	0.0277	0.001	0.001	0.001	0.001			0.001	0.0134	0.0043
$mass$	77	77	77	77	77	77	77	77	77			77	77	77
T_{shift}	0	0	0	0	0	0	0	0	0			0	0	0
td	0.4804	0.1967	0.2912	0.3411	0.0995	0	0.7556	0.2066	0.2233			0.3463	0.1987	0.1809
T	0.1305	0.1363	0.1511	0.12	0.12	0.1599	0.1475	0.1376	0.16			0.1324	0.1375	0.14
J_{min}	0.012	0.0128	0.0064	0.0094	0.0083	0.013	0.0149	0.0245	0.0156			0.0137	0.0125	0.0148

Upper body motion + data shift

Run 26	S1	S2
α	0.298	0.2809
k_1	0.2576	0.2874
μ	0.0258	0.0051
$mass$	77	77
T_{shift}	-0.0308	-0.0113
td	0.1974	0.2735
T	0.135	0.1485
J_{min}	0.0122	0.0154
x	0.1077	0.1439
y	0.8029	0.5461
dx	0.0799	0.0738
dy	0.2868	0.2873
F	78	88

Run 38 - Constant upper body

Run 38	L1	L2	L3	L4	L5	L6	R1	R2	R3	R4	R5	R6	S1	S2
α	0	0	0	0	0	0	0	0	0	0	0	0	0	0
k_1	0.01	0.01	0.01	0.01	0.01	0.01	0.1723	0.01	0.1964	0.2471	0.01	0.01	0.01	0.01
μ	0.001	0.001	0.001	0.001	0.001	0.001	0.0254	0.1532	0.0356	0.1507	0.1232	0.001	0.001	0.001
$mass$	85	85	85	85	85	85	85	85	85	85	85	85	85	85
J_{min}	0.0349	0.0164	0.0146	0.0312	0.0102	0.0157	0.0083	0.0104	0.0108	0.0096	0.0083	0.0156	0.1189	0.0206
x	0.1156	0.0339	0.0172	0.0071	0.0151	0.0506	0.0495	0.0677	0.0183	0.0254	0.0345	0.019	0.2105	0.2168
y	0.5384	0.078	0.0528	0.05	0.0649	0.1795	0.1264	0.133	0.0881	0.1103	0.084	0.0703	0.8055	1.09
dx	0.1532	0.057	0.0458	0.0338	0.0573	0.1226	0.0976	0.1218	0.0633	0.0928	0.0637	0.0336	0.0655	0.1189
dy	0.7418	0.1876	0.1528	0.1807	0.2362	0.6342	0.5196	0.5908	0.3217	0.5953	0.2089	0.1799	0.2561	0.5705
F	149	112	111	179	97	116	75	79	77	61	77	97	107	100

Run 38 - Data shift

Run 38	L1	L2	L3	L4	L5	L6	R1	R2	R3	R4	R5	R6	S1	S2
α	1	0.5847	0	0	0		0.5896	0.3321	0	0	0			0
k_1	0.01	0.2511	0.2441	0.2908	0.2441		0.225	0.2472	0.01	0.2548	0.2188			0.0298
μ	0.001	0.0026	0.1	0.1	0.1		0.0109	0.1639	0.0558	0.1555	0.1155			0.001
$mass$	85	85	77	77	77		85	85	85	85	85			77
T_{shift}	0.0967	0.0768	0.0391	9.20E-03	0.0319		0.0035	0.0015	0.0001	0.0099	0.0278			0.0136
J_{min}	0.0336	0.0267	0.0056	0.0085	0.0056		0.0085	0.0104	0.0107	0.0076	0.0053			0.0192

Ackland, Blanksby, et al. (2013). Mass and moment of inertia of body parts. http://www.phys.washington.edu/users/jeff/courses/ken_young_webs/208A/body_segment_mass.txt.

Akman, O. (2012). Robust Augmented Reality. PhD, Technical University Delft.

Allinger, T. L. and A. J. v. Bogert (1997). "Skating technique for the straights, based on the optimization of a simulation model." Medicine & Science in Sports & Exercise **29**(2): 279-286.

Andreas Stelzer, K. P., Alexander Fischer (2004). "Concept and Application of LPM—A Novel 3-D Local Position Measurement System." IEEE TRANSACTIONS ON MICROWAVE THEORY AND TECHNIQUES **52**(12).

Boer, R. W. d. and K. L. Nilsen (1989). "The gliding and push-off technique of male and female Olympic speed skaters." Int. J. Sport. Biomech. **5**: 119-134.

Brendle, J. and S. Hoy (2011). "Investigation of distances covered by fattening pigs measured with VideoMotionTracker®." Applied Animal Behaviour Science **132**(1–2): 27-32.

de Koning, J. J., G. de Groot, et al. (1992). "A power equation for the sprint in speed skating." Journal of Biomechanics **25**(6): 573-580.

Depenthal, C. (2010). iGPS A new system for static and kinematic measurements. FIG Congress 2010 - TS 2C – Low Cost GNSS and New Positioning Techniques. Sydney.

Field;, A. (2005). Discovering statistics using SPSS. London, SAGE publications.

Fintelman, D. M. (2010). "Literature study: Biomechanical models for speed skating."

Fintelman, D. M. (2011). Simplest skater model. Master Final Thesis, Technical University of Delft.

Garcia, M., A. Chatterjee, et al. (1998). "The Simplest Walking Model: Stability, Complexity, and Scaling." ASME Journal of Biomechanical Engineering.

Houdijk, H., M. F. Bobbert, et al. (2003). "The effects of klapskate hinge position on push-off performance: a simulation study." Medicine & science in sports & exercise: 2077-2084.

Hughes, B., A. Forbes, et al. (2012). iGPS Capability study. National Physical Laboratory (NPL). MiddleSex, England.

Ingen Schenau, G. J. v. (1982). "The influence of air friction in speed skating." Journal of Biomechanics **15**(6): 449-458.

Inmotio. (2013). "http://www.inmotio.eu/."

Klous, M., E. Muller, et al. (2010). "Collecting kinematic data on a ski/snowboard track with panning, tilting and zooming cameras: Is there sufficient accuracy for a biomechnical analysis?" Journal of Sports Sciences **28**(12): 1345-1353.

Koning, J. J. d., C. Foster, et al. (2005). "Experimental evaluation of the power balance model of speed skating." Journal of Applied Physiology **98**(1): 227-233.

Koning, J. J. d., G. d. Groot, et al. (1992). "Ice friction during speed skating." Journal of Biomechanics **25**(6): 565-571.

Kruk, E. v. d. (2013). Smooth measuring: finding accurate kinematic data of skaters on an ice rink, Technical University Delft.

Kurita, K. (2011). "Novel non-contact and non-attached technique for detecting sports motion." Measurement **44**(8): 1361-1366.

Lee, J. B., B. J. Burkett, et al. (2011). "Inertial sensor, 3D and 2D assessment of stroke phases in freestyle swimming." Procedia Engineering **13**(0): 148-153.

Mosqueira, G., J. Apetz, et al. (2012). "Analysis of the indoor GPS system as feedback for the robotic alignment of fuselages using laser radar measurements as comparison." Robotics and Computer-Integrated Manufacturing **28**(6): 700-709.

Nikon. (2013). "http://www.nikonmetrology.com/en_EU/Products/Large-Volume-Applications/iGPS/iGPS/(brochure)."

Owen, C. B., F. Xiao, et al. (2002). "What is the best fiducial?" The First IEEE International Augmented Reality Toolkit Workshop: 98-105.

Press, W. H., B. P. Flannery, et al. (1992). "Runge Kutta Method and Adaptive Step Size Control for Runge-Kutta." Numerical Recipes in FORTRAN: The Art of Scientific Computing; Cambridge Univeristy Press: 704-716.

ProMove-3D. (2013). "Wireless Inertial and Orientation Sensor Platform U.M. v1.3.2."
Schwieger, V. (2012). Challenges of kinematic measurements. Multi-Sensor Systems. Rome.
van Ingen Schenau, G. J., G. de Groot, et al. (1985). "The control of speed in elite female speed skaters." Journal of Biomechanics **18**(2): 91-96.
Xsens. (2013). "http://www.xsens.com/."
Zhong, D. and S.-F. Chang (2004). "Real-time view recognition and event detection for sports video." Journal of Visual Communication and Image Representation **15**(3): 330-347.
Zohlandt, C., L. Walk, et al. (2012). Classification of Vault Jumps in Gymnastics. B. B. Engineering. Delft, Technical University Delft.